DYNAMIC STABILITY OF CYLINDRICAL SHELLS UNDER STEP LOADING

Thesis by

Yukio Stephen Tamura

In Partial Fulfillment of the Requirements

For the Degree of

Aeronautical Engineer

California Institute of Technology

Pasadena, California

1973

(Submitted May 20, 1973)

ACKNOWLEDGEMENT

The author is sincerely grateful to Dr. Charles D. Babcock for his patient guidance and encouragement during the course of this research. He is also indebted to Dr. Johann Arbocz for many helpful discussions and suggestions, and to Dr. Ernest E. Sechler for his support and encouragement. Thanks are also due Mrs. Elizabeth Fox for excellent typing of the manuscript and Mrs. Betty Wood for drawing the figures. Finally the author wishes to thank his many colleagues, the Computing Center, and the staff in the Aeronautics Department, who have given helpful comments and encouragement along the way.

The financial support of the California Institute of Technology in the form of a Graduate Research Assistantship and a Graduate Teaching Assistantship is gratefully acknowledged. Thanks are also due to the U. S. Air Force for their support under Contract AFOSR 73-2447.

ABSTRACT

A study has been made to determine the dynamic stability of an imperfect circular cylindrical shell subject to a step loading in the axial direction. In the analysis, the radial displacement of the shell is approximated by a finite degree of freedom system. To assure that the created model is proper, its static buckling behavior was studied. It was found that the model gives the proper imperfection sensitivity behavior.

The dynamic analysis includes not only the effect of the radial inertia, but also that due to the axial inertia in an approximate manner. The critical loads are determined by numerical integration of the equation of motion. In addition a study is carried out to consider the effects of wave number of the radial mode shape, mass on the loaded edge of the shell and damping of the axial motion. Compared with the static case, there is a significant reduction of the dynamic buckling load for the high wave numbers of the radial modes. Also, there is a critical damping value, above which the dynamic buckling load is close to the static buckling load. The dynamic buckling load approaches half of the static buckling load with increasing mass on the loading edge. Through the parametric studies of the wave number, mass, and damping factor it is concluded that due to frequency coupling between axial and radial motions, the axial inertia plays an essential role in characterizing the dynamic instability of a finite length shell.

LIST OF SYMBOLS

Symbol	Definition
c	$\sqrt{3(1-\nu^2)}$
c^*	Speed of sound in the material, $\sqrt{\frac{E}{\rho}}$
C_i, Q_i	Coefficients of system equations
$\hat{C}_i, \hat{Q}_i$	Coefficients of strain energy expression
D	Bending rigidity, $Eh^3/12(1-\nu^2)$
E	Young's modulus
h	Shell thickness
$H(t)$	Unit step function
i	Half axial wave number for axisymmetric mode
k	Half axial wave number for asymmetric mode
ℓ	Full circumferential wave number
L	Shell length
$\overline{m}$	Nondimensional mass
$\overline{p}(t)$	λ/c
R	Shell radius
t	Time
u, v, w	Axial, circumferential and radial displacement
u_h, v_h	Homogeneous solutions of inplane equation
u_{BL}, v_{BL}	Boundary layer type solutions in u_h, v_h
$\overline{w}$	Initial imperfection function
x, y, z	Longitudinal, circumferential and radial coordinates
ρ	Density of shell
$\xi_1(t)$	Axisymmetric mode
$\xi_2(t)$	Asymmetric mode

LIST OF SYMBOLS (Cont'd)

$\xi_3(t)$	Uniform radial expansion mode
$\xi_o(t)$	Axial mode
ξ_o^*	$= \xi_o(cR/L)$
$\overline{\xi}_1$	Imperfection amplitude for axisymmetric mode
$\overline{\xi}_2$	Imperfection amplitude for asymmetric mode
λ	Nondimensional load parameter, σ/σ_{cl}
λ_D	Dynamic buckling load
λ_s	Static buckling load
ω_i	Frequency of axisymmetric mode
ω_k	Frequency of asymmetric mode
ω_3	Frequency of uniform radial mode
ω_o	Frequency of axial mode
ζ	Coefficient of critical damping
σ	Applied stress
σ_{cl}	Classical buckling load, $Eh/R\sqrt{3(1-\nu^2)}$
ν	Poisson's ratio
τ	Nondimensional time, c^*t/R
$\overline{\tau}$	$\omega_o\tau$

LIST OF FIGURES

LIST OF FIGURES (Cont'd)

TABLE OF CONTENTS

TABLE OF CONTENTS (Cont'd)

I. INTRODUCTION

Research concerned with the elastic stability of cylindrical shells has been carried out by many authors since the early nonlinear investigations by Donnell (ref. 1) and Kármán and Tsien (ref. 2). A great amount of effort has been put forth to explain the large discrepancy between experimental results and the classical buckling load. Geometrical imperfections have been recognized as the main contribution to this discrepancy (ref. 3). However most of the investigations have been limited to a static analysis. On the other hand, interest in the dynamic stability of thin shells has been increased during the last decade. This work can be largely divided into two categories.

The first categories of the problem are analogous to static buckling problems in that, for subcritical values of the load the measure of the response is small, whereas for supercritical values of the load the response is large (refs. 4-6). The critical load is defined as that load for which a discrete change in response is obtained with a small change in the loading parameter.

The second categories of problems are those similar to the one studied by Goodier and McIvor (ref. 7), Lindberg and Herbert (refs. 8, 9), etc. who study how the selected modes of response grow. This growth may occur during a single oscillation of the fundamental response or over many cycles of the fundamental oscillation. In general there is not a discrete change of amplitude, but one says that if the amplitude grows, say to 1000 times some initial imperfections (ref. 10), the structure has dynamically buckled.

Pioneering analytical work in the first category of dynamic buckling problems for the cylindrical shells subject to longitudinal dynamic loads was carried out by Volmir (ref. 11) where a two degrees of freedom system was obtained by Galerkin's method. A recent study due to Coppa and Nash (ref. 12) used the potential energy method and also studied a two degrees of freedom model. Roth and Klosner (ref. 13) applied a similar analysis to obtain a four degree system which they studied numerically.

The axial impacted cylindrical shell problem dealt with by these investigators was an axisymmetric structure subjected to an axisymmetric load. It is clear that there must be some trigger mechanism such as an asymmetric initial velocity or displacement or some asymmetric initial imperfection. In most previous work this triggering mechanism was assumed arbitrarily since better information on, say, initial imperfections did not exist. None of these studies assessed the influence of a realistic triggering mechanism on the calculated dynamic buckling loads. In addition, all of these investigators neglected the influence of inplane inertia in the analysis. Among other things, this simplification is equivalent to assuming if an axial load is applied to the end of a cylindrical shell the resultant axial stress is felt everywhere in the shell simultaneously.

To begin a dynamic buckling analysis of a shell structure, the governing differential equation must be simplified in some appropriate manner. This is usually accomplished by discretizing the system using an energy approach, finite elements, finite differ-

ences or Galerkin's procedure. One must then establish that the resulting model created is realistic. This step has not been carried out in the most dynamic buckling investigations. Some discrete models have displayed static equilibrium positions which the continuous structure did not possess (refs. 14, 15).

In the present analysis of the dynamic buckling problem, the static problem was thoroughly studied to determine whether the model was realistic or not. The model which had the proper static behavior among the various models attempted was chosen. Then this model was investigated with various modes of radial deflection to determine which were important in the static buckling problem. This static investigation incorporated a realistic distribution of initial imperfections (ref. 16). This imperfection model gives a balance between the amplitude of imperfection in any mode of deformation and the sensitivity of the structure to that mode of imperfection.

In the present dynamic buckling analysis the following points are emphasized:

(i) The analysis includes the effect of axial inertia in an approximate manner. The case of a shell with a mass on its loading edge is also treated.

(ii) The discrete model used in the dynamic analysis is based on the study of static buckling behavior.

(iii) Experimental results are used for values of the initial imperfections.

II. ANALYTICAL FORMULATION

The governing differential equations for a cylindrical shell to be used in this study are the nonlinear Donnell's equations (ref. 1). In previous investigations using these equations they have usually been written in terms of the inplane stress function and the out-of-plane displacement. The procedure used is to assume an expression for the out-of-plane displacement and find the solution of the compatibility equation. The out-of-plane equilibrium equation is then satisfied by Galerkin's procedure or an energy method. The inplane displacements must be obtained from the stress function and checked to see if they satisfy the circumferential periodicity condition. In the present analysis the two inplane equilibrium equations are directly solved after an assumption on the radial displacement has been made. The following procedure is used.

1. Assume an appropriate radial displacement function w and an initial imperfection function $\overline{w}$.
2. Find the displacement u and v from the inplane equilibrium equations and in turn the stresses σ_x, σ_y and τ_{xy}.
3. Evaluate the total potential energy and the kinetic energy of the system.
4. Apply Hamilton's principle by carrying out the variation with respect to the variables in the assumed expression for w. A set of nonlinear ordinary differential equations is obtained.

The geometry of the system is shown in Fig. 1, where u, v, and w

are the axial, circumferential and radial displacements of the median surface, respectively. It should be noted that radial displacement is positive inward.

2.1 Equilibrium Equations

The nonlinear strain-displacement relationship for thin cylindrical shells of radius R having initial imperfection $\bar{w}$, are based on the work of Donnell (ref. 1)

$$\epsilon_x = \frac{\partial u}{\partial x} + \frac{1}{2}\left(\frac{\partial w}{\partial x}\right)^2 + \frac{\partial \bar{w}}{\partial x}\frac{\partial w}{\partial x} - z\frac{\partial^2 w}{\partial x^2} \tag{1a}$$

$$\epsilon_y = \frac{\partial v}{\partial y} - \frac{w}{R} + \frac{1}{2}\left(\frac{\partial w}{\partial y}\right)^2 + \frac{\partial \bar{w}}{\partial y}\frac{\partial w}{\partial y} - z\frac{\partial^2 w}{\partial y^2} \tag{1b}$$

$$\gamma_{xy} = \frac{\partial u}{\partial y} + \frac{\partial v}{\partial x} + \frac{\partial w}{\partial x}\frac{\partial w}{\partial y} + \frac{\partial \bar{w}}{\partial x}\frac{\partial w}{\partial y} + \frac{\partial \bar{w}}{\partial y}\frac{\partial w}{\partial x} - 2z\frac{\partial^2 w}{\partial x \partial y} \tag{1c}$$

The static equilibrium equations can be found by applying a variation principle. The total strain energy, considered as an implicit function of displacements, is made stationary by setting the total variation with respect to u, v, w equal to zero. The resulting three equations are:

$$\frac{D}{h}\nabla^4 w = \frac{\partial}{\partial x}\left(\sigma_x \frac{\partial w}{\partial x}\right) + \frac{\partial}{\partial y}\left(\tau_{xy}\frac{\partial w}{\partial x}\right) + \frac{\partial}{\partial x}\left(\tau_{xy}\frac{\partial w}{\partial y}\right) + \frac{\partial}{\partial y}\left(\sigma_x \frac{\partial w}{\partial y}\right) + \frac{\sigma_y}{R} \tag{2a}$$

$$\frac{\partial \sigma_x}{\partial x} + \frac{\partial \tau_{xy}}{\partial y} = 0 \tag{2b}$$

$$\frac{\partial \sigma_y}{\partial y} + \frac{\partial \tau_{xy}}{\partial x} = 0 \tag{2c}$$

Finding the stresses in terms of the displacements by using the usual form of Hooke's law, equation (2) is expressed in the following form:

$$\frac{D}{h}\nabla^4 w = \frac{\partial}{\partial x}\left(\sigma_x \frac{\partial w}{\partial x}\right) + \frac{\partial}{\partial y}\left(\tau_{xy} \frac{\partial w}{\partial x}\right) + \frac{\partial}{\partial x}\left(\tau_{xy} \frac{\partial w}{\partial y}\right) + \frac{\partial}{\partial y}\left(\sigma_y \frac{\partial w}{\partial y}\right) + \frac{\sigma_y}{R} \quad (2a)$$

$$\frac{1}{(1-\nu^2)} \frac{\partial^2 u}{\partial x^2} + \frac{1}{2(1-\nu)} \frac{\partial^2 v}{\partial x \partial y} + \frac{1}{2(1+\nu)} \frac{\partial^2 u}{\partial y^2} = \frac{1}{(1-\nu^2)} \left\{ \frac{\partial^2 \overline{w}}{\partial x^2} \frac{\partial w}{\partial x} + \frac{\partial \overline{w}}{\partial x} \frac{\partial^2 w}{\partial x^2} + \nu \left(\frac{\partial^2 \overline{w}}{\partial x \partial y} \frac{\partial w}{\partial y} + \frac{\partial \overline{w}}{\partial y} \frac{\partial^2 w}{\partial x \partial y} \right) \right\}$$

$$- \frac{1}{2(1+\nu)} \left(\frac{\partial^2 \overline{w}}{\partial x \partial y} \frac{\partial w}{\partial y} + \frac{\partial^2 w}{\partial y^2} \frac{\partial \overline{w}}{\partial x} + \frac{\partial^2 \overline{w}}{\partial y^2} \frac{\partial w}{\partial x} + \frac{\partial \overline{w}}{\partial x} \frac{\partial^2 w}{\partial x \partial y} \right) \quad (3a)$$

$$\frac{1}{(1-\nu^2)} \frac{\partial^2 v}{\partial x^2} + \frac{1}{2(1-\nu)} \frac{\partial^2 u}{\partial x \partial y} + \frac{1}{2(1+\nu)} \frac{\partial^2 v}{\partial x^2} = \frac{1}{1-\nu^2} \left\{ \frac{\partial^2 \overline{w}}{\partial y^2} \frac{\partial w}{\partial y} + \frac{\partial \overline{w}}{\partial y} \frac{\partial^2 w}{\partial y^2} + \nu \left(\frac{\partial^2 \overline{w}}{\partial x \partial y} \frac{\partial w}{\partial x} + \frac{\partial \overline{w}}{\partial x} \frac{\partial^2 w}{\partial x \partial y} \right) \right\}$$

$$- \frac{1}{2(1+\nu)} \left(\frac{\partial^2 w}{\partial x \partial y} \frac{\partial \overline{w}}{\partial x} + \frac{\partial^2 \overline{w}}{\partial x^2} \frac{\partial w}{\partial y} + \frac{\partial^2 w}{\partial x^2} \frac{\partial \overline{w}}{\partial y} + \frac{\partial w}{\partial x} \frac{\partial^2 \overline{w}}{\partial x \partial y} \right) \quad (3b)$$

where $\nabla^4 = \left(\frac{\partial}{\partial x^2} + \frac{\partial}{\partial y^2} \right)^2$

The mathematical problem then resolves itself to solving three non-linear partial differential equations (2a), (3a) and (3b). The corresponding equations for the dynamic problem are obtained by adding inertia terms to the above equations. Boundary conditions and initial conditions must also be specified for a proper solution.

2.2 Approximate Displacement Funcation and Initial Imperfections

Rather than attempt to solve this set of equations directly, a technique was used whereby approximate functions for w and $\overline{w}$

were substituted into the inplane equilibrium equations (3a) and (3b).

The inplane displacement u and v are then found from these equations. The approximate radial deflection function w was chosen to have the following form, which includes both axisymmetric and asymmetric modes.

$$w = h\left[\xi_1(t)\cos\frac{i\pi x}{L} + \xi_2(t)\sin\left(\frac{k\pi x}{L}\right)\sin\left(\frac{\ell y}{R}\right) + \xi_3(t)\right] \tag{4}$$

where ξ_1, ξ_2, and ξ_3 can be functions of time (t) for the dynamic problem, and i and k are integers for the half wave numbers in the axial direction, which will be called axial wave numbers in the present report. ℓ is the number of full waves in the circumferential direction.

This form, which is a cosine-sine representation in the axisymmetric and asymmetric modes, respectively, was found to be the simplest and the best approximation among the combinations of trigonometric functions attempted. (Ref. Appendix A.) The initial imperfections of the shell were chosen to be

$$\bar{w} = h\left[\bar{\xi}_1\cos\left(\frac{i\pi x}{L}\right) + \bar{\xi}_2\sin\left(\frac{k\pi x}{L}\right)\sin\left(\frac{\ell y}{R}\right)\right] \tag{5}$$

2.3 Solutions of Inplane Equilibrium Equations

The substitution of the expressions for w and $\bar{w}$ into the right-hand side of equations (3a) and (3b) results in the following.

$$\frac{1}{(1-\nu^2)}\frac{\partial^2 u}{\partial x^2} + \frac{1}{2(1-\nu)}\frac{\partial^2 v}{\partial x\partial y} + \frac{1}{2(1+\nu)}\frac{\partial^2 u}{\partial y^2} = p_1\sin\hat{a}_i x + p_2\sin 2\hat{a}_i x + p_3\sin 2\hat{a}_k x$$
$$+ p_4\cos\hat{a}_k x\sin\hat{\beta}y + p_5\cos\hat{a}_{i+k}x\sin\hat{\beta}y + p_6\cos\hat{a}_{i-k}x\sin\hat{\beta}y$$
$$+ p_7\sin 2\hat{a}_k x \tag{6b}$$

$$\frac{1}{1-\nu^2}\frac{\partial^2 v}{\partial y^2} + \frac{1}{2(1-\nu)}\frac{\partial^2 u}{\partial x \partial y} + \frac{1}{2(1+\nu)}\frac{\partial^2 v}{\partial x^2}$$

$$= q_1 \sin\hat{\alpha}_{i-k}x \cos\hat{\beta}y + q_2 \sin\hat{\alpha}_{i+k}x \cos\hat{\beta}y + q_3 \sin\hat{\alpha}_k x \cos\hat{\beta}y$$

$$+ \hat{q}_4 \sin 2\hat{\beta}y + q_5 \cos 2\hat{\alpha}_k x \sin 2\hat{\beta}y \qquad (6b)$$

The particular solutions, u_p and v_p are found to be

$$u_p = b_1 \sin\hat{\alpha}_i x + b_2 \sin 2\hat{\alpha}_i x + b_3 \sin 2\hat{\alpha}_k x + b_4 \cos\hat{\alpha}_k x \sin\hat{\beta}y$$

$$+ b_5 \cos\hat{\alpha}_{i+k}x \sin\hat{\beta}y + b_6 \cos\hat{\alpha}_{i-k}x \sin\hat{\beta}y + b_7 \sin 2\hat{\alpha}_k x \cos 2\hat{\beta}y \quad (7)$$

$$v_p = e_1 \sin\hat{\alpha}_{i-k}x \cos\hat{\beta}y + e_2 \sin\hat{\alpha}_{i+k}x \cos\hat{\beta}y + e_3 \sin\hat{\alpha}_k x \cos\hat{\beta}y$$

$$+ e_4 \sin 2\hat{\beta}y + e_5 \cos 2\hat{\alpha}_k x \sin 2\hat{\beta}y \qquad (8)$$

Coefficients b_i and e_i are listed in Appendix B-1. Now consider the solution form such as to satisfy the boundary conditions of the shell. The homogeneous solutions of the inplane equilibrium equations (6a), (6b) are then found. An example of this type of solution is given in Appendix A. The appropriate homogeneous solution consists of a boundary layer type solution plus a simple function of x.

$$u_h = Ax + B + u_{BL}$$

$$v_h = v_{BL}$$

where A and B are constant or functions of time and u_{BL} and v_{BL} are boundary type solutions. The complete solutions for u and v are

then given as

$$u = u_p + Ax + B + u_{BL}$$

$$v = v_p + v_{BL}$$

The boundary conditions to be satisfied at $x = 0, L$ are as follows,

$$u = 0, \quad v = 0 \quad \text{at} \quad x = 0$$

$$u = \xi_o(t), \quad v = 0 \quad \text{at} \quad x = L$$

The substitution of the above condition gives at $x = 0$

$$u = (b_4+b_5+b_6)\sin\hat{\beta}y + B + u_{BL}(0, y) = 0$$

$$v = (e_4+e_5)\sin 2\hat{\beta}y + v_{BL}(0, y) = 0$$

As shown in Appendix A, the boundary-type solutions can be chosen to cancel the first terms and B then becomes zero.

at $x = L$

$$u = (-1)^k(b_4+b_5+b_6)\sin\hat{\beta}y + AL + u_{BL}(L, y) = \xi_o(t)$$

$$v = (e_4+e_5)\sin 2\hat{\beta}y + v_{BL}(L, y) = 0$$

Again the boundary-type solutions can be chosen to cancel the first terms, therefore

$$A = \frac{\xi_o(t)}{L}$$

It should be noted that a new time-dependent variable $\xi_o(t)$, which

represents a motion in an axial direction, has been introduced. This is a crucial assumption in the present analysis. Finally, the approximate displacement field of the system is summarized as follows,

$$\frac{w(x,y,t)}{h} = \left[\xi_1(t)\cos\left(\frac{i\pi x}{L}\right) + \xi_2(t)\sin\left(\frac{k\pi x}{L}\right)\sin\left(\frac{\ell y}{R}\right)+\xi_3(t)\right] \quad (4)$$

$$u(x,y,t) = up(x,y,t) - \frac{\xi_o(t)}{L}x \quad (10)$$

$$v(x,y,t) = vp(x,y,t) \quad (11)$$

The boundary layer type solutions in u and v have been dropped. Now we are ready to evaluate the equations resulting from the above assumption.

2.4 System Equations by the Energy Method

Using the displacement functions, (4), (10) and (11), found in the previous section, a set of differential equations for the four variables, ξ_o, ξ_1, ξ_2 and ξ_3 can be found by the application of Hamilton's principle. In order to perform this calculation the potential and kinetic energies of the shell must be evaluated. The expressions used for this calculation are consistent with the assumptions made in the Donnell equations. The elastic strain energy corresponding to the membrane stresses is

$$V_1 = \frac{h}{2E}\int_o^L\int_o^{2\pi R}\left[(\sigma_x+\sigma_y)^2-2(1+\nu)(\sigma_x\sigma_y-\tau_{xy}^2)\right]dxdy \quad (12)$$

The elastic bending strain energy of the shell is given as

$$V_2 = \frac{D}{2}\int_o^L\int_o^{2\pi R}\left[\left(\frac{\partial^2 w}{\partial x^2}+\frac{\partial^2 w}{\partial y^2}\right)^2-2(1-\nu)\left(\frac{\partial^2 w}{\partial x^2}\frac{\partial^2 w}{\partial y^2}-\left(\frac{\partial^2 w}{\partial x\partial y}\right)^2\right)\right]dxdy \quad (13)$$

The potential of the applied axial load, p(t), can be expressed as

$$V_3 = h \int_0^{2\pi R} p(t)\, u(L, y)dy$$

Finally, the expression for the kinetic energy of the system can be written as

$$T = \frac{1}{2} \rho h \int_0^L \int_0^{2\pi R} \left[\left(\frac{\partial w}{\partial t}\right)^2 + \left(\frac{\partial u}{\partial t}\right)^2 + \left(\frac{\partial v}{\partial t}\right)^2\right] dxdy + \frac{1}{2} m \left(\frac{\partial u}{\partial t}\right)^2_{x=L} \quad (15)$$

where ρ is the mass density of the shell, and m is the mass at the loaded end of the shell. The only axial inertia term taken into account results from the variable $\xi_o(t)$, while the circumferential inertia terms will be completely neglected. This assumption is shown to be valid over the range of wave numbers i, k, and ℓ of importance in the present analysis (ref. 17).

If the expressions for σ_x, σ_y, τ_{xy}, w and $\overline{w}$ are substituted into equations (12) to (15) and the integration performed, then

$$V_1 = \frac{\pi E h^3 L}{R} \left\{ \hat{C}_1 (\xi_2^2 + 2\overline{\xi}_2 \xi_2)^2 + \hat{C}_2 (\xi_1 \xi_2 + \overline{\xi}_1 \xi_2 + \overline{\xi}_2 \xi_1)^2 \right.$$

$$\left. + \hat{C}_3 \left[\xi_2^2 + \frac{1}{2} \xi_1^2 + [\overline{g}_x(\xi)]^2 + [\overline{g}_y(\xi)]^2 + 2\nu \overline{g}_x(\xi) g_y(\xi) \right] \right\}$$

$$+ \frac{\pi E h^3 L}{R} \left\{ \hat{Q}_1 \xi_1 (\xi_2^2 + 2\overline{\xi}_2 \xi_2) + \hat{Q}_2 \xi_2 (\xi_1 \xi_2 + \overline{\xi}_1 \xi_2 + \overline{\xi}_2 \xi_1) \right\} \quad (16)$$

$$V_2 = \frac{\pi E h^3 L}{R} \left\{ \hat{C}_4 \xi_1^2 + \hat{C}_5 \xi_2^2 \right\} \quad (17)$$

where $\hat{Q}_1$ and $\hat{Q}_2$ appear only under the restriction i = 2k,

$$\bar{g}_x(\xi) = \frac{1}{1-\nu^2}\left[\frac{R}{L}\xi_o + \nu\xi_3 - \hat{C}_6(\xi_2^2+2\xi_2\bar{\xi}_2) - \hat{C}_7(\xi_1^2+2\bar{\xi}_1\xi_1)\right] \quad (18)$$

$$\bar{g}_y(\xi) = \frac{1}{1-\nu^2}\left[-\xi_3 - \frac{\nu R}{L}\xi_o + \hat{C}_8(\xi_2^2+2\bar{\xi}_2\xi_2) + \hat{C}_9(\xi_1^2+2\bar{\xi}_1\xi_1)\right] \quad (19)$$

Coefficients $\hat{C}_i$ and $\hat{Q}_i$ are listed in Appendix B-2. The potential energy of the applied axial load is given as

$$V_3 = -2\pi h^2 E\,\hat{p}(t)\xi_o(t)$$

$$\text{where} \quad \hat{p}(t) = \frac{p(t)R}{Eh}$$

Finally, the kinetic energy of the system can be easily evaluated.

$$T = \pi\rho h^3 RL\left[\frac{1}{2}\left(\frac{d\xi_1}{dt}\right)^2 + \frac{1}{4}\left(\frac{d\xi_2}{dt}\right)^2 + \left(\frac{d\xi_3}{dt}\right)^2 + \left(\frac{1}{3}+\bar{m}\right)\left(\frac{d\xi_o}{dt}\right)^2\right] \quad (21)$$

$$\text{where} \quad \bar{m} = \frac{m}{2\pi\rho hRL}$$

Now applying Hamilton's principle

$$\delta\int_{t_1}^{t_2}\left[T-(V_1+V_2+V_3)\right]\,d\tau = 0 \quad (22)$$

and carrying out the variation with respect to the four dependent variables ξ_1, ξ_2, ξ_3, and ξ_o, we obtain the following set of simultaneous nonlinear differential equations,

$$\left(\frac{1}{2a_i^2}\right)\ddot{\xi}_1 + \left[\lambda_{c_i} - c\bar{g}_x(\xi)\right]\xi_1 + C_3(\xi_1\xi_2+\bar{\xi}_1\xi_2+\bar{\xi}_2\xi_1)(\xi_2+\bar{\xi}_2)$$

$$+ Q_1(\xi_2^2 + 2\bar{\xi}_2\xi_2) + Q_2(\xi_2^2 + \bar{\xi}_2\xi_2) = c\bar{\xi}_1\bar{g}_x(\xi) \quad (23a)$$

$$\left(\frac{1}{2a_k^2}\right)\ddot{\xi}_2 + [\lambda_{c_k} - c\bar{g}_x(\xi)]\xi_2 + C_1(\xi_2^2 + 2\bar{\xi}_2\xi_2)(\xi_2 + \bar{\xi}_2)$$

$$+ C_2(\xi_1\xi_2 + \bar{\xi}_2\xi_1 + \bar{\xi}_1\xi_2)(\xi_1 + \bar{\xi}_1) + C_4 c(\xi_2 + \bar{\xi}_2)\bar{g}_y(\xi)$$

$$+ Q_3\xi_1(\xi_2 + \bar{\xi}_2) + Q_4(2\xi_1\xi_2 + \xi_1\bar{\xi}_2 + 2\bar{\xi}_1\xi_2) = c\bar{\xi}_2\,\bar{g}_x(\xi) \qquad (23b)$$

$$\ddot{\xi}_3 + \frac{1}{1-\nu^2}\left[\xi_3 + \frac{\nu R}{L}\xi_o - \hat{C}_8(\xi_2^2 + 2\bar{\xi}_2\xi_2) - \hat{C}_9(\xi_1^2 + 2\bar{\xi}_1\xi_1)\right] = 0 \qquad (23c)$$

(i.e., $\ddot{\xi}_3 + \bar{g}_y(\xi) = 0$)

$$\left(\frac{1}{3} + \bar{m}\right)\ddot{\xi}_o + \frac{R}{L(1-\nu^2)}\left[\frac{R}{L}\xi_o + \nu\xi_o - \hat{C}_6(\xi_2^2 + 2\bar{\xi}_2\xi_2) - \hat{C}_7(\xi_1^2 + 2\bar{\xi}_1\xi_1)\right]$$

$$= \left(\frac{R}{L}\right)\hat{p}(t) \qquad (23d)$$

(i.e., $\left(\frac{1}{3} + \bar{m}\right)\ddot{\xi}_o + \frac{R}{L}\bar{g}_x(\xi) = \frac{R}{L}\hat{p}(t)$)

where the nondimensional time is defined as

$$\tau = \frac{t}{R}\sqrt{\frac{E}{\rho}}$$

and $\dot{\xi} = \frac{\partial\xi}{\partial\tau}$

λ_{c_i}, λ_{c_k}, C_i, Q_i are listed in Appendix B-3.

III. STATIC ANALYSIS

Before attempting to analyze the dynamic behavior of the shell using the four degrees of freedom model, the static buckling load and post-buckling behavior of the model should be investigated. This step is necessary to insure the existence of post-buckling equilibrium positions. As mentioned in the Introduction there must be more than one stable equilibrium position under a given load, if dynamic buckling, as defined in this paper, is to occur.

3.1 Formulation

The static buckling behavior of the model can be obtained from the set of dynamic differential equations (23a-23d) in the following manner. Dropping the inertia terms and setting the end load equal to a constant, allows one to solve directly for $\bar{g}_x(\xi)$ and $\bar{g}_y(\xi)$. Then substitution of $\bar{g}_x$ and $\bar{g}_y$ into equations (23a) and (23b) gives the two nonlinear algebraic equations, which are

$$(\lambda_{c_i}-\lambda)\xi_1 + C_3[(\xi_2+\bar{\xi}_2)\xi_1+\bar{\xi}_1\xi_2](\bar{\xi}_2+\xi_2) + Q_1(\xi_2^2+2\bar{\xi}_2\xi_2)$$

$$+Q_2(\xi_2^2+\bar{\xi}_2\xi_2) = \bar{\xi}_1\lambda \tag{24}$$

$$(\lambda_{c_k}-\lambda)\xi_2 + C_1(\xi_2^2+2\bar{\xi}_2\xi_2)(\bar{\xi}_2+\xi_2)+C_2[(\bar{\xi}_2+\xi_2)\xi_1+\bar{\xi}_1\xi_2](\bar{\xi}_1+\xi_1)$$

$$+Q_3\xi_1(\xi_2+\bar{\xi}_2) + Q_4(2\xi_1\xi_2+\xi_1\bar{\xi}_2+2\bar{\xi}_1\xi_2) = \lambda\bar{\xi}_2 \tag{25}$$

where $\lambda = \dfrac{p\sqrt{3(1-\nu^2)}}{E}\dfrac{R}{h} = \sigma/\sigma_{c\ell}$

and C_i, Q_i is given in Appendix B-3. It should be mentioned here

that the solution for $\bar{g}_y(\xi)$ (i. e., $\bar{g}_y(\xi) = 0$) is the same as the periodicity condition usually enforced (ref. 1). Also the set of nonlinear algebraie equations (24) and (25), which are obtained from minimizing the potential energy are exactly the same equation obtained by Galerkin's method (ref. 3). A solution of these nonlinear equations yields the equilibrium configuration of the finite length shell as a function of λ. If λ, the axial compression loads, attain a local maximum, then this is the value of the static buckling load called λ_s.

A typical path of λ is a function of the variable ξ_1, and ξ_2 is schematically shown in Fig. 2. The response is dependent upon the size and sign of the initial imperfection $\bar{\xi}_1$ in the axisymmetric mode. However, the asymmetric response is the same for a plus or minus sign of $\bar{\xi}_2$, which can be seen from the algebraic equations (24) and (25). If $\bar{\xi}_1$ is positive, then the shell has a higher buckling load than classical buckling load and if $\bar{\xi}_1$ is negative, a lower buckling load is obtained. This result is due to the coupling between the asymmetric mode and the axisymmetric mode of response.

3.2 Numerical Procedure

In order to determine the static buckling load and post-buckling behavior, the two nonlinear algebraic equations (24) and (25) must be solved numerically for the given wave numbers and the imperfections. The following procedure was employed. ξ_1 is eliminated from the two equations to obtain the following third order polynomial in λ

$$\lambda^3 + p_1(\xi_2)\lambda^2 + p_2(\xi_2)\lambda + p_3(\xi_2) = 0 \qquad (29)$$

The load-deflection curve, i.e., the relation between ξ_2 and λ is obtained by finding the minimum real root of equation (29) for a given ξ_2.

Differentiating with respect to ξ_2 yields,

$$\frac{d\lambda}{d\xi_2} = - \frac{p_1'(\xi_2)\lambda^2 + p_2'(\xi_2) + p_3'(\xi_2)}{3\lambda^2 + 2\lambda p_1(\xi_2) + p_2(\xi_2)} = 0 \qquad (30)$$

To find only the static buckling load, equation (30) must be also satisfied. The two equations (29) and (30) are solved numerically by a modified Newton's method.

3.3 Results and Discussion

The algebraic equations (24) and (25) contain several parameters which must be chosen in the numerical study. These are the three wave numbers i, k and ℓ and the initial imperfections, $\bar{\xi}_1$ and $\bar{\xi}_2$. The wave parameters are not independent and can be chosen in the following manner. Without the condition of $i = 2k$, all the quadratic terms in equations (24) and (25) would vanish identically and the resulting equation would describe a system which can be shown to be insensitive to initial imperfections. In other words, this system is not expected to have a dynamic buckling load as defined in this report. In addition to this condition, the asymmetric wave parameter must be selected to minimize the asymmetric buckling load (ref. 3). This requirement is the same as saying that the asymmetric buckling mode lies on the Koiter circle (ref. 18). The condition is written as $a_k^2 - a_k + \beta^2 = 0$.

Next the amplitudes of the initial imperfection must be selected for the numerical study. The following formula is employed, based on the results by Arbocz and Babcock (ref. 16),

$$\bar{\xi}_1 = -\frac{0.256}{i^{1.18}} \tag{27a}$$

$$\bar{\xi}_2 = \frac{3.26}{k^{1.01}\,\ell^{1.33}} \tag{27b}$$

This imperfection distribution uses the decrease in imperfection amplitude with i, k and ℓ as determined from experimental results. However, the amplitude has been doubled from the results as measured on high quality electroformed shells. This was necessary to produce significant reduction of the imperfect shell buckling load, λ_s.

The load-deflection behavior of an imperfect shell for different wave numbers k is shown in Fig. 3. From this figure, the static buckling load is determined as the local maximum point. In addition, the existence of multiple equilibrium positions at a given load is seen. Therefore, this indicates that the radial-displacement assumption employed at the beginning of analysis is physically appropriate and one can use the present model for a dynamic buckling problem under step loading.

Fig. 4 and Table 1 summarize the static buckling load as a function of the axial wave number, k. Fig. 4 indicates that there are two possible wave numbers which produce a minimum static buckling load. One of them is at the lowest wave number, i.e., $k = 1$, $i = 2$, $\ell = 9$, and the other is at a rather higher number near

$a_k = \beta = 0.5$ and $a_i = 1$. This occurs since the shell is very sensitive to imperfections in the high wave number mode. On the other hand, the shell is not particularly sensitive to the imperfection, k = 1, but it has the largest amplitude.

IV. DYNAMIC INSTABILITY

Now that the four degrees of freedom model has been shown to exhibit the proper static behavior, the dynamic equations will be solved. First the numerical method used will be discussed and then the results presented.

4.1 Numerical Method

The set of four simultaneous nonlinear ordinary differential equations (23a) to (23d) is integrated numerically for given initial conditions and initial imperfections under a specified step load. For these calculations the initial conditions (i.e., velocity and displacement) are set equal to zero.

The differential equations can be written in vector form,

$$\ddot{\underset{\sim}{\xi}} = \underset{\sim}{f}(\underset{\sim}{\xi})$$

Letting $x = \dot{\xi}$ the above equation can be written in a scalar form,

$$\begin{aligned}
\dot{x}_1 &= f_1(\xi_o, \xi_1, \xi_2, \xi_3) \\
\dot{x}_2 &= f_2(\xi_o, \xi_1, \xi_2, \xi_3) \\
\dot{x}_3 &= f_3(\xi_o, \xi_1, \xi_2, \xi_3) \\
\dot{x}_4 &= f_4(\xi_o, \xi_1, \xi_2, \xi_3) \\
\dot{\xi}_o &= x_1 \\
\dot{\xi}_1 &= x_2 \\
\dot{\xi}_2 &= x_3 \\
\dot{\xi}_3 &= x_4
\end{aligned} \tag{28}$$

Using a Runge-Kutta numerical-integration scheme for the starting solutions, the integration was switched to a 6th order predictor-

corrector method. The interval of integration was controlled to obtain the desired accuracy of each integrated point. The interval was selected as large as possible within the above restriction in order to save computing time.

The Runge-Kutta method employed in the present analysis can be written symbolically for any variable y_j as (ref. 19),

$$y_{j,i+1} = y_{ji} + \Delta t \left(\frac{1}{6} k_{j1} + \frac{1}{3} k_{j2} + \frac{1}{3} k_{j3} + \frac{1}{6} k_{j4}\right)$$

where $k_{j1} = f_j (\Delta t, y_{1i}, y_{2i}, \ldots . y_{Ni})$

$$y^*_{ji} = y_{ji} + \frac{1}{2} \Delta t \, k_{j1}$$

$$k_{j2} = f_j \left(t_i + \frac{\Delta t}{2}, \; y^*_{1i}, \; y^*_{2i}, \; \ldots . \; y^*_{Ni}\right)$$

$$\bar{y}_{ji} = y_{ji} + \frac{1}{2} \Delta t \, k_{j2}$$

$$k_{j3} = f_j \left(t_i + \frac{\Delta t}{2}, \; \bar{y}_{1i}, \; \bar{y}_{2i} \ldots . \bar{y}_{Ni}\right)$$

$$\bar{y}^*_{ji} = y_{ji} + \frac{1}{2} \Delta t \, k_{j3}$$

$$k_{j4} = f_j \left(t_i + \frac{\Delta t}{2}, \; \bar{y}^*_{1i}, \; \bar{y}^*_{2i}, \ldots . \bar{y}^*_{Ni}\right)$$

where j is a subscript for the jth variable of the system.

i is a subscript of an integration point.

The predicted solution y_{i+1} is computed, by using the following 6th order Milne-method, (ref. 19).

$$y_{i+1} = y_{i-5} + \frac{3\Delta t}{10}\,(11f_i - 14f_{i-1} + 26f_{i-2} - 14f_{i-3} + 11f_{i-4})$$

Finally, the Milne-corrector equation is solved to obtain a more accurate solution, which is given as

$$y'_{i+1} = y_{i-3} + \frac{2\Delta t}{45}\,(7f_{i+1} + 32f_i + 12f_{i-1} + 32f_{i-2} + 7f_{i-3})$$

If the difference between the predicted value y_{i+1} and corrected value y'_{i+1} is within the desired tolerance, then the integration proceeds to the next step. Otherwise, the interval of integration is changed by a factor of two. The details of computer programming are shown in the flow chart (Appendix C).

4.2 Results and Discussion

The set of differential equations (23a-d) were numerically integrated with a specified load, given initial imperfections and the selected modes of deformation. The behavior of the generalized coordinates ξ_o, ξ_1, ξ_2 and ξ_3 were then determined as a function of time.

Let us consider a typical numerical result. The response of the ξ_o mode (motion in the axial direction), ξ_1 (axisymmetric mode in the radial direction) and ξ_2 (asymmetric mode in the radial direction) are shown in Figs. 5-a, 5-b and 5-c, respectively. A distinguishable change in the amplitude of the ξ_o-mode and the ξ_1-mode can be seen. This change occurs with a small change in the loading parameter (i.e., 2.1% from $\lambda = 0.792$ to 0.809). As shown in Fig. 6, if the magnitudes of the maximum amplitude of ξ_2 taken over time are plotted against load, this discrete change is more precisely

recognized.

Figs. 7-a and 7-b provide an interesting result which shows the path of motion on the generalized coordinate ξ_1-ξ_2 plane. This is obtained by eliminating the parameter time from the previous response of the ξ_1 and ξ_2 modes. The detail of this path in the neighborhood of origin is shown in Fig. 7-b. It is quite clear that only the axisymmetric mode, ξ_1, is initially oscillating. This oscillation occurs for several cycles before a significant asymmetric response, ξ_2, builds up. After the build-up of ξ_2, the trajectory of the system is direct to the post-buckling equilibrium position. The system then oscillates about this position. This behavior is typical of the many example cases which were run. From this result it seems reasonable to establish the stability criteria by the response of the ξ_2-mode rather than any other measure of response.

The value of the dynamic buckling load will depend on the following parameters:

(i) Modes of radial deformation (i, k and ℓ)

(ii) "Mass" at the loaded end of shell ($\overline{m}$)

(iii) Damping of the motion (ζ)

(iv) Initial imperfections ($\overline{\xi}_1$ and $\overline{\xi}_2$)

(v) Geometric parameters and material constants of the shell

Item (iv) were previously mentioned in the section of the static buckling problems. The same formula (equations (27a) and (27b)) giving the imperfection distribution was used for the present dynamic analysis. Concerning item (v), it can be seen from the dynamic

equations (23a-d) that only the nondimensional shell parameters (R/h) and (L/R) and Poisson's ratio (ν) must be taken into account. For the numerical results, R/h is set equal to 1000 and L/R equal to 2 with ν equal to 0.30. In this section the effects of wave number and the effect of "mass" on dynamic instability are covered, in addition to the consideration of the damping effect on the axial motion.

4.2.1 Selection of Deflection Modes

The wave numbers of the axisymmetric mode and the asymmetric mode are represented by (i) and (k, ℓ), respectively, where i and k are the number of half waves in the axial direction and ℓ is the number of full waves in the circumferential direction. As mentioned before in the static analysis, however, only k can be chosen as an arbitrary integer among i, k and ℓ, if ℓ is determined from the condition that the asymmetric modes lie on the Koiter's circle and the restriction, i = 2k. The investigation of the static buckling problem (Fig. 4 summarizes the effect of wave number k on the static buckling load) indicated that there were two local minimum buckling loads. One of these is at k = 1 and ℓ = 9 (the lowest wave number) and the other is near k = 17 and ℓ = 29 which gives $\alpha_k \approx \beta \approx 0.5$.

Fig. 8 shows the results of the dynamic buckling load for the various wave numbers k. The static buckling load denoted by the upper dotted line is traced from Fig. 4. The lower dotted line indicates the minimum post-buckling equilibrium position for that particular value of k; that is, the local minimum load, λ_{min}, in the load-deflection curve. The dynamic buckling loads as depicted in Fig. 8 were determined by numerical integration of the equations of

motion. The maximum response of the shell must be determined for all time under a specified load level in order to find the critical load. Of course, the integration time must be truncated at some finite value. For most of the integration the maximum value of non-dimensional time, τ, was taken to be 150. A few cases were run to determine if this upper limit was adequate. Except for the low wave numbers, the upper limit of 150 was found to be satisfactory ($\tau = 150$ is equivalent to approximately 3.1 msec for an 8 inch diameter aluminum shell).

It is quite clear that there is a significant decrease of the dynamic buckling load in the neighborhood of k = 15, compared with the static case. On the other hand, in the range of lower wave numbers ($k \leq 4$), the numerical results showed even higher values than the static buckling loads. This has also been observed for the nonlinear analysis of a shallow arch (ref. 20). In order to understand the dynamic buckling behavior at low values of k, one must examine the frequencies of the system. This is of course most easily done from the linearized equations. These frequencies are shown in Fig. 9, as a function of wave number k. As can be observed, the frequency of the asymmetric mode, ω_k, is much less than that of the driven mode, ω_o, at small values of k. In addition, the frequency of the uniform expansion mode can be calculated as

$$\frac{\omega_3}{\omega_o} = \frac{1}{\sqrt{3}} \frac{L}{R} = 1.15 \quad \text{for} \quad \frac{L}{R} = 2.0$$

Since these two modes, ξ_o and ξ_3 are directly excited by the step

loading and they have much higher frequencies than the major response mode, ξ_2, it is reasonable to neglect the inertia of these two modes for the values of k. This neglect is based upon the assumption that the damping in the system would suppress the dynamic response of these modes before the asymmetric response in the ξ_2 mode occured. For the two mode case the shell response from the numerical integration ($\tau_{max} = 1000$) for the case k = 1 is shown in Fig. 10. The buckling load is seen to lie between λ equal to 0.82 and 0.86.

Secondly, it should be pointed out for the case k = 8 and k = 10 in Fig. 8 that a definite dynamic buckling load is established. However, the system did not buckle for the time of numerical integration ($\tau = 200$) if the load is increased approximately 3 percent larger than the critical load. A typical response of the case k = 8 is shown in Figs. 11-a, 11-b and 11-c. An applied load $\lambda = 0.892$ obviously gives the buckling behavior, while the amplitude of the response for $\lambda = 0.92$ is much smaller than the case $\lambda = 0.892$. The reason for this behavior is that the integration time is probably not sufficiently long for the system to reach the saddle point* on the potential energy surface. In addition there exists a complex coupling of frequencies between the ξ_1 and ξ_o mode. The nature of this coupling is affected by the load level, λ.

Thirdly, the buckling load at extremely high wave numbers,

---

* There are generally three kinds of equilibrium positions, a stable center, an unstable center and a saddle point for the two degrees of freedom system for a given applied load. Of all the paths connecting two stable equilibrium positions, the path which has the least increase of potential energy goes through the saddle point.

say k = 20 to 24, should be discussed. The dynamic buckling loads in Fig. 8 for these wave numbers are less than the value of the minimum post-buckled equilibrium position. Since there is only the unbuckled equilibrium position for the value of λ less than λ_{min}, one would not expect a dynamic buckling characterized by a jump of response with increasing λ, for the load less than λ_{min} (ref. 23). However, these buckling loads were defined from the response calculated by numerical integration and some judgement must be used in picking out the dynamic buckling load. Figs. 12-a, 12-b and 12-c show the response of ξ_2, ξ_1 and ξ_o mode for the case of k equal to 23 at different applied loads. A distinguishable jump of the response with a small change in load parameter λ is not quite clear, but one cannot but admit that the buckling has occurred at $\lambda = 0.728$, in spite of the fact that λ is less than $\lambda_{min} = 0.75$. The explanation of this phenomenon will be given by some observation of the present system equations in the following discussion. Also, for such high wave numbers of the radial modes, the potential energy surface of the system may consist of a shallow surface. This makes it difficult to define the dynamic buckling load.

Finally, the concluding remark concerning Fig. 8 is that, compared with the static case, there is a significant reduction of the dynamic buckling load in the range of high wave number k. The dominant reason for these numerical results will be given by the following consideration of the present system of equations.

To study further the effects of wave number k, let us consider the linearized frequencies which are functions of the wave

numbers. First, by simplifying the set of nonlinear differential equations (23), the following set of simplified equations is obtained.

$$\frac{1}{\omega_i^2}\ddot{\xi}_1 + \left(1 - \frac{\xi_o^*}{\lambda_{c_i}}\right)\xi_1 = \frac{\xi_o^*}{\lambda_{c_i}}\xi_1 \tag{31a}$$

$$\frac{1}{\omega_k^2}\ddot{\xi}_2 + \left(1 - \frac{\xi_o^*}{\lambda_{c_k}}\right)\xi_2 = \frac{\xi_o^*}{\lambda_{c_k}}\xi_2 \tag{31b}$$

$$\frac{1}{\omega_o^2}\ddot{\xi}_o^* + \xi_o^* = \lambda H(t) \tag{31c}$$

where all the cubic and quadratic terms except $\xi_o\xi_1$ and $\xi_o\xi_2$ terms have been dropped and Poisson's ratio was set to zero. The frequencies of each mode are

$$\omega_k = \sqrt{2a_k^2 \lambda_{c_k}} \tag{32a}$$

$$\omega_i = \sqrt{2a_i^2 \lambda_{c_i}} \tag{32b}$$

$$\omega_o = \sqrt{\left(\frac{R}{L}\right)^2 \frac{1}{m+\frac{1}{3}}} = \frac{R}{L}\sqrt{3} \tag{32c}$$

where $\xi_o^* = \frac{cR}{L}\xi_o$

The assumption of zero Poisson's ratio yields the uniform radial motion equal to zero ($\xi_3 \equiv 0$). It should be noticed that the frequency of axial mode, ω_o, is approximately the same value as the axial frequency of a cylindrical shell with one end fixed. Now substitution of a solution of equation (31c) into equation (31a) and (31b) yields the following Mathieu-type equations

$$\frac{d^2\xi_1}{d\bar{\tau}^2} + \left[\left(1 - \frac{\lambda}{\lambda_{c_i}}\right)\left(\frac{\omega_i}{\omega_o}\right)^2 + \frac{\lambda}{\lambda_{c_i}}\left(\frac{\omega_i}{\omega_o}\right)^2 \cos\bar{\tau}\right]\xi_1 = \frac{\lambda(1-\cos\bar{\tau})\bar{\xi}_1}{\lambda_{c_i}} \tag{33}$$

$$\frac{d^2\xi_2}{d\bar{\tau}^2} + \left[\left(1 - \frac{\lambda}{\lambda_{c_k}}\right)\left(\frac{\omega_k}{\omega_o}\right)^2 + \frac{\lambda}{\lambda_{c_k}}\left(\frac{\omega_k}{\omega_o}\right)^2 \cos\bar{\tau}\right]\xi_2 = \frac{\lambda(1-\cos\bar{\tau})\bar{\xi}_2}{\lambda_{c_R}} \tag{34}$$

where $\bar{\tau} = \omega_o \tau$. Each solution of equations (33) and (34) would lead to an instability of the Mathieu type for certain combinations of $\frac{\lambda}{\lambda_{c_k}}$ and $\frac{\omega_k}{\omega_o}$, or $\frac{\lambda}{\lambda_{c_i}}$ and $\frac{\omega_i}{\omega_o}$. Such combinations were given by D. A. Danielson (ref. 22). According to his analysis, $\frac{\omega_i}{\omega_o}$, $\frac{\omega_k}{\omega_o} = 0.5$, 1.0, 1.5, ... give an instability condition for any load parameter $\lambda > 0$. $\frac{\omega_i}{\omega_o}$ and $\frac{\omega_k}{\omega_o}$ are written in the following forms.

$$\left(\frac{\omega_k}{\omega_o}\right) = \frac{\pi}{\sqrt{c}}\sqrt{\frac{h}{R}}\, k\, \sqrt{\frac{1}{3} + \bar{m}} = 0.0773\, k \sqrt{\frac{1}{3} + \bar{m}}$$

$$\left(\frac{\omega_i}{\omega_o}\right) = 2\left(\frac{\omega_k}{\omega_o}\right)\sqrt{\lambda_{c_i}}$$

$$\left(\frac{\omega_k}{\omega_i}\right) = \frac{1}{2\sqrt{\lambda_{c_i}}}$$

where R/h = 1000

These frequency ratios are plotted as a function of k in Fig. 9. It is found from the upper two lines in Fig. 9 that if k is chosen to be close to 12, then the condition $\frac{\omega_k}{\omega_o} \approx 0.5$ will be satisfied and if k is 17, then the condition $\frac{\omega_i}{\omega_o} \approx 1.5$ will be obtained. Therefore in the range of $12 \leq k \leq 17$ the axisymmetric mode, ξ_1, as well as the

asymmetric mode, ξ_2, would have a Mathieu-type instability by coupling with the axial mode ξ_o.

For the next stage, let us consider the nonlinear coupling between the asymmetric mode and the axisymmetric mode. The nature of the interaction between ξ_1 and ξ_2 modes can be demonstrated by the approximate equations of motion. If the cubic terms $\xi_1\xi_2^2$, $\xi_1^2\xi_2$ and ξ_2^3 in equations (23a) and (23b) are neglected, these simplified equations are written as

$$\ddot{\xi}_2 + \omega_k^2\left(1 - \frac{\xi_o^*}{\lambda_{c_k}}\right)\xi_2 + q_2\xi_1\xi_2 = \frac{\omega_k^2}{\lambda_{c_k}}\xi_o^*\,\bar{\xi}_2 \tag{35}$$

$$\ddot{\xi}_1 + \omega_i^2\left(1 - \frac{\xi_o^*}{\lambda_{c_i}}\right)\xi_1 + q_2\xi_2^2 = \frac{\omega_i^2}{\lambda_{c_i}}\xi_o^*\,\bar{\xi}_1 \tag{36}$$

where $q_1 = \hat{Q}_1 + \hat{Q}_2$

$q_2 = 4(\hat{Q}_1 + \hat{Q}_2)$, $\hat{Q}_1$ and $\hat{Q}_2$ are listed in Appendix (B-2).

From these two equations (35) and (36) we see that the parametric excitation of the asymmetric mode ξ_2 arises through the term $q_2\xi_1$ in equation (35). The interaction of this mode with the symmetric mode arises through the term $q_1\xi_2^2$ in equation (36). Considering the effect of wave number k, the conditions of k = 16 gives not only large values of q_1 and q_2 but also $\frac{\omega_k}{\omega_i} \approx 0.5$. The fact that the frequency of the axisymmetric mode, ω_i, is twice that of the asymmetric mode, ω_k, leads to a favorable coupling between these two modes. This coupling, which results from the shell attempting to vibrate without stretching, has been previously pointed out (ref. 24).

Therefore, the analysis including the quadratic terms indicates that the system has a strong coupling between the axisymmetric mode and the asymmetric mode at k = 16. Consequently this interaction can be considered to lead to dynamic buckling loads much less than the static load in the high wave number range.

Now referring to the numerical results, the previous explanation will be demonstrated. For the case of k = 15, which shows a typical response in the high wave numbers, $12 \leq k \leq 20$, the buckled and unbuckled response of the ξ_1, ξ_2 and ξ_o modes are shown in Figs. (13a, b, c). The linearized frequency ratios for each mode are given as follows,

$$\frac{\omega_k}{\omega_o} = 1.67$$

$$\frac{\omega_i}{\omega_o} = 1.39$$

$$\frac{\omega_k}{\omega_i} = 1.48$$

The average frequency ratios (denoted by $\frac{\bar{\omega}_k}{\bar{\omega}_o}$ and $\frac{\bar{\omega}_i}{\bar{\omega}_o}$) are obtained from counting the cycles of the numerical unbuckled response as follows,

$$\frac{\bar{\omega}_k}{\bar{\omega}_o} \approx 0.50$$

$$\frac{\bar{\omega}_i}{\bar{\omega}_o} \approx 1.07$$

$$\frac{\bar{\omega}_k}{\bar{\omega}_i} \approx 0.46$$

There appears to be a Mathieu-type coupling phenomenon between the ξ_1 mode and the ξ_o mode. As depicted in Figs. 13-a and 13-b, the initial motion of the asymmetric mode is small. However the axisymmetric mode ξ_1 is initially oscillating with almost the same frequency as the ξ_o mode and the amplitude of the ξ_1 mode exponentially builds up. After five cycles, the influence of this motion can be observed in the asymmetric ξ_2 mode. This "parametrically induced buckling" process (i.e., the ξ_1 mode excited by the ξ_o mode causes the triggering mechanism for the large deformation of the ξ_2 mode) can be understood through Figs. 13-a, 13-b and 13-c.

On the other hand, in the low wave number range ($k \leqslant 10$), the axisymmetric mode, ξ_1, is comparatively not as strongly coupled with the ξ_o mode. Also, as the wave number k decreases, the magnitude of q_2 of the coupling from equation (35) becomes smaller. It will be considered that these two reasons essentially give the relatively high dynamic buckling load for the wave number k less than 10.

It is clearly understood through the study of the effect of the wave number that the presence of axial-mode ξ_o plays an essential role in determining the dynamic instability. If the axial inertia were neglected, the resulting dynamic buckling load would be higher than the present analysis, and would, in fact, be associated with the "direct-buckling" phenomena (which will be discussed in section (4.2.4)).

4.2.2 Effect of Mass on the Loading Edge of the Shell

In investigating the dynamic stability of a cylindrical shell

experimentally, a certain amount of structure is required on the loading edge in order to transfer the load from the loading device to the shell. This transfer device is generally a ring or a circular plate of some kind. Therefore, the effects of mass of the end fixture should be taken into account in the analysis. From this point of view, the present analysis including the motion in the longitudinal direction will be applied in a study of the effect of mass on the dynamic stability of a cylindrical shell.

Fig. 14 summarizes the numerical results concerning the effect of mass on the dynamic buckling load. The buckling loads for the two cases of the wave number k = 14 and 20 are plotted as a function of mass, $\overline{m}$, where $\overline{m}$ is a nondimensional mass (end mass divided by the shell' s own mass). Although the critical values at the negative mass are physically meaningless, these points were evaluated in order to obtain the more information at near $\overline{m} = 0.0$. If $\overline{m}$ is equal to $-\frac{1}{3}$, the inertia term in equation (23d) vanishes and the system is mathematically equivalent to the three degrees of system where the axial inertia is neglected. The buckling load resulting from the three mode system is found to be close to the static buckling load (see section 4.2.4). On the other hand, as the mass increases, the asymptotic value of critical load of the system subject to a step loading should be nearly half of the static buckling load. This is quite obvious from the fact that when the mass becomes large, the shell is subject to a load almost twice as large as the static load. The numerical results of $\overline{m}$ greater than 5.0 turns out to be approximately 55 percent of the static buckling load.

For the case k = 14 and $\overline{m}$ = 1.0, the resulting dynamic buckling load shows a higher value than the $\overline{m}$ = 0.0. This phenomenon can be explained due to the frequency coupling between the ξ_o mode and the ξ_2 mode, as shown in the previous section.

A typical response for the case of $\overline{m}$ = 5.0 and k = 20 is shown in Figs. 15-a, 15-b and 15-c. This particular choice of the wave number and mass yields $\omega_k \approx 0.77$ for the asymmetric mode, $\omega_i \approx 1.56$ for the axisymmetric mode and $\omega_o \approx 0.216$ for the axial mode. The average frequencies, $\overline{\omega}_k$ and $\overline{\omega}_o$, found from the response of Figs. 15-a and 15-b approximately agree with the above linearized frequencies. This is a quite different phenomenon, comparing with the case of $\overline{m}$ = 0.0, where the ξ_1 mode oscillates at the same frequency as the ξ_o mode (see, for example, Figs. 13-b and 13-c). The response of the radial motion is not at the frequency of the ξ_o mode, but can be understood as if this system were subject to the double magnitude of the quasi-static* loading. Consequently the dynamic buckling load will be close to half of the static buckling load, if the size of the mass satisfies the condition such that $\overline{m}$ is greater than about 4.0.

As shown, the mass directly affects only the fundamental frequency of the axial motion. However, the wave number of the radial motion which is induced by the axial motion, would be influenced. If the wave number were chosen differently, for instance,

---

*From a judgement of the rise time of the axial response, we call this type of loading quasi-static for convenience's sake.

such as to couple with the axial mode, then the resulting buckling load must be changed. The radial motion of the shell subject to the axial load with a low frequency can be expected to have a small value of the wave number k. In this sense, if a shell has a rather heavy mass, or if a load is statically applied, the shell would prefer to buckle with a small wave number.

4.2.3 Effect of Viscous Damping

From the experimental observation of a cylindrical shell subjected to a step loading, it is known that the damping of the axial motion is much more pronounced than that of the radial motion. It is considered reasonable to include the effect of damping on the axial motion only in the present analysis. The inclusion of viscous damping of the axial vibrations, ξ_o mode, was found to have an appreciable effect on the critical loads. This effect is particularly marked in those cases where the buckling loads were determined by a "parametrically induced" buckling phenomenon.

Typical examples of the response for the damping factor, $\zeta = 0.1$, were shown in Figs. 5a, b, c. Comparing these figures with the response of an undamped system, it is noted that the response with damping is much more reasonable. The large amplitudes of the ξ_1 mode and the ξ_2 mode develop during buckling. Then the system vibrates about the second equilibrium configuration, while the axial motion ξ_o decays to a constant value with increasing time.

The effect of the magnitude of the damping factor on the critical loads is studied for the case of the wave number, $k = 14$. It should be remembered that the minimum dynamic buckling load

was obtained at this wave number by "parametrically induced" buckling. Fig. 16 shows the dynamic buckling load for the various values of ζ, where ζ is the ratio of damping of the system to critical damping. The buckling load for $\zeta = 0.05$ is 48 percent above the value corresponding to the undamped system, and is close to the static critical value for $\zeta \geq 0.2$.

The response for the value of ζ equal to 0.2 is shown in Figs. 17-a, 17-b and 17-c. The resulting critical load is approximately equal to the static critical value. This can be explained as follows. In this case the ξ_1 and ξ_2 modes initially oscillate due to the motion of the ξ_o mode. However, at the time when the ξ_1 mode starts to play a triggering mechanism for the ξ_2 mode, the axial ξ_o mode has already decayed to the static value due to the damping. Additional computer results for larger values of τ_{max} showed that a buckling was achieved at a value of λ slightly lower than the static buckling load. Also this result demonstrated that the buckling was due to the coupling motion between the axisymmetric and asymmetric modes.

Another interesting feature of the effect of damping is that the quasi-static response can be obtained by considering the dynamic problem with very large damping in the axial motion. This is illustrated in Figs. 18-a and 18-b which show the response obtained by setting the damping factor equal to 2.0 and the applied load one percent higher than the static buckling load. The amplitudes of the ξ_1 and ξ_2 modes grow simultaneously without oscillation before the buckling occurs.

Through the study of damping in the axial motion, it can be more clearly understood that the dynamic response of the system is sensitive to the coupling between the radial and axial motion as well as the ξ_1 and ξ_2 modes. Damping is particularly important when the stability is governed by "parametrically induced" buckling. In those cases, a small amount of damping has a large influence on the stability. However, buckling loads for the lower wave numbers of the radial mode are not affected.

4.2.4 Comparison with the Analysis Excluding Axial Inertia

It has been shown in the previous sections on the effects of wave numbers, mass, and damping that the axial inertia plays an important role in determining the dynamic stability of a shell. It is interesting to compare the present results with the numerical results based upon the analysis which does not include the axial inertia but has the same radial displacement as the present analysis.

The governing differential equations for this case can be directly obtained from the system of equations (23a) through (23d) by the following procedure. Dropping the axial inertia term, $\ddot{\xi}_o$, in equation (23d), ξ_o can be eliminated from the set of equations. The resulting three differential equations of motion are listed in Appendix D. The response of the asymmetric and the axisymmetric modes for the wave number k = 15, is shown in Figs. 19-a and 19-b, respectively. From the relation between load and the maximum amplitude of the displacement, the critical load, λ, of this system is found to lie between 0.88 and 0.89. This is significantly higher than the critical load (λ = 0.54) resulting from the previous four degrees of

freedom system which includes the axial inertia term. These results are in good agreement with the results obtained by Budiansky and Hutchinson (ref. 25) who also neglected axial inertia. The equations used by Budiansky and Hutchinson are slightly different since they neglected the cubic terms and terms of the order $\xi\bar{\xi}$. Their justification for neglecting the axial inertia is that the ratio of time it takes an axial compressive wave to travel half of a buckle length to one quarter of the free vibration period has the small value

$$\delta = \frac{2}{\sqrt{c}} \sqrt{\frac{h}{R}}$$

for all of the radial modes. This means, for practical purposes, the stress in the shell remains steady at the value of the applied step function. This is only true for an infinite length shell. However, for finite length shells, reflections of the axial stress waves must be taken into account. In other words, a more appropriate measure for neglecting the axial inertia is that the ratio of the time the axial stress wave takes to travel the length of the shell to the period of radial vibration should be small compared to unity. This condition is not met in the present analysis.

Fig. 20 shows schematically the difference in shell motion if the system of equations includes the axial inertia or not. The motion in the axial direction of the loaded edge is shown by the solid line and the radial displacements at the same time are represented by the dotted lines in this figure. In Case (A) of Fig. 20, the axial motion ξ_o has two time-dependent contributions, namely (i) primary contribution due to the applied load which excites an axial vibration

and (ii) secondary contribution due to the end shortening accompanying radial motion. However in Case (B), due to the absence of the axial inertia, the first contribution is not oscillatory and the time-dependent axial motion is because of the end shortening only. From Fig. 20 it is apparent that while Case (A) with axial inertia included represents the response of the shell under step force, Case (B) without axial inertia represents the response more like that due to a step axial displacement. The resulting mathematical model does not properly represent the shell behavior subject to a step force, if there is likely to be interaction between the axial vibration mode and radial response mode.

V. SUMMARY AND CONCLUSIONS

The critical step loads required to produce buckling of a cylindrical shell were determined by an approximate method, taking into account the inertia in the axial direction. Also, the dynamic buckling mechanism of the system was investigated. The analysis makes several important assumptions regarding the nature of the boundary conditions, the response modes, and the circumferential inertia. The boundary conditions that were not satisfied in the present analysis were analytically shown to affect the shell only near the ends. The radial response modes studied consisted of a coupled axisymmetric mode and an asymmetric mode, in addition to a uniform expansion mode. The axial and circumferential displacements were found using the inplane equilibrium equations, taking into account the axial inertia in an approximate manner.

A study of the numerical results of the "mathematical model" with four degrees of freedom, for which the static buckling behavior is well defined, led to the following conclusions.

(i) The dynamic buckling criterion can be defined by a sharp jump in amplitude of the asymmetric mode with a small change in load parameter.

(ii) The present analysis leaves the wave numbers of the radial modes as arbitrary parameters. However the parametric study of the wave number, k, with the restriction that the asymmetric mode lies on the Koiter circle, shows that there is a significant reduction of the dynamic buckling load in the range of high wave numbers. A minimum critical load is found near $\alpha_k \approx \beta \approx 0.5$.

This can be explained by the Mathieu-type instability of the system. There is a strong frequency coupling between the radial modes and the axial mode. Also there is a nonlinear coupling arising from the quadratic terms of the radial modes. These two coupling phenomena play an essential role in reducing the dynamic buckling load in the range of high wave numbers.

(iii) The mass on the loaded edge of a shell is important in the dynamic buckling load. If the mass is several times greater than that of the shell, the resulting dynamic critical loads approach approximately half of the static buckling load.

(iv) According to a study of the effect of damping in the axial motion, it is found that its effect is particularly marked in the case where critical loads are controlled by the "parametrically induced buckling." The damping suppresses the parametric resonance between the radial and axial modes. The buckling load for the system with the damping factor equal to or greater than 0.2 is close to the static value.

(v) To demonstrate the importance of axial inertia, the results of the present analysis are compared with those from a study which does not include axial inertia terms. The buckling loads from the latter analysis are found to be much higher than those from the present analysis, due to the absence of any coupling between radial and axial motion. Therefore, if the axial inertia is ignored, for the finite length cylindrical shell problem, the resulting model cannot properly describe the shell behavior subject to a step force.

From the above observations, it can be concluded that the axial inertia has a very significant influence on the dynamic stability of a shell subject to a step force.

REFERENCES

1. Donnell, L. H., "A New Theory for the Buckling of Thin Cylindrical Shells under Axial Compression and Bending," ASME Transactions, 56(11), 1934, pp. 795-806.

2. Karman, T. von, and Tsien, H. S., "The Buckling of Thin Cylindrical Shells Under Axial Compression," J. Aero. Sci., 8, 1941, pp. 303-312.

3. Arbocz, J. and Babcock, C. D., "The Effect of General Imperfections on the Buckling of Cylindrical Shells," J. of Appl. Mech., March 1969.

4. Lock, M. H., "Snapping of a Shallow Sinusoidal Arch Under a Step Pressure Load," AIAA Journal, Vol. 4, No. 7, July 1966, pp. 1249-1256.

5. Lock, M. H., Okubo, S. and Whittier, J. S., "Experiments on the Snapping of a Shallow Dome under a Step Pressure Load," AIAA Journal, vol. 6, No. 7, 1967, pp. 1320-1326.

6. Cheung, M. C. and Babcock, C. D., "An Energy Approach to the Dynamic Stability of Arches," ASME Transaction, December 1970, pp. 1012-1018.

7. Goodier, J. N., and McIvor, I. K., "The Elastic Cylindrical Shell under Nearly Uniform Radial Impulse," ASME Transaction, June 1964, pp. 259-266.

8. Lindberg, H. E., "Impact Buckling of a Thin Bar," Journal of Applied Mechanics, vol. 32, ASME Transaction vol. 87, 1965, pp. 315-322.

9. Lindberg, H. E., and Herbert, R. E., "Dynamic Buckling

REFERENCES (Cont'd)

of a Thin Cylindrical Shell Under Axial Impact," ASME Transaction, March 1966, pp. 105-110.

10. Abrahamson, G. R. and Lindberg, H. E., "Peak Load-impulse Characterication of Critical Pulse Loads in Structural Dynamics," Dynamic Response of Structures, Proceedings of Symposium at Stanford Univ., June 1971, pp. 31-53.

11. Volmir, A. S., "On the Stability of Dynamically Loaded Cylindrical Shells," Diklady Academi Nauk SSSR, Vol. 123, No. 5, 1958, pp. 806-808 (in Russian). Translated in Soviet Physics-Doklady, Vol. 3, 1958, pp. 1287-1289.

12. Coppa and Nash, "Dynamic Buckling of Shell Structure Subject to Longitudinal Impact," Technical Documentary Report No. FDL-TDR-64-65.

13. Roth, R. S. and Klosner, J. P., "Nonlinear Response of Cylindrical Shells with Initial Imperfections Subjected to Dynamic Axial Loads," Avco Corp. RAD-TM-63-43, 31 July 1963.

14. Humphreys, J. S., "A Note on the Adequacy of Energy Criteria for Dynamic Buckling of Arches," AIAA Journal, vol. 4, No. 5, 1966, pp. 921-923.

15. Vahidi, B., "Non-existence of Snap-through for Clamped Shallow Elastic Arches Subjected to Impulsive Loading." AFOSR Scientific Report Grant AF-AFOSR 1226-6X, March 1968.

REFERENCES (Cont'd)

16. Arbocz, J. and Babcock, C. D., "On the Role of Imperfections in Shell Buckling," Proc. of The XIII IUTAM Congress at Moscow in USSR, August 1972.

17. El Raheb, M., "Some Approximations in the Dynamic Shell Equations," Ph.D. Thesis, California Institute of Technology, Dec. 1, 1969.

18. Koiter, W. J., "The Stability of Elastic Equilibrium," Technical Report AFFDL-TR-70-25, Feb. 1970.

19. Carnaham, B., Luther, H. A., and Wilkers, J. O., "Applied Numerical Methods," 1969, Wiley.

20. Lock, M. H. "The Snapping of a Shallow Sinusoidal Arch Under a Step Pressure Load," SSD-TR-65-107, July 1965.

21. Budiansky, B., "Dynamic Buckling of Elastic Structures: Criteria and Estimates," Proceedings of an International Conference at Northwestern Univ., Evanston, Illinois, Oct. 1965, pp. 83-106.

22. Danielson, D. A., "Dynamic Buckling Loads of Imperfection-Sensitive Structure from Perturbation Procedure," AIAA Journal, vol. 7, No. 8, 1968, pp. 1506-1510.

23. Bhatia, P. and Babcock, C. D., "Dynamic Buckling of Structures," California Institute of Technology GALCIT Report SM 73-1, Feb. 1973.

REFERENCES (Cont'd)

24. Chen, Jay-Chung, "Nonlinear Vibration of Cylindrical Shell," Ph. D. Thesis, California Institute of Technology, 1972.

25. Budiansky, B. and Hutchinson, J. W., "Dynamic Buckling of Imperfection Sensitive Structures," Proc. XI International Congress Applied Mechanics, Munich, 1964.

APPENDIX A

Analysis of Sine-Representation

The radial displacement and initial imperfection are assumed as the following forms,

$$\frac{w}{h} = \xi_1 \sin(\frac{i\pi x}{L}) + \xi_2 \sin(\frac{k\pi x}{L}) \sin(\frac{\ell y}{R}) + \xi_3 \tag{A-1}$$

$$\frac{\overline{w}}{h} = \overline{\xi}_1 \sin(\frac{i\pi x}{L}) + \overline{\xi}_2 \sin(\frac{k\pi x}{L}) \sin(\frac{\ell y}{R}) \tag{A-2}$$

(A-1) Boundary Layer-type Solutions

The particular solutions u_p and v_p of the inplane equations are obtained as

$$u_p = b_1 \sin\alpha_{i-k} x \sin\beta y + b_2 \sin\alpha_{i+k} \sin\beta y + b_3 \cos\alpha_k x \sin\beta y$$

$$+ b_4 \sin 2\alpha_k x + b_5 \cos\alpha_i x + b_6 \sin 2\alpha_k x \cos 2\beta y + b_7 \sin 2\alpha_i x \tag{A-3}$$

$$v_p = e_1 \cos\alpha_{i-k} x \cos\beta y + e_2 \cos\alpha_{i+k} x \cos\beta y + e_3 \sin\alpha_\pi x \cos\beta y$$

$$+ e_4 \sin\beta y + e_5 \cos 2\alpha_k x \sin 2\beta y \tag{A-4}$$

The homogeneous solutions for the simple support boundary condition are obtained in the following form,

$$u_h = f_2(x)\sin\beta y + f_3(x)\cos 2\beta y + f_1(x) \tag{A-5}$$

$$v_h = f_4(x)\sin 2\beta y + f_5(x)\cos 2\beta y \tag{A-6}$$

and

and $f_1(x) = \xi_o x - b_5$

$$f_2(x) = \frac{-b_3}{(\sinh\beta L+\gamma L)} \left\{ \gamma \left[x\cosh\beta(L-x)+(L-x)\cosh\beta x \right] \right.$$

$$\left. + \left[\sinh\beta x+\sinh\beta(L-x) \right] \right\}$$

$$+ \frac{(e_1+e_2)\gamma}{(\sinh\beta L-\gamma L)} \left[(L-x)\sinh\beta x-x\sinh\beta(L-x) \right] \qquad \text{(A-7)}$$

$$f_3(x) = \frac{-2(e_1+e_2)\gamma}{(\sinh 2\beta L-2\gamma L)} \left[(L-x)\sinh 2\beta x-x\sinh 2\beta(L-x) \right] \qquad \text{(A-8)}$$

$$f_4(x) = \frac{(e_4+e_5)}{(\sinh 2\beta L-2\gamma L)} \left\{ 2\gamma \left[(L-x)\cosh 2\beta x + x\cosh 2\beta(L-x) \right] \right.$$

$$\left. - \left[\sinh 2\beta x + \sinh 2\beta(L-x) \right] \right\} \qquad \text{(A-9)}$$

$$f_5(x) = \frac{-b_3\gamma}{(\sinh\beta L+\gamma L)} \left[(L-x)\sinh\beta x - x\sinh\beta(L-x) \right]$$

$$+ \frac{(e_1+e_2)}{(\sinh\beta L-\gamma L)} \left\{ \gamma \left[x\cosh(L-x)+(L-x)\cosh\beta x \right] \right.$$

$$\left. - \left[\sinh\beta x + \sinh\beta(L-x) \right] \right\} \qquad \text{(A-10)}$$

where $\gamma = \frac{\beta(1+\nu)}{3-\nu}$

The boundary layer-type solutions, $f_2(x)$ through $f_5(x)$ are shown in Fig. 21-a and 21-b. All coefficients are listed at the end of this section.

The list of Coefficients in Appendix A

$$b_1 = \left\{ \frac{a_i^2\beta^2(\beta^2 - \nu a_{i-k}^2)}{2a_{i-k}(a_{i-k}^2+\beta^2)^2} - \frac{a_i a_k}{2a_{k-i}} \right\} (\xi_1\xi_2+\bar{\xi}_1\xi_2+\bar{\xi}_2\xi_1)$$

$$b_2 = \left\{ \frac{a_i^2\beta^2(\nu a_{i+k}^2 - \beta^2)}{2a_{i+k}(a_{i+k}^2+\beta^2)^2} - \frac{a_i a_k}{2a_{k+i}} \right\} (\xi_1\xi_2+\bar{\xi}_1\xi_2+\bar{\xi}_2\xi_1)$$

$$b_3 = \frac{a_k(\beta^2 - \nu a_k^2)}{R(a_k^2+\beta^2)^2}\ \xi_2$$

$$b_4 = \frac{\nu\beta^2 - a_k^2}{16a_k}\ (\xi_2^2 + 2\bar{\xi}_2\xi_2)$$

$$b_5 = -\frac{\nu}{a_i R}\ \xi_1$$

$$b_6 = \frac{a_k}{16}\ (\xi_2^2 + 2\bar{\xi}_2\xi_2)$$

$$b_7 = -\frac{a_i}{8}\ (\xi_1^2 + 2\bar{\xi}_1\xi_1)$$

$$e_1 = \frac{a_i^2\beta^2(a_{i-k}^2 - \nu\beta^2)}{2(a_{i-k}^2+\beta^2)^2}\ (\xi_1\xi_2 + \bar{\xi}_1\xi_2 + \bar{\xi}_2\xi_1)$$

$$e_2 = \frac{a_i^2\beta^2(a_{i+k}^2 - \nu\beta^2)}{2(a_{i+k}^2+\beta^2)^2}\ (\xi_1\xi_2 + \bar{\xi}_1\xi_2 + \bar{\xi}_2\xi_1)$$

$$e_3 = -\frac{\beta[\beta^2+(\nu+2)a_k^2]}{R(a_k^2+\beta^2)^2}\ \xi_2$$

$$e_4 = \frac{\nu a_k^2 - \beta^2}{16\beta} (\xi_2^2 + 2\bar{\xi}_2\xi_2)$$

$$e_5 = \frac{\beta}{16} (\xi_2^2 + 2\bar{\xi}_2\xi_2)$$

where $a_i = \frac{i\pi}{L}$, $a_k = \frac{k\pi}{L}$, $a_{i\pm k} = \frac{(i\pm k)\pi}{L}$, and $\beta = \frac{\ell}{R}$

(A-2) Algebraic Equations for Static Buckling

The method employed in the present analysis yields the following set of two nonlinear algebraic equations,

$$(\hat{\lambda}_{c_i} - \lambda)\,\xi_1 + C_3[(\xi_2+\bar{\xi}_2)\xi_1 + \bar{\xi}_1\xi_2](\bar{\xi}_2+\xi_2) + Q_1(\xi_2^2+2\bar{\xi}_2\xi_2)$$

$$+ Q_2\xi_2(\bar{\xi}_2+\xi_2) = \lambda\bar{\xi}_1 \qquad \text{(A-11)}$$

$$(\lambda_{c_k} - \lambda)\,\xi_2 + C_1(\xi_2^2+2\bar{\xi}_2\xi_2)(\bar{\xi}_2+\xi_2) + C_2[(\xi_1+\bar{\xi}_1)\xi_2+\bar{\xi}_2\xi_1](\bar{\xi}_1+\xi_1)$$

$$+ Q_3\,\xi_1(\bar{\xi}_2+\xi_2) + Q_4(2\xi_1\xi_2+2\bar{\xi}_1\xi_2+\bar{\xi}_2\xi_1) = \lambda\bar{\xi}_2 \qquad \text{(A-12)}$$

Note: quadratic terms Q_i appear in equations (A-11) and (A-12) only if i = odd numbers.

Numerical Results of the System of Equations (A-11) and (A-12)

The system has a local maximum in the variation of load parameter, λ, and displacements, ξ_1 and ξ_2, only for the particular combination of the wave numbers. The wave numbers have to satisfy the following conditions

$i = 2k+1$ or $i = 2k-i$, and $i \geq 17$

where $\frac{R}{L} = 0.5$, $\frac{h}{R} = 0.001$

The list of coefficients of equations (A-11) and (A-12)

$$\hat{\lambda}_{c_i} = \lambda_{c_i} - \left(\frac{2}{\pi i}\right)^2 \frac{1}{a_i^2}$$

$$Q_1 = \frac{D_1}{4a_i^2}$$

$$Q_2 = \frac{D_2}{2a_i^2}$$

$$Q_3 = \frac{D_1}{a_k^2}$$

$$Q_4 = \frac{D_2}{a_k^2}$$

$$D_1 = -\frac{2ic\beta^2}{(4k^2-i^2)\pi}$$

$$D_2 = -\frac{2kc\, a_i^2 a_k^2 \beta^2}{i(2k-i)\pi(a_k^2+\beta^2)} \left\{ \frac{1}{a_{i-k}^2+\beta^2} + \frac{1}{a_{i+k}^2+\beta^2} \right\}$$

$$- \frac{2(1+\nu)ca_k^2\beta^2}{i\pi(a_k^2+\beta^2)^2} \left\{ \frac{2i\,a_k a_{i+k} - k a_i^2}{(2k+i)(a_{i+k}^2+\beta^2)^2} + \frac{2ia_k a_{i-k} - k a_i^2}{(2k-i)(a_{i-k}^2+\beta^2)^2} \right\}$$

λ_{c_i}, λ_{c_k}, C_1, C_2, C_3, a_i, a_k, β, a_{i-k}, and a_{i+k} are the same as Appendices B-2 and B-3.

APPENDIX B

(B-1) Coefficient of Particular Solutions of Inplane Equations, u_p and v_p

$$\hat{\alpha}_i = \frac{i\pi}{L}$$

$$\hat{\alpha}_k = \frac{k\pi}{L}$$

$$\hat{\alpha}_{i+k} = \frac{(i+k)\pi}{L}$$

$$\hat{\alpha}_{i-k} = \frac{(i-k)\pi}{L}$$

$$\hat{\beta} = \frac{\ell}{R}$$

For solution u_p

$$b_1 = \frac{\nu}{R\hat{\alpha}_i}\,\xi_1$$

$$b_2 = \frac{\hat{\alpha}_i(\xi_1^2+2\bar{\xi}_1\xi_1)}{8}$$

$$b_3 = -\frac{(\hat{\alpha}_k^2-\nu\beta^2)(\xi_2^2+2\bar{\xi}_2\xi_2)}{16\hat{\alpha}_k}$$

$$b_4 = \frac{\hat{\alpha}_k^2(\hat{\beta}^2-\nu\hat{\alpha}_k^2)\xi_2}{R(\hat{\alpha}_k^2+\hat{\beta}^2)^2}$$

$$b_5 = \left[\frac{\hat{\alpha}_i^2\hat{\beta}^2(\hat{\beta}^2-\nu\hat{\alpha}_{i+k}^2)}{2\hat{\alpha}_{i+k}(\hat{\alpha}_{i+k}^2+\hat{\beta}^2)^2} + \frac{\hat{\alpha}_i\hat{\alpha}_k}{2\hat{\alpha}_{i+k}}\right](\xi_1\xi_2+\bar{\xi}_1\xi_2+\bar{\xi}_2\xi_1)$$

$$b_6 = \left[\frac{\hat{\alpha}_i^2\hat{\beta}^2(\hat{\beta}^2-\nu\hat{\alpha}_{i-k}^2)}{2\hat{\alpha}_{i-k}(\hat{\alpha}_{i-k}^2+\hat{\beta}^2)^2} - \frac{\hat{\alpha}_i\hat{\alpha}_k}{2\hat{\alpha}_{i-k}}\right](\xi_1\xi_2+\bar{\xi}_1\xi_2+\bar{\xi}_2\xi_1)$$

$$b_7 = \frac{\hat{\alpha}_k(\xi_2^2+2\bar{\xi}_2\xi_2)}{16}$$

For solution v_p

$$e_1 = \frac{\hat{\alpha}_i^2\hat{\beta}(\hat{\alpha}_{i-k}^2 - \nu\hat{\beta}^2)}{2(\hat{\alpha}_{i-k}^2+\hat{\beta}^2)^2} (\xi_1\xi_2 + \bar{\xi}_1\xi_2 + \bar{\xi}_2\xi_1)$$

$$e_2 = \frac{\hat{\alpha}_i^2\hat{\beta}(\hat{\alpha}_{i+k}^2 - \nu\hat{\beta}^2)}{2(\hat{\alpha}_{i+k}^2+\hat{\beta}^2)^2} (\xi_1\xi_2 + \bar{\xi}_1\xi_2 + \bar{\xi}_2\xi_1)$$

$$e_3 = \frac{1}{R\hat{\beta}}\left[\frac{\hat{\alpha}_k^2(\hat{\alpha}_k^2+\nu\hat{\beta}^2)}{(\hat{\alpha}_k^2+\hat{\beta}^2)^2} - 1\right]\xi_2$$

$$e_4 = \frac{(\nu\hat{\alpha}_k^2-\hat{\beta}^2)(\xi_2^2+2\bar{\xi}_2\xi_2)}{16\hat{\beta}}$$

$$e_5 = \frac{\hat{\beta}}{16}(\xi_2^2 + 2\bar{\xi}_2\xi_2)$$

(B-2) Coefficients of Energy Expressions in Equations (16), (17)

$$a_i^2 = i^2\left(\frac{Rh}{2c}\right)\left(\frac{\pi}{L}\right)^2$$

$$a_k^2 = k^2\left(\frac{Rh}{2c}\right)\left(\frac{\pi}{L}\right)^2$$

$$a_{i-k}^2 = (i-k)^2\left(\frac{Rh}{2c}\right)\left(\frac{\pi}{L}\right)^2$$

$$a_{i+k}^2 = (i+k)^2\left(\frac{Rh}{2c}\right)\left(\frac{\pi}{L}\right)^2$$

$$\beta^2 = \ell^2 \left(\frac{Rh}{2c}\right) \left(\frac{1}{R}\right)^2$$

$$\hat{C}_1 = \frac{c^2(a_k^4+\beta^4)}{32}$$

$$\hat{C}_2 = \frac{c^2 a_i^2 \beta^4}{4} \left[\frac{1-\delta_{ik}}{(a_{i-k}^2+\beta^2)^2} + \frac{1}{(a_{i+k}^2+\beta^2)^2}\right] (\xi_1\xi_2+\bar{\xi}_1\xi_2+\bar{\xi}_2\xi_1)^2$$

where IF $i = k$, $\delta_{ik} = 1$

IF $i \neq k$, $\delta_{ik} = 0$

$$\hat{C}_3 = \frac{a_k^4}{4(a_k^2+\beta^2)^2}$$

$$\hat{C}_4 = \frac{(a_k^2+\beta^2)^2}{4}$$

$$\hat{C}_5 = \frac{a_i^4}{2}$$

$$\hat{C}_6 = \frac{c(a_i^2+\nu\beta^2)}{4}$$

$$\hat{C}_7 = \frac{c a_i^2}{2}$$

$$\hat{C}_8 = \frac{c(\beta^2+\nu a_k^2)}{8}$$

$$\hat{C}_9 = \frac{c\nu a_i^2}{2}$$

$$\hat{Q}_1 = \frac{c\beta^2}{4} \quad , \quad \text{where} \quad \text{If } i \neq 2k, \quad \hat{Q}_1 = 0$$

$$\hat{Q}_2 = \frac{c a_i^2 a_k^2 \beta^2}{2(a_k^2+\beta^2)^2} \quad , \quad \text{where} \quad \text{If } i \neq 2k, \quad \hat{Q}_2 = 0$$

(B-3) Coefficients of Nonlinear Differential Equations

$$\lambda_{c_i} = \frac{1}{2}\left(a_i^2 + \frac{1}{a_i^2}\right)$$

$$\lambda_{c_k} = \frac{1}{2}\left[\frac{(a_k^2+\beta^2)^2}{a_k^2} + \frac{a_k^2}{(a_k^2+\beta^2)^2}\right]$$

$$C_1 = \frac{c^2}{8}\left(\frac{\beta^4}{a_k^2} + a_k^2\right)$$

$$C_2 = \frac{c^2 a_i^4 \beta^4}{2a_k^2}\left[\frac{1-\delta_{ik}}{(a_{i-k}^2+\beta^2)^2} + \frac{1}{(a_{i+k}^2+\beta^2)^2}\right]$$

$$C_3 = \frac{c^2 a_i^2 \beta^4}{4}\left[\frac{1-\delta_{ik}}{(a_{i-k}^2+\beta^2)^2} + \frac{1}{(a_{i+k}^2+\beta^2)^2}\right]$$

where If $i = k$, $\delta_{ik} = 1$

If $i \neq k$, $\delta_{ik} = 0$

$$C_4 = \frac{\beta^2}{a_k^2}$$

$$C_5 = \frac{c(a_k^2+\nu\beta^2)}{4}$$

$$C_6 = \frac{c a_i^2}{2}$$

$$C_7 = \frac{c(\nu a_k^2 + \beta^2)}{4}$$

$$C_8 = \frac{c \nu a_i^2}{2}$$

$$Q_1 = \frac{1}{2a_i^2}\left(\frac{c\beta^2}{4}\right)$$

$$Q_2 = \frac{1}{2a_i^2}\left[\frac{c a_i^2 a_k^2 \beta^2}{2(a_k^2+\beta^2)^2}\right]$$

$$Q_3 = \frac{2}{a_k^2}\left(\frac{c\beta^2}{4}\right)$$

$$Q_4 = \frac{1}{a_k^2}\left[\frac{c a_i^2 a_k^2 \beta^2}{2(a_k^2+\beta^2)^2}\right]$$

where if $i \neq 2k$, then $Q_j = 0 \qquad j = 1, 2, 3, 4$

a_i^2, a_k^2, β^2, a_{i-k}^2 and a_{i+k}^2 are defined in Appendix (B-2).

APPENDIX C

THE FLOW CHART OF COMPUTER PROGRAM

The set of four simultaneous nonlinear ordinary differential equations is integrated numerically for given initial imperfections and under step loading. Numerical methods of Runge-Kutta and Milne predictor-corrector can be found in reference 19.

The present program was optimized in accuracy and time. The essence of the employed technique is in choosing an appropriate interval of integration. The procedure is to use the 4th order Runge-Kutta method to generate the starting values and then switch to use the Milne predict-correction method. If the error of the corrected value is bigger than the maximum tolerance, the interval is halved and if the error is smaller than the minimum tolerance, the interval can be doubled.

The details of the involved technique are shown in the following flow chart.

LIST OF NOTATION

YR Vector of solution

FR Vector of derivative approximations

H Step size

COUNT Step counter

RUNGE Subroutine of Runge-Kutta

PRECOR Subroutine of predict-corrector

FUN(J) Function of derivative

PCC Control parameter

ERROR Difference between predicted value and correct value

EPS Upper bound of error tolerance

SPS Lower bound of error tolerance

TMAX Upper limit of integration

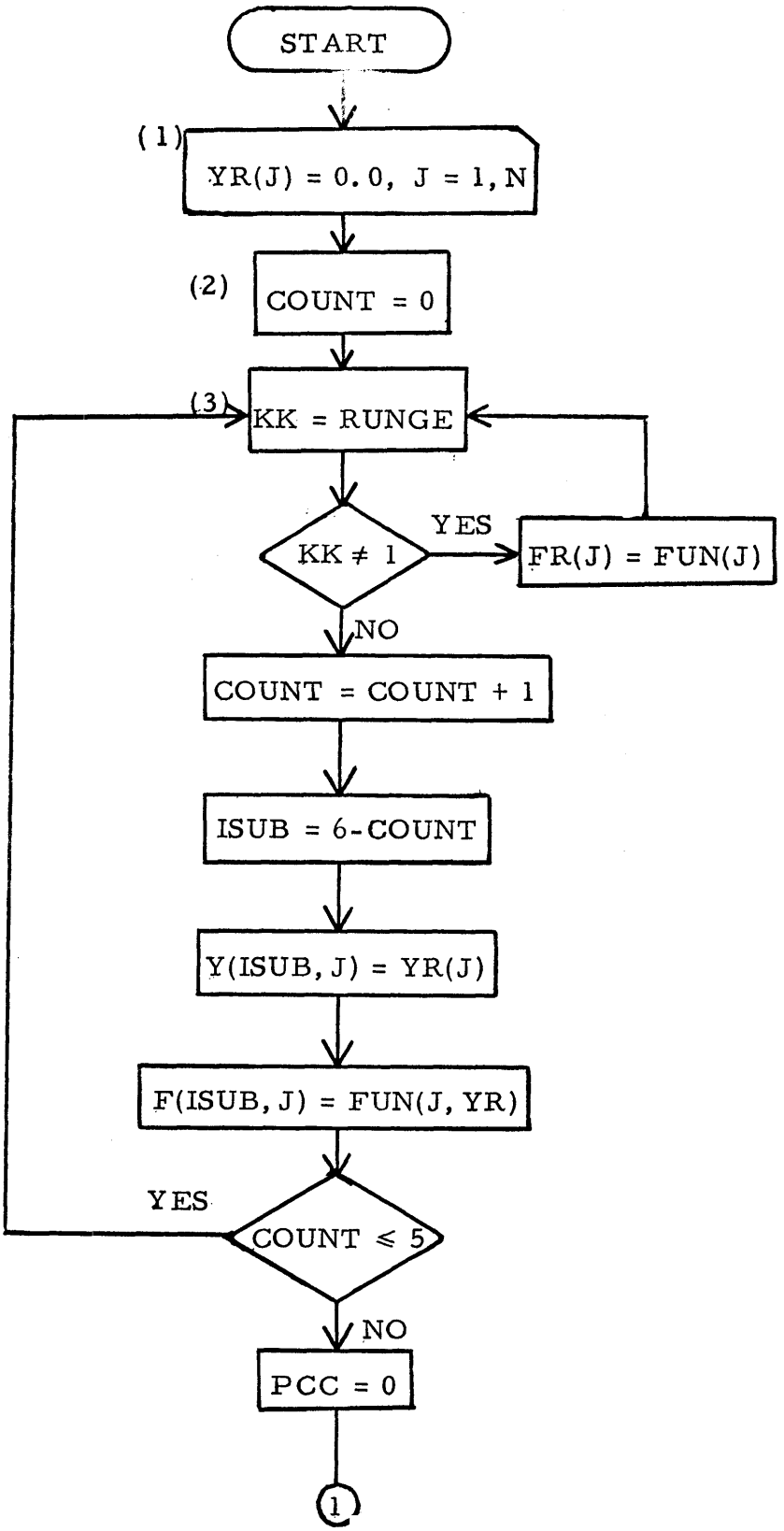
START
(1)
YR(J) = 0.0, J = 1, N
(2)
COUNT = 0
(3)
KK = RUNGE
KK ≠ 1
YES
FR(J) = FUN(J)
NO
COUNT = COUNT + 1
ISUB = 6-COUNT
Y(ISUB, J) = YR(J)
F(ISUB, J) = FUN(J, YR)
YES
COUNT ≤ 5
NO
PCC = 0
1

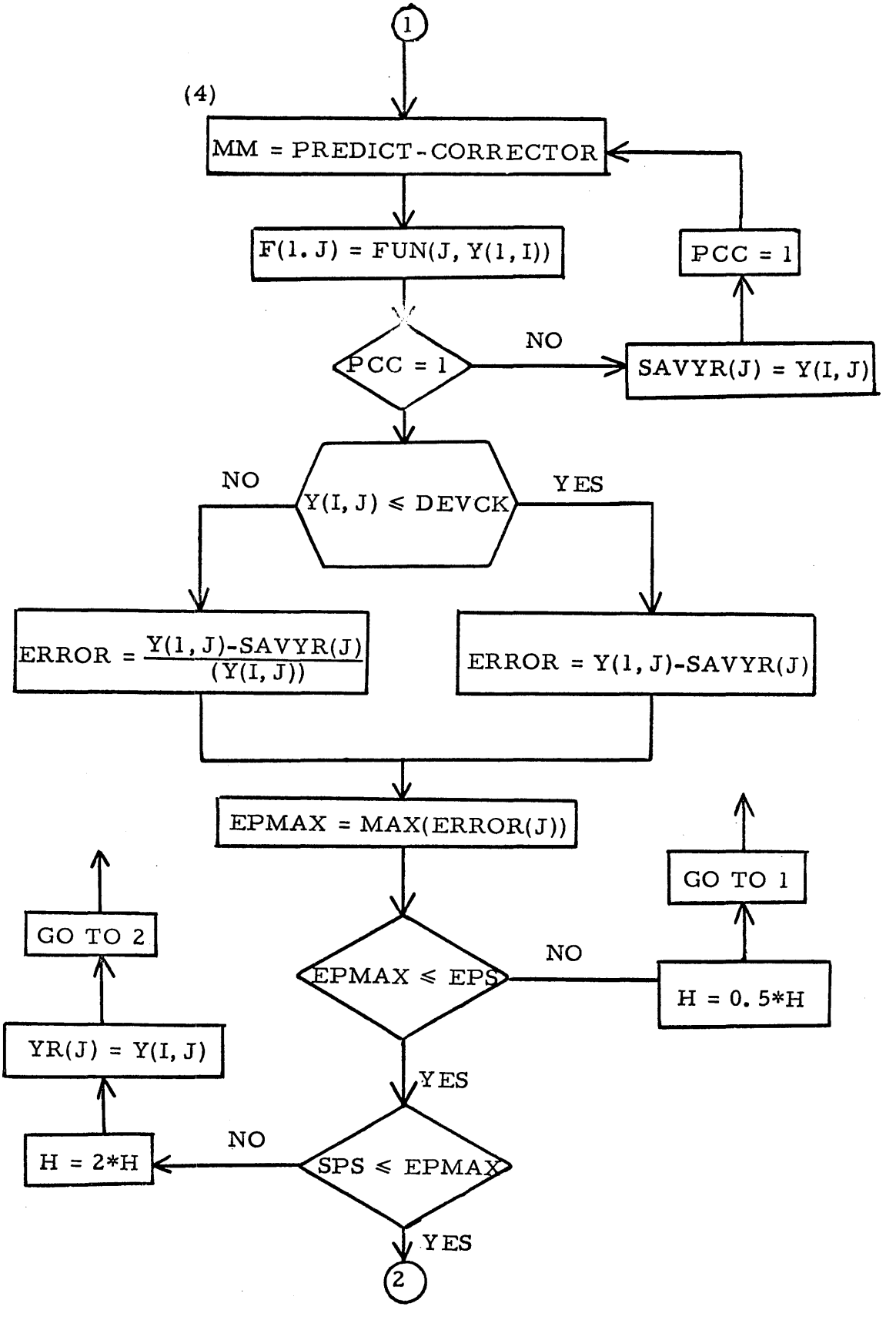
1
(4)
MM = PREDICT-CORRECTOR
F(1. J) = FUN(J, Y(1, I))
PCC = 1
PCC = 1
NO
SAVYR(J) = Y(I, J)
NO
Y(I, J) ≤ DEVCK
YES
ERROR = Y(1, J)-SAVYR(J) / (Y(I, J))
ERROR = Y(1, J)-SAVYR(J)
EPMAX = MAX(ERROR(J))
GO TO 1
GO TO 2
EPMAX ≤ EPS
NO
H = 0. 5*H
YR(J) = Y(I, J)
YES
H = 2*H
NO
SPS ≤ EPMAX
YES
2

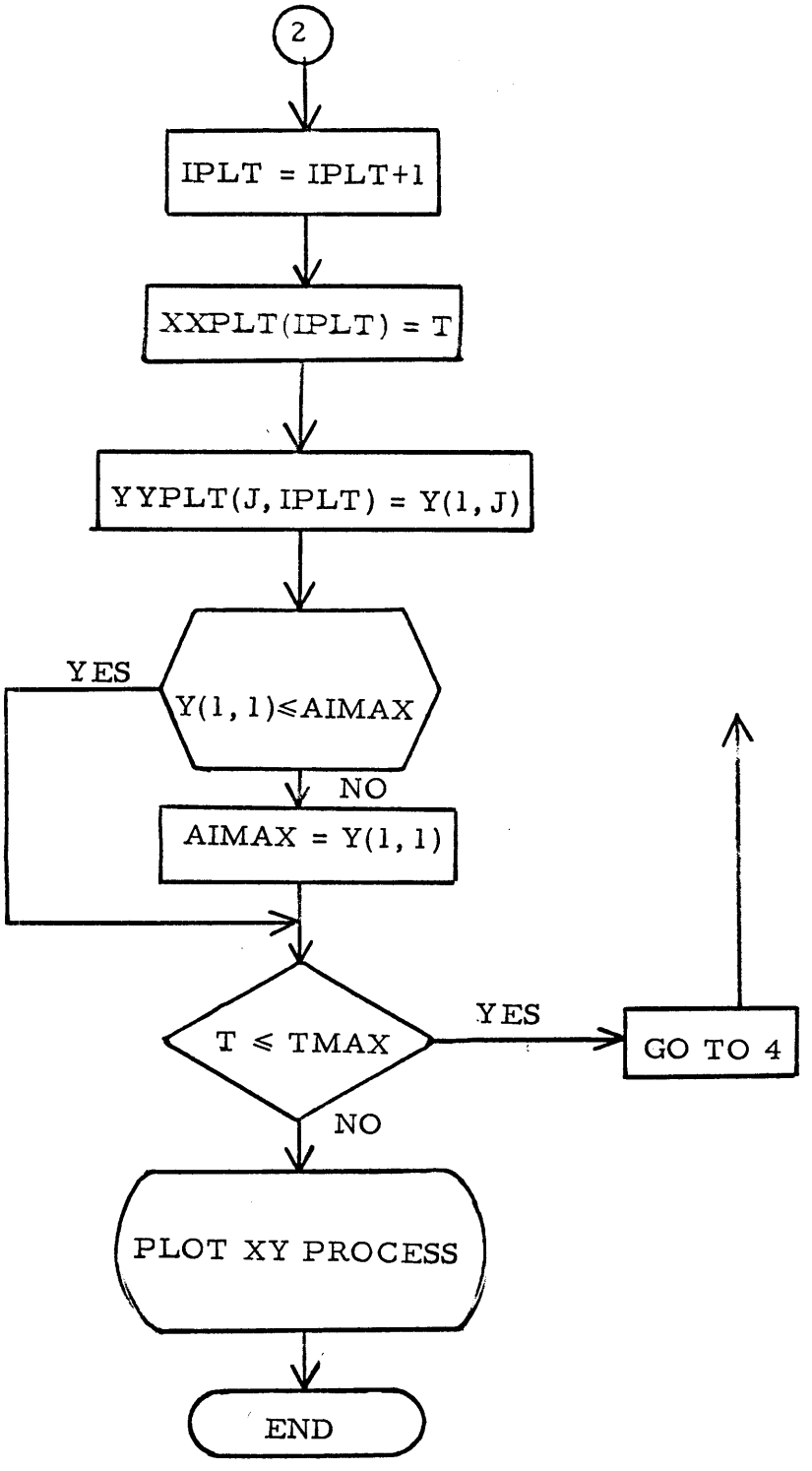
2
IPLT = IPLT+1
XXPLT(IPLT) = T
YYPLT(J, IPLT) = Y(1, J)
YES
Y(1, 1)≤AIMAX
NO
AIMAX = Y(1, 1)
T ≤ TMAX
YES
GO TO 4
NO
PLOT XY PROCESS
END

APPENDIX D

THE SYSTEM EQUATIONS WITHOUT AXIAL INERTIA

The governing differential equations which do not include the axial inertia but have the same radial displacement as the present analysis can be directly obtained from the system of equations (23a through 23d). The resulting three differential equations of motion are given as follows.

$$\left(\frac{1}{2a_i^2}\right)\ddot{\xi}_1 + \left[\lambda_{c_i} - c\bar{p}(t)\right]\xi_1 + C_3(\xi_1\xi_2+\bar{\xi}_1\xi_2+\bar{\xi}_2\xi_1)(\xi_2+\bar{\xi}_2)$$

$$+Q_1(\xi_2^2+2\bar{\xi}_2\xi_2) + Q_2(\xi_2^2+\bar{\xi}_2\xi_2) = c\bar{p}(t)\bar{\xi}_1 \qquad \text{(D-1)}$$

$$\left(\frac{1}{2a_k^2}\right)\ddot{\xi}_2 + \left[\lambda_{c_k} - c\bar{p}(t)\right]\xi_2 + C_1(\xi_2^2+2\bar{\xi}_2\xi_2)(\xi_2+\bar{\xi}_2)$$

$$+C_2(\xi_1\xi_2+\xi_2\xi_1+\bar{\xi}_1\xi_2)(\xi_1+\bar{\xi}_1) + C_4\, c(\xi_2+\bar{\xi}_2)\,\bar{g}_y(\xi)$$

$$+Q_3\xi_1(\xi_2+\bar{\xi}_2) + Q_4(2\xi_1\xi_2+\xi_1\bar{\xi}_2+2\bar{\xi}_1\xi_2) = c\bar{p}(t)\,\bar{\xi}_2$$

$$\ddot{\xi}_3 + \xi_3 - \frac{c\beta^2}{4}(\xi_2^2+2\bar{\xi}_2\xi_2) = -\nu\bar{p}(t)$$

$$\bar{g}_y(\xi) = -\nu\bar{p}(t) - \xi_3 + \frac{c\beta^2}{4}(\xi_2^2+2\bar{\xi}_2\xi_2)$$

where λ_{c_i}, λ_{c_k}, C_i and Q_i are listed in Appendix (B-3).

TABLES

FIGURES

TABLE 1. STATIC BUCKLING LOAD

ASYM k	AXI-SYM i	CIRCUMF ℓ	BUCKLING LOAD λ_s	ASYM-IMP $\bar{\xi}_2$	AXI-IMP $\bar{\xi}_1$
1	2	9	0.8765	0.1754	-0.1130
2	4	13	0.8962	0.0534	-0.0499
3	6	16	0.9111	0.0269	-0.0309
4	8	18	0.9173	0.0172	-0.0220
5	10	20	0.9230	0.0119	-0.0169
6	12	21	0.9254	0.0093	-0.0136
7	14	23	0.9274	0.0071	-0.0114
8	16	24	0.9263	0.0058	-0.0097
9	18	25	0.9249	0.0049	-0.0085
10	20	26	0.9226	0.0042	-0.0075
11	22	26	0.9186	0.0038	-0.0067
12	24	27	0.9120	0.0033	-0.0060
13	26	28	0.9057	0.0029	-0.0055
14	28	28	0.8970	0.0027	-0.0050
15	30	28	0.8896	0.0025	-0.0049
16	32	29	0.8838	0.0022	-0.0043
17	34	29	0.8812	0.0021	-0.0040
18	36	29	0.8831	0.0020	-0.0037
19	38	29	0.8894	0.0019	-0.0035
20	40	29	0.9000	0.0018	-0.0033
21	42	28	0.9120	0.0018	-0.0031
22	44	28	0.9246	0.0017	-0.0029
23	46	28	0.9367	0.0016	-0.0028
24	48	27	0.9480	0.0016	-0.0027
25	50	27	0.9568	0.0016	-0.0025
26	52	26	0.9647	0.0016	-0.0024
27	54	25	0.9718	0.0616	-0.0023
28	56	24	0.9787	0.0016	-0.0022
29	58	23	******	0.0017	-0.0021

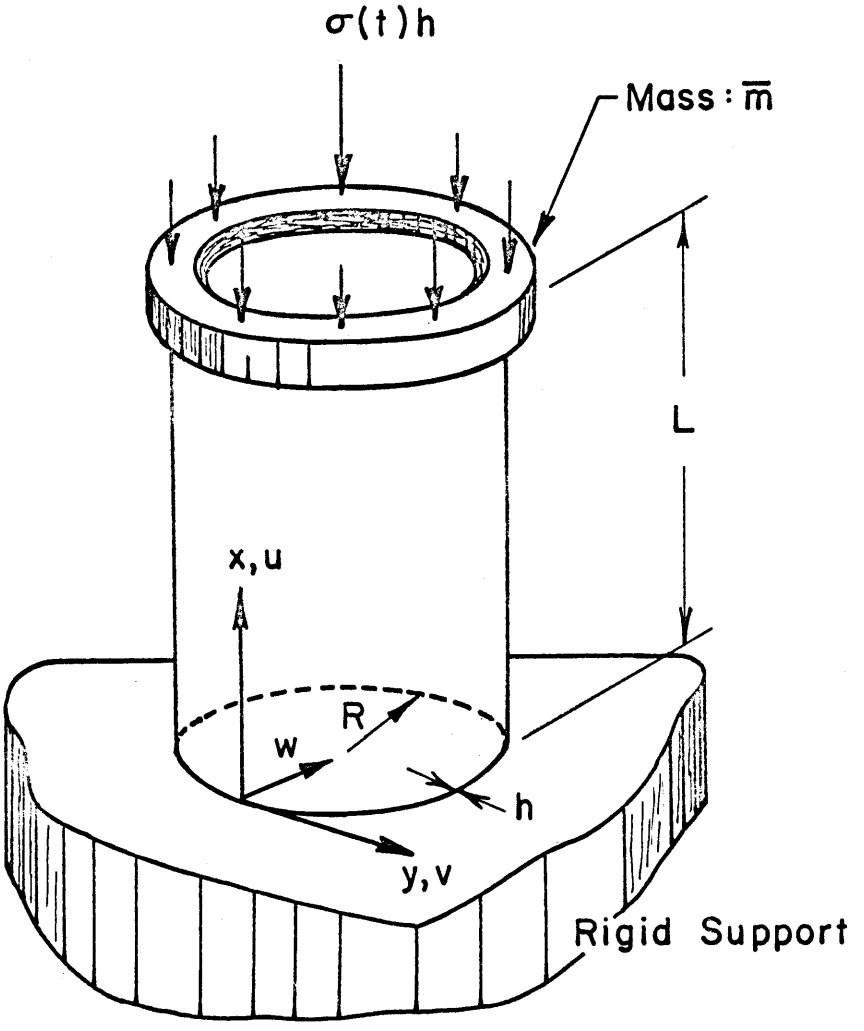

FIG. I SHELL GEOMETRY AND COORDINATE SYSTEM

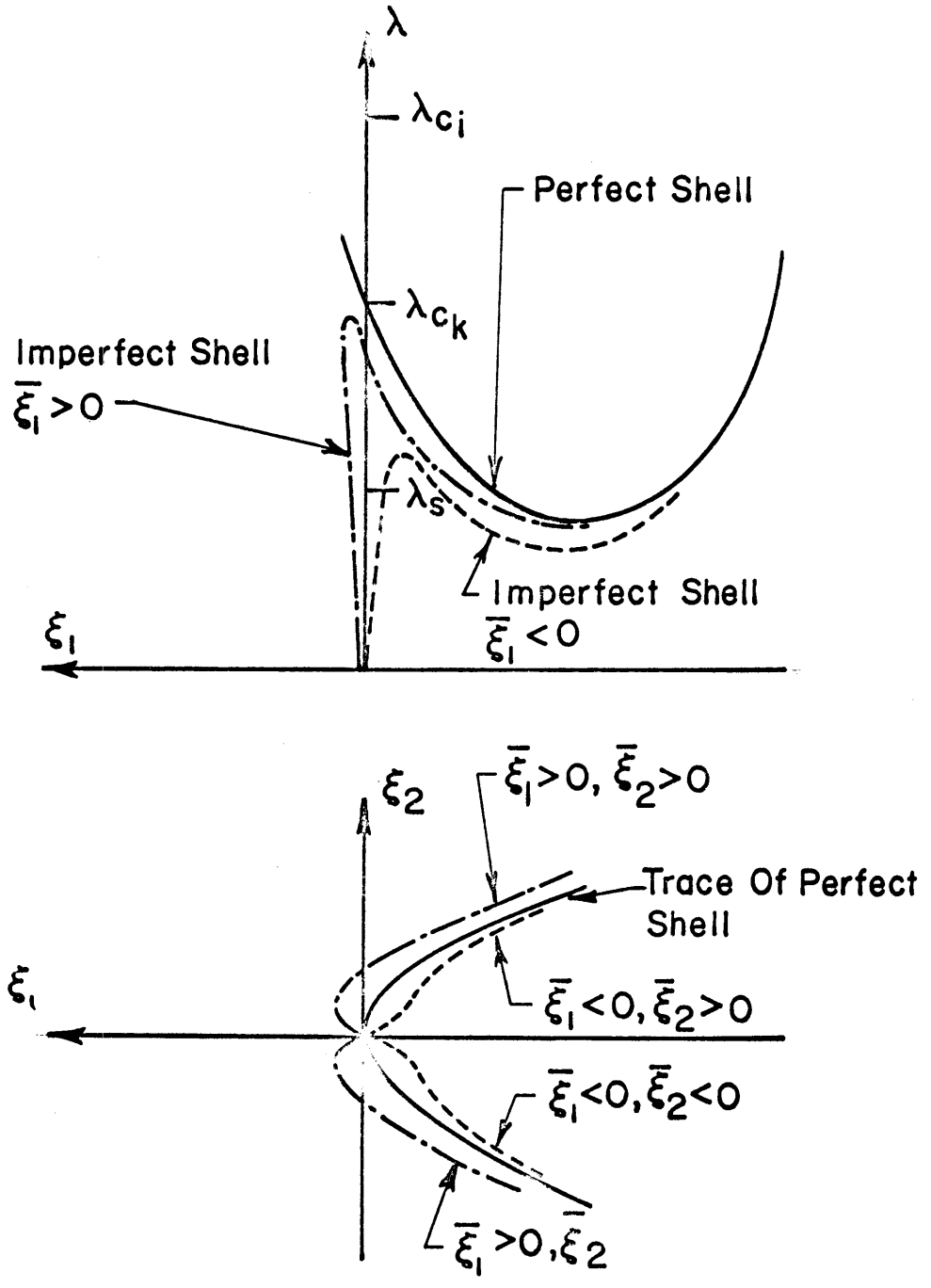

FIG. 2 EQUILIBRIUM PATHS FOR PERFECT AND IMPERFECT SHELLS

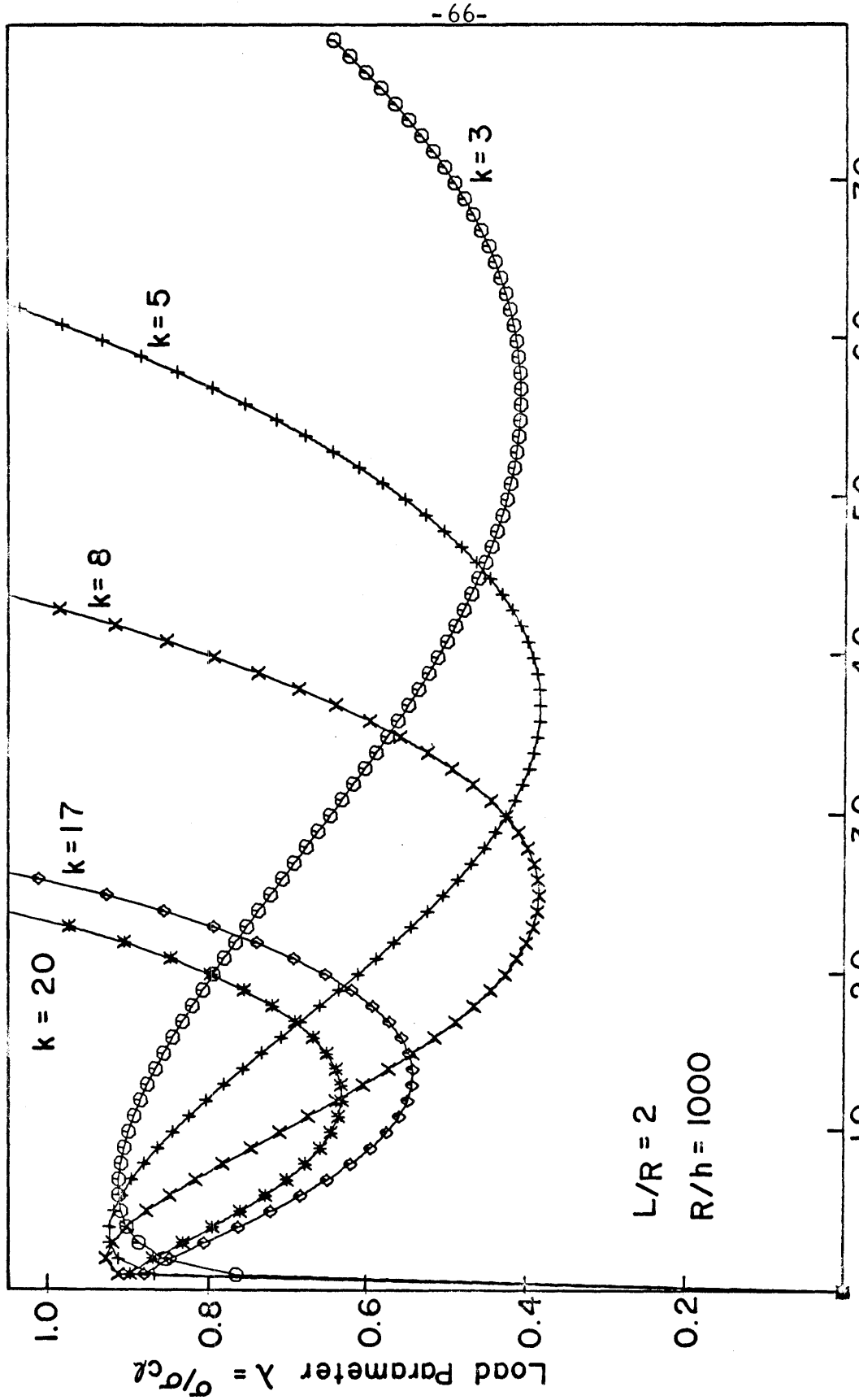

FIG.3 LOAD-DEFLECTION CURVES FOR DIFFERENT WAVE NUMBERS (k)

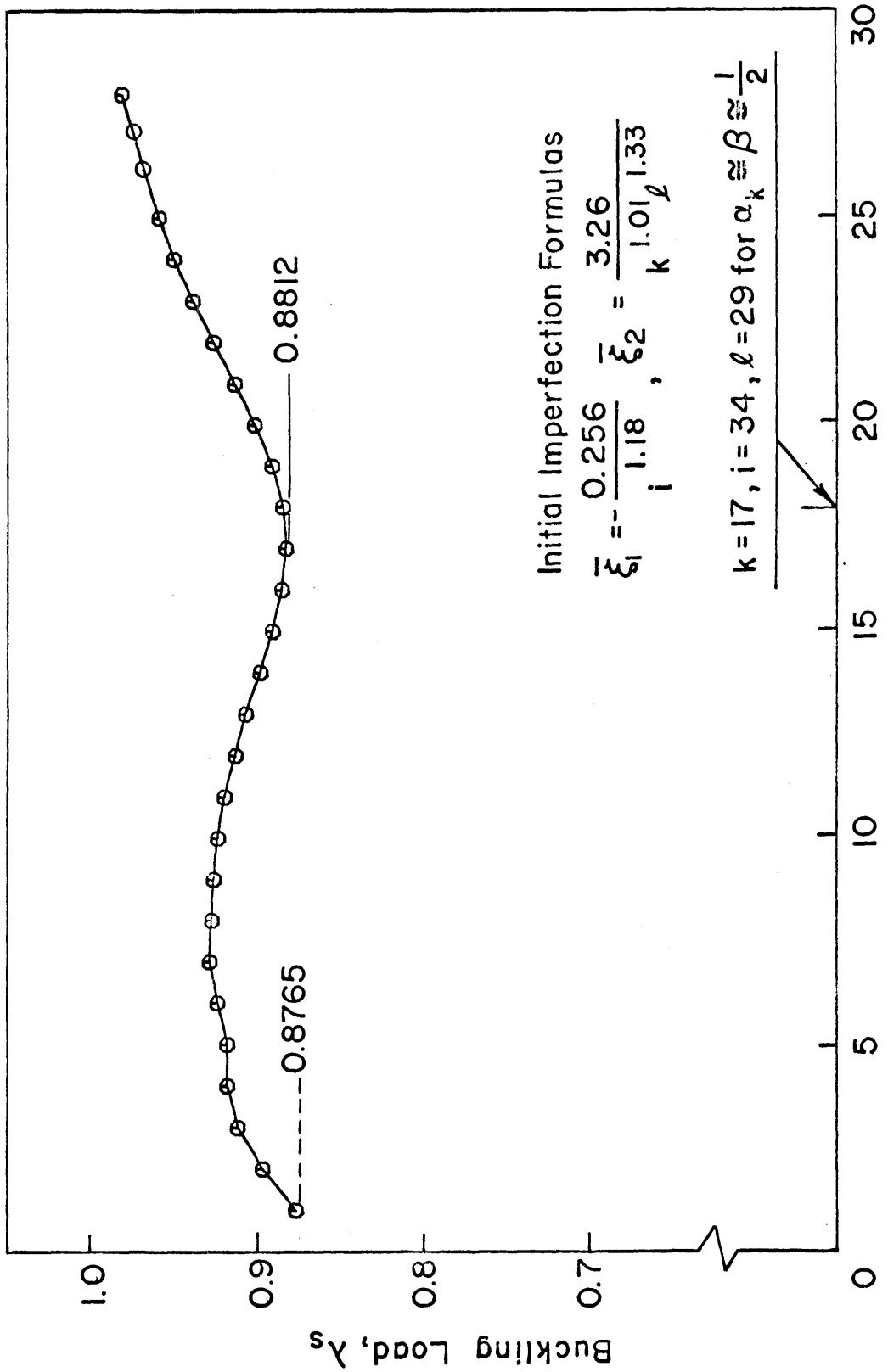

FIG. 4 STATIC BUCKLING LOAD VS. WAVE NUMBER

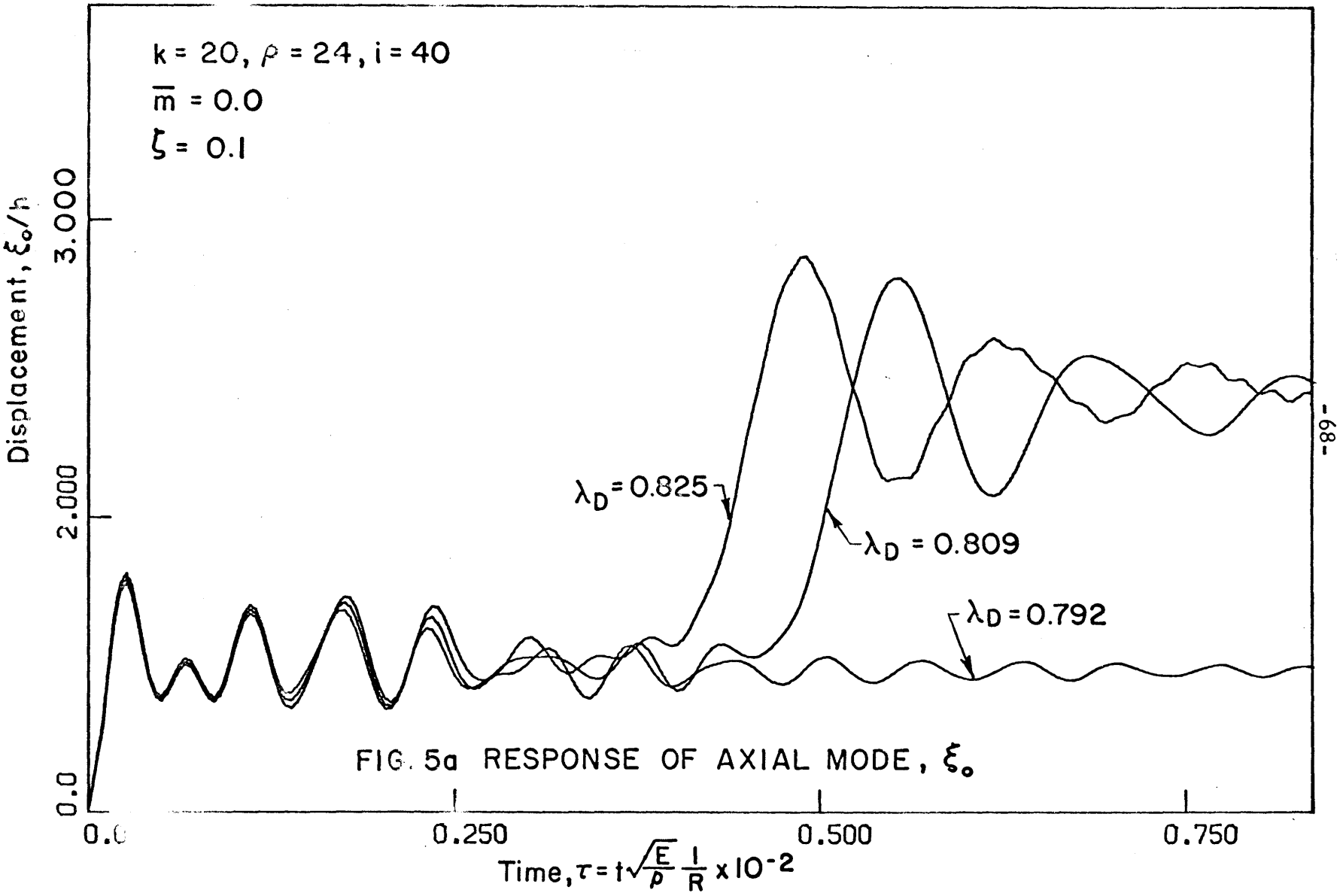

FIG. 5a RESPONSE OF AXIAL MODE, ξ_o

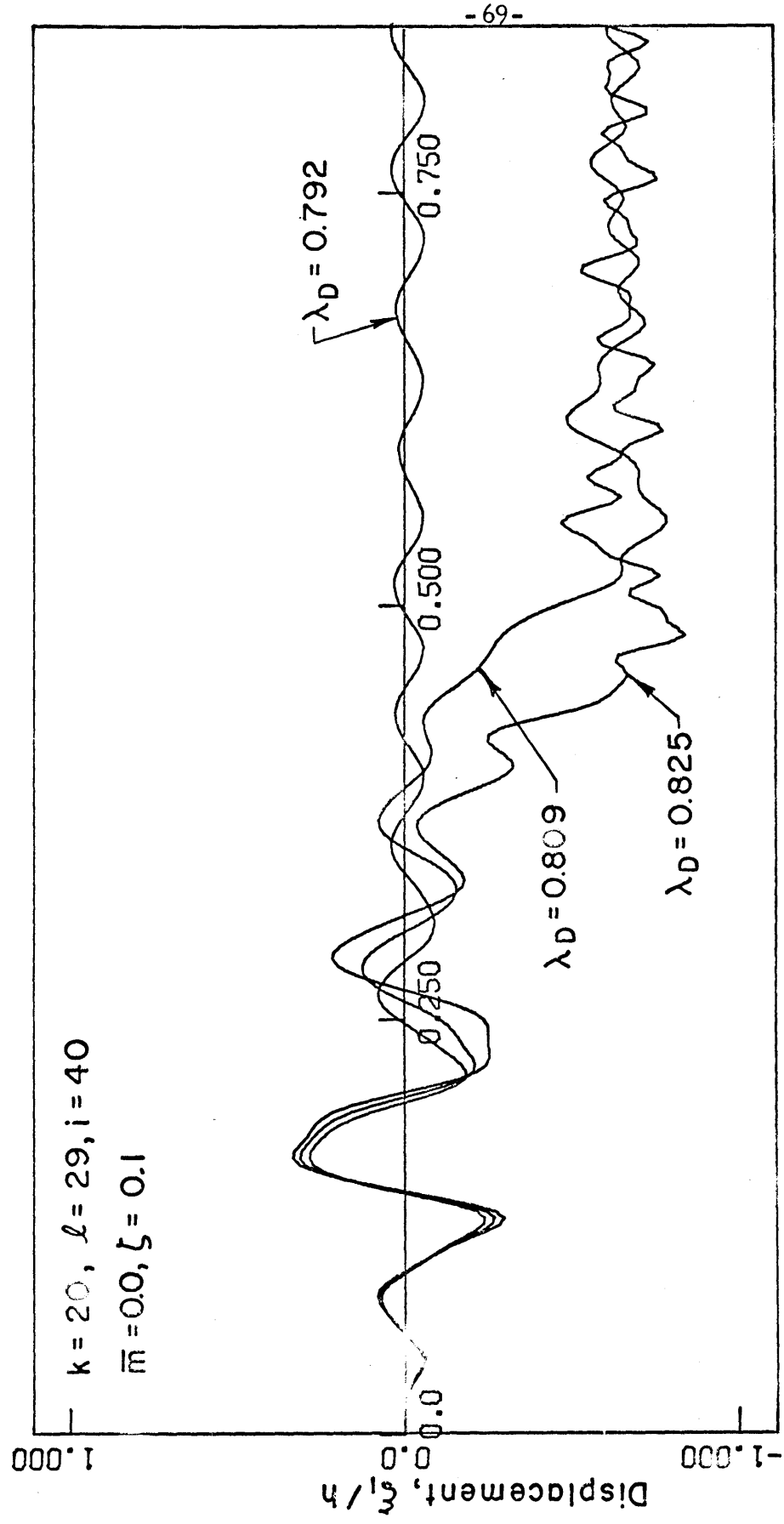

FIG. 5b RESPONSE OF AXISYMMETRIC MODE, ξ_1

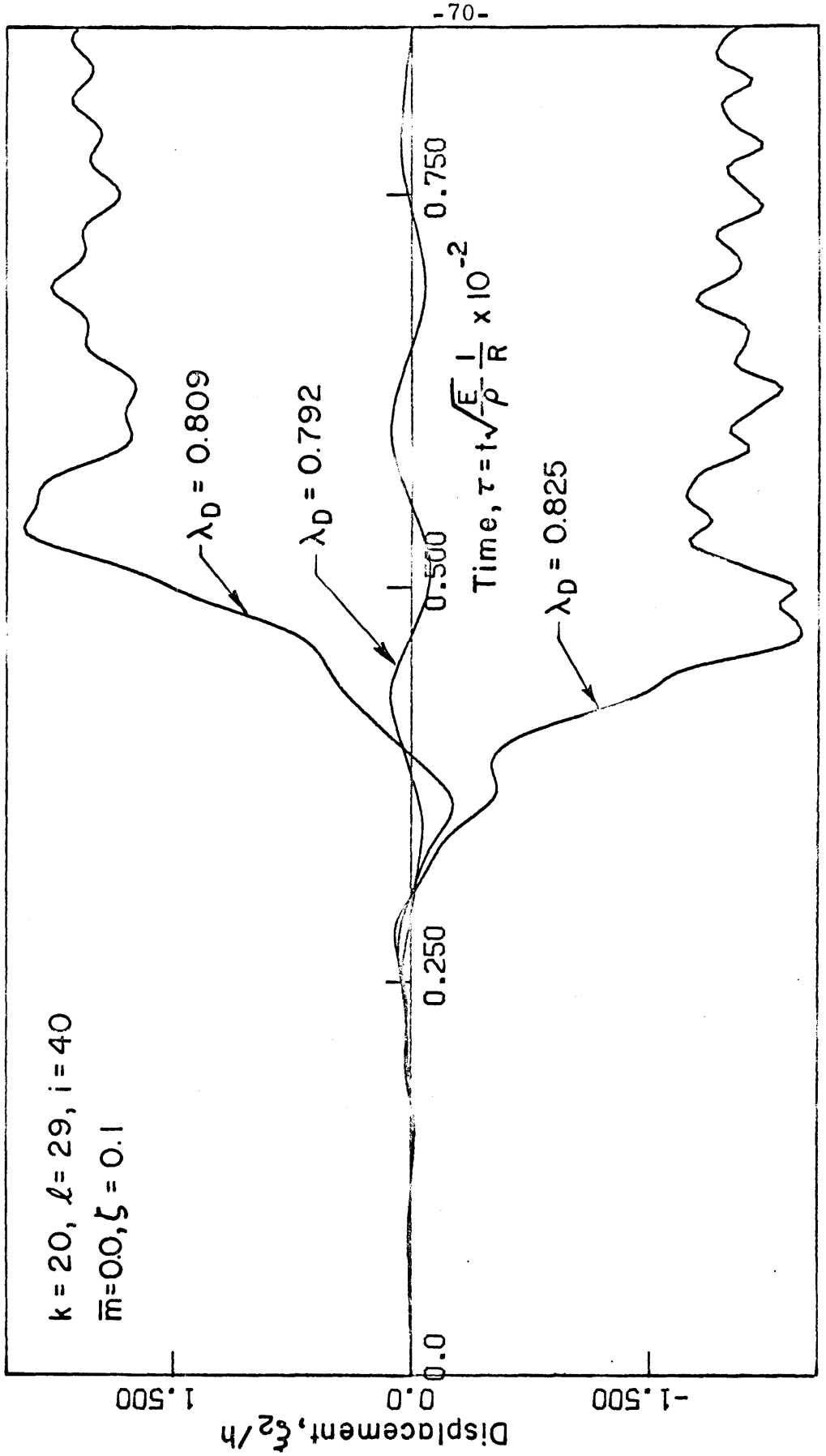

FIG. 5c RESPONSE AT ASYMMETRIC MODE, ξ_2

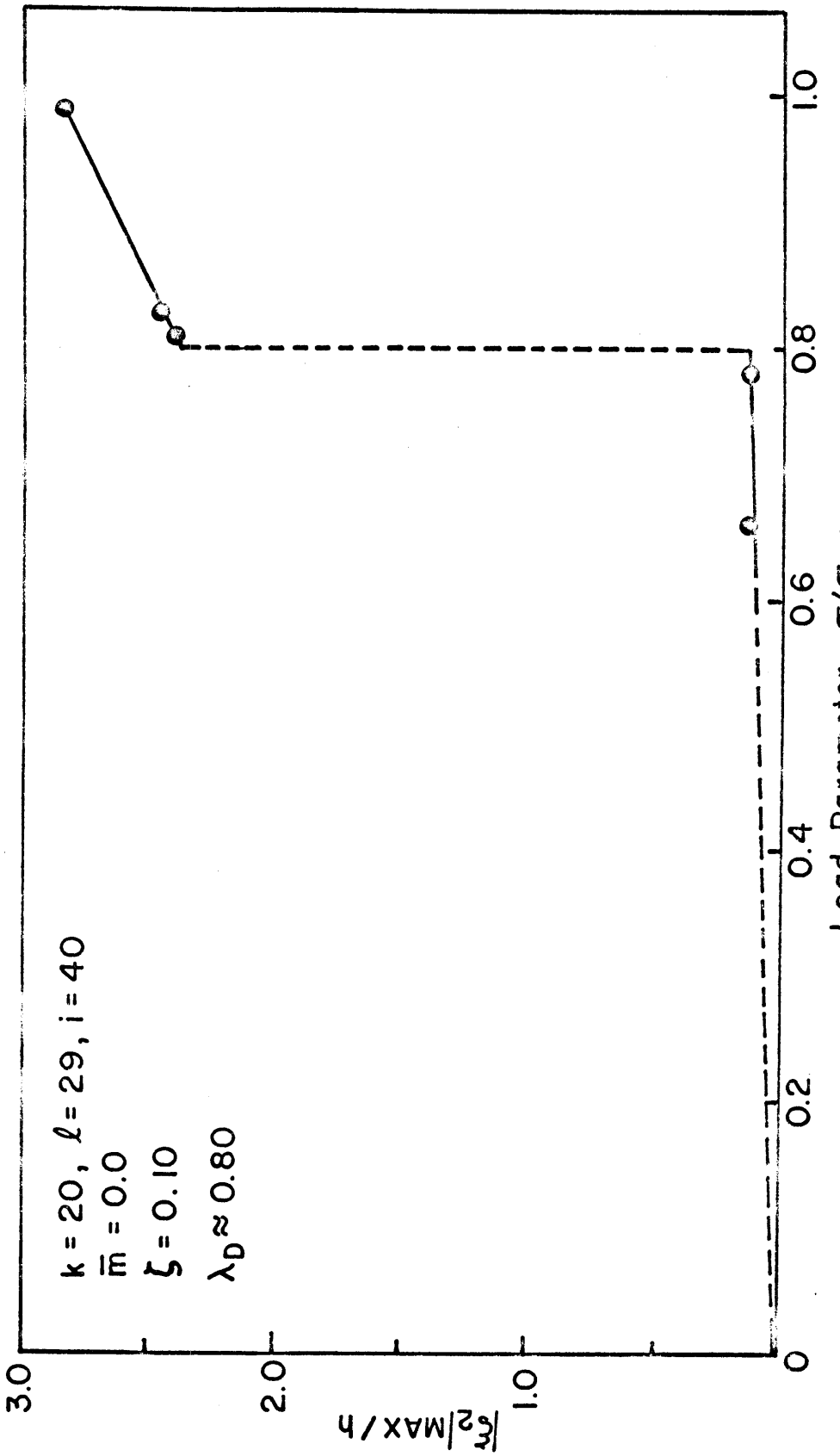

FIG. 6 VARIATION OF $(\xi_2)_{MAX}$ WITH LOAD

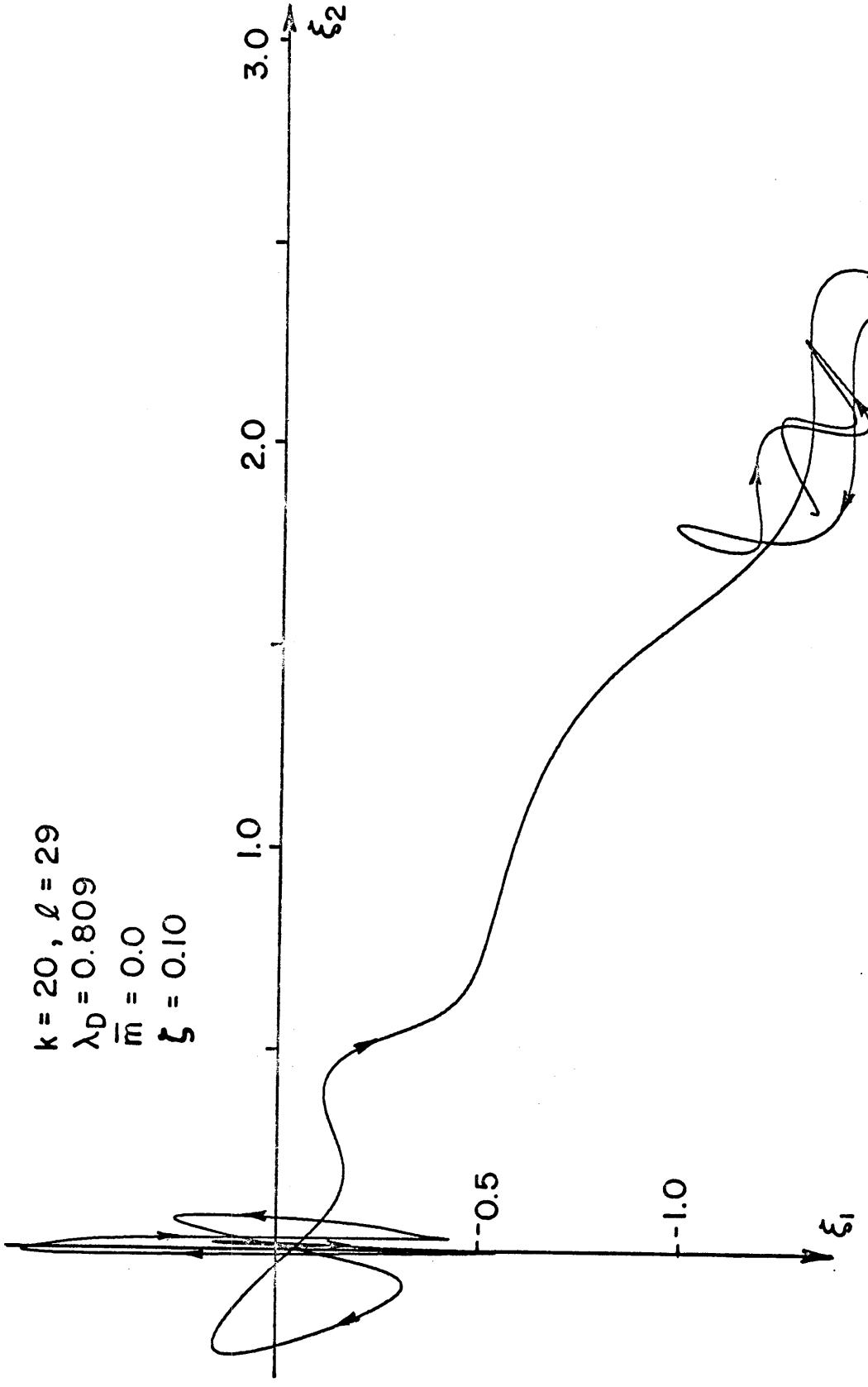

FIG. 7a DYNAMICAL PATH ON $\xi_1 - \xi_2$ PLANE

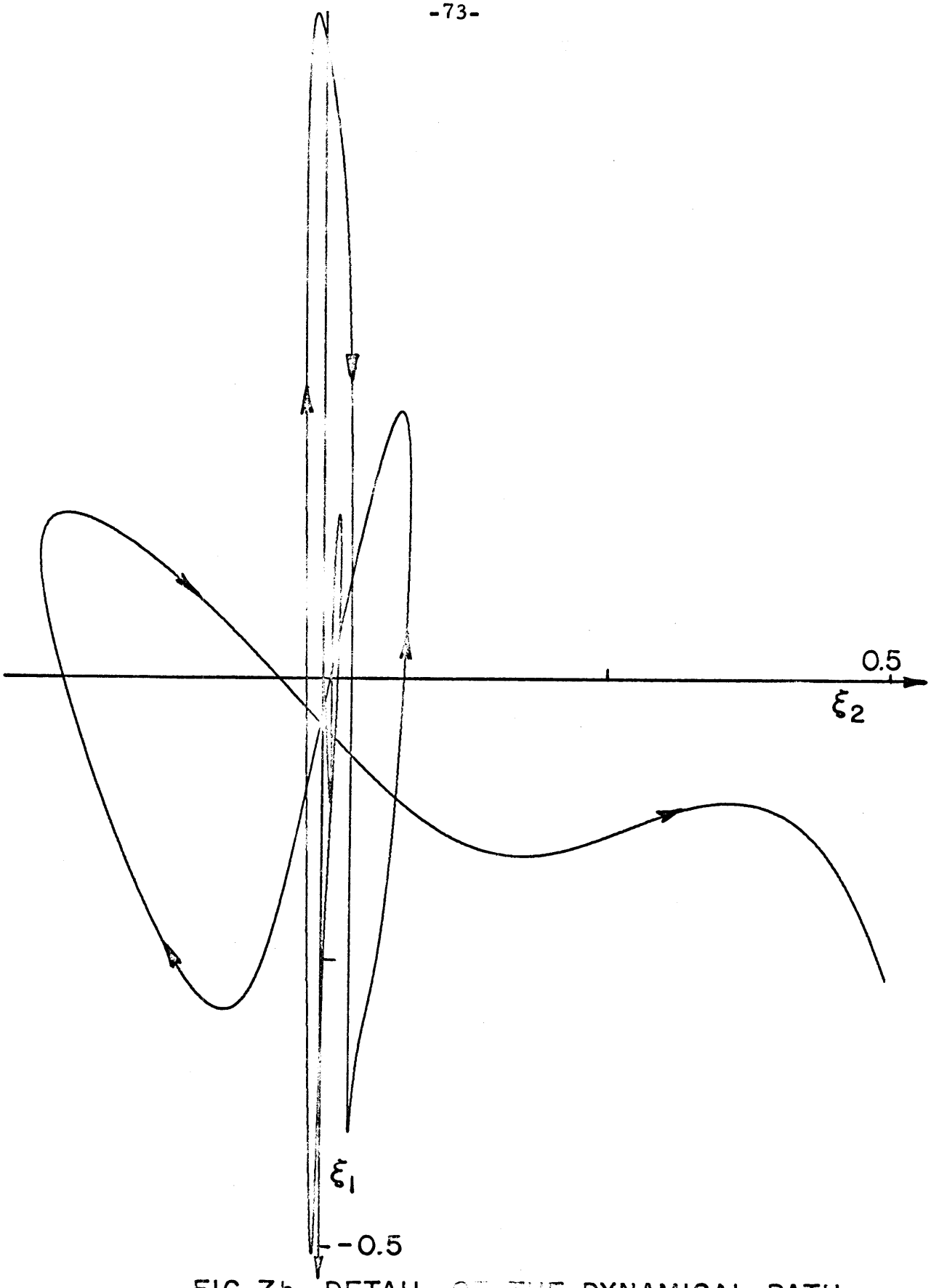

FIG. 7b DETAIL OF THE DYNAMICAL PATH

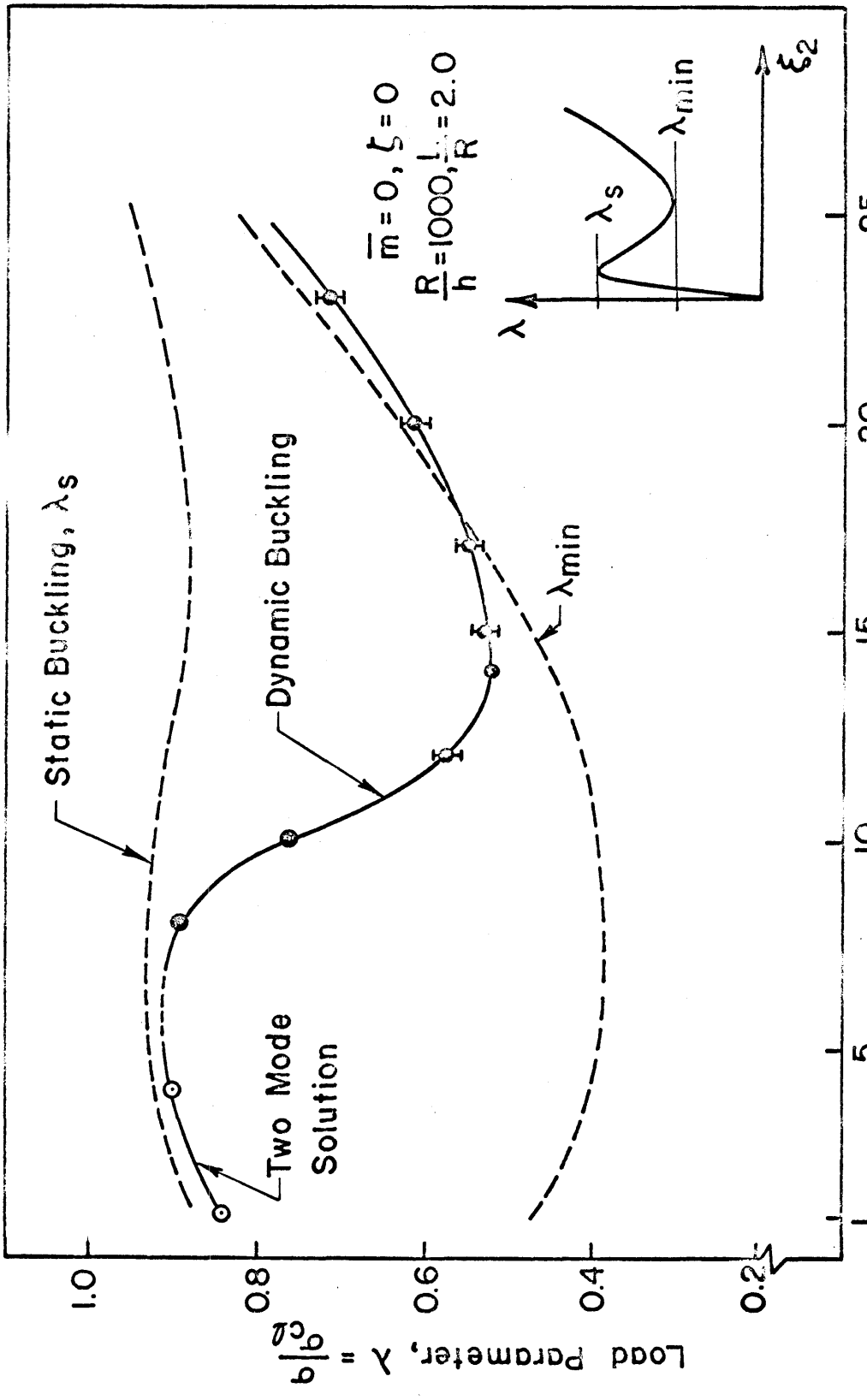

FIG.8 DYNAMIC BUCKLING LOAD VS. WAVE NUMBER

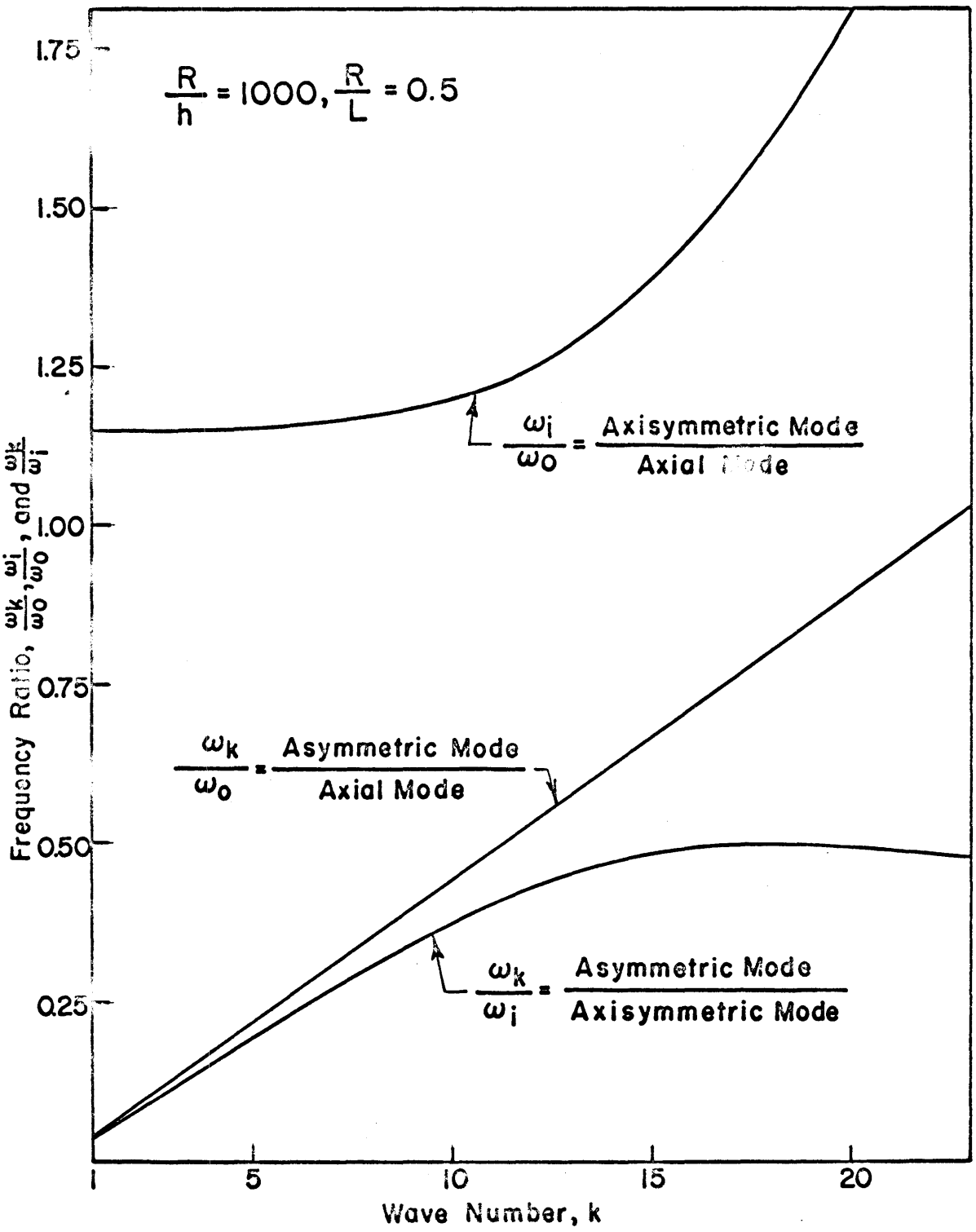

FIG. 9 FREQUENCY RATIO VS. WAVE NUMBER

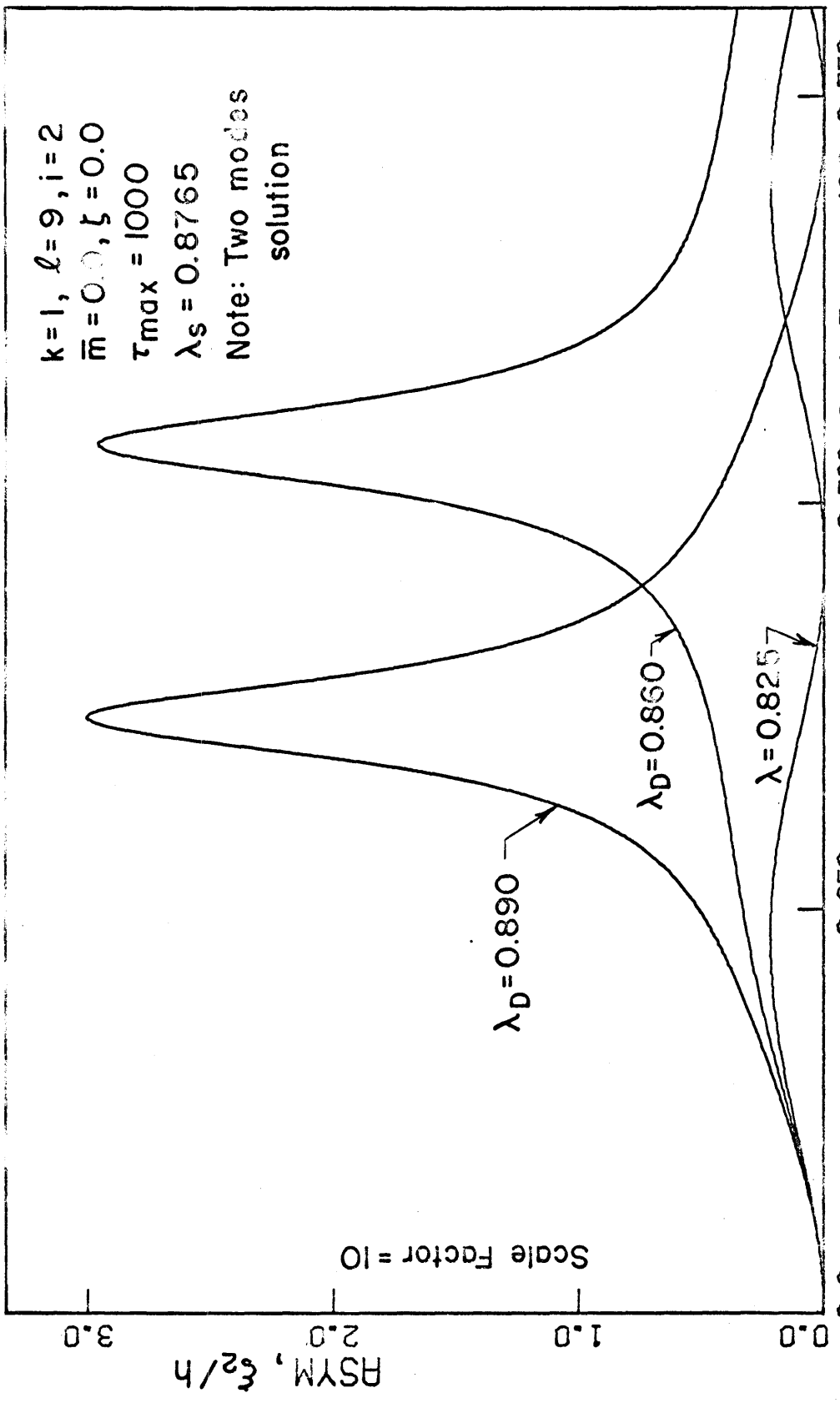

FIG. 10 RESPONSE OF THE LOWEST WAVE NUMBER

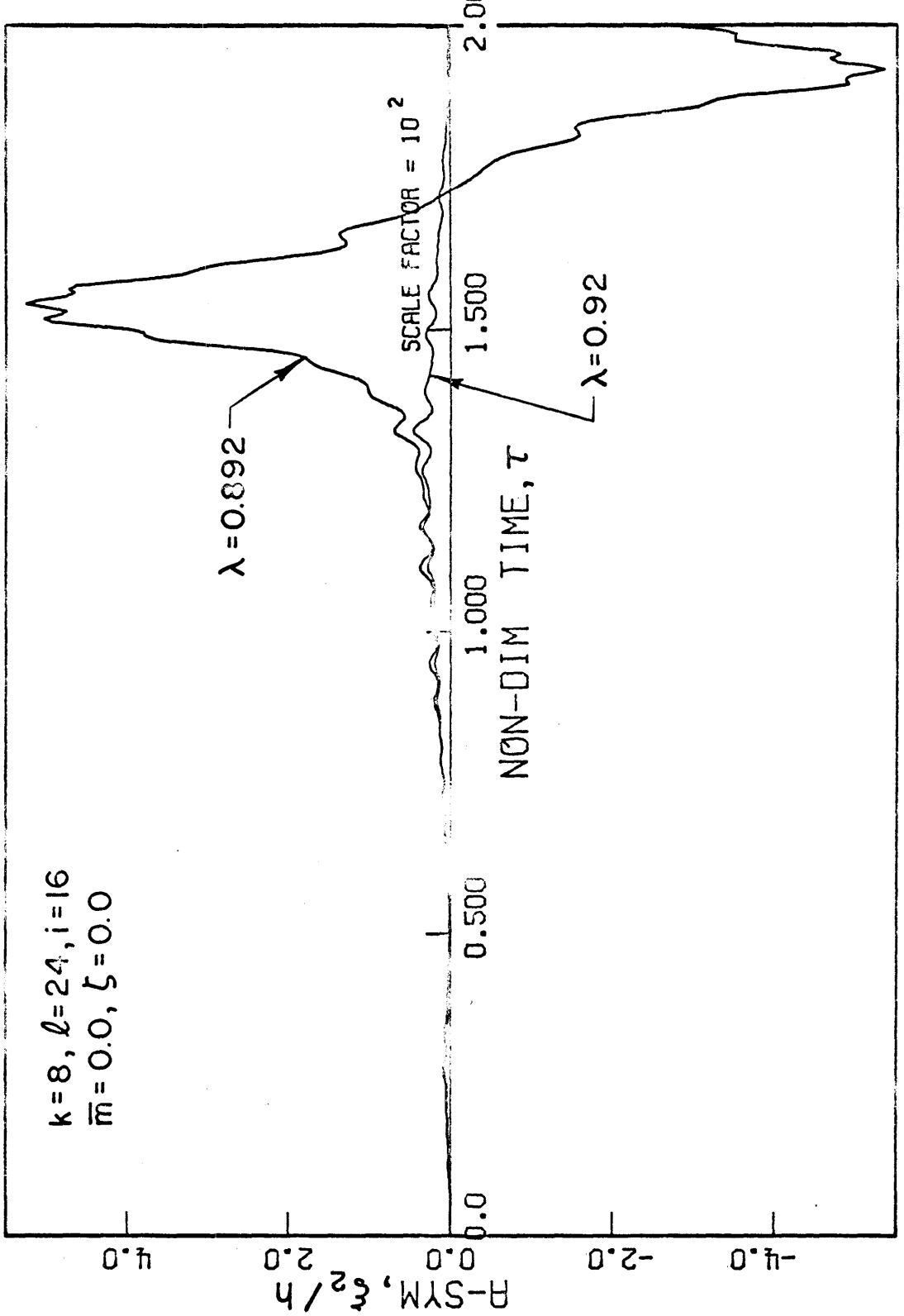

FIG. II-4 RESPONSE OF ASYMMETRIC MODE FOR k = 8

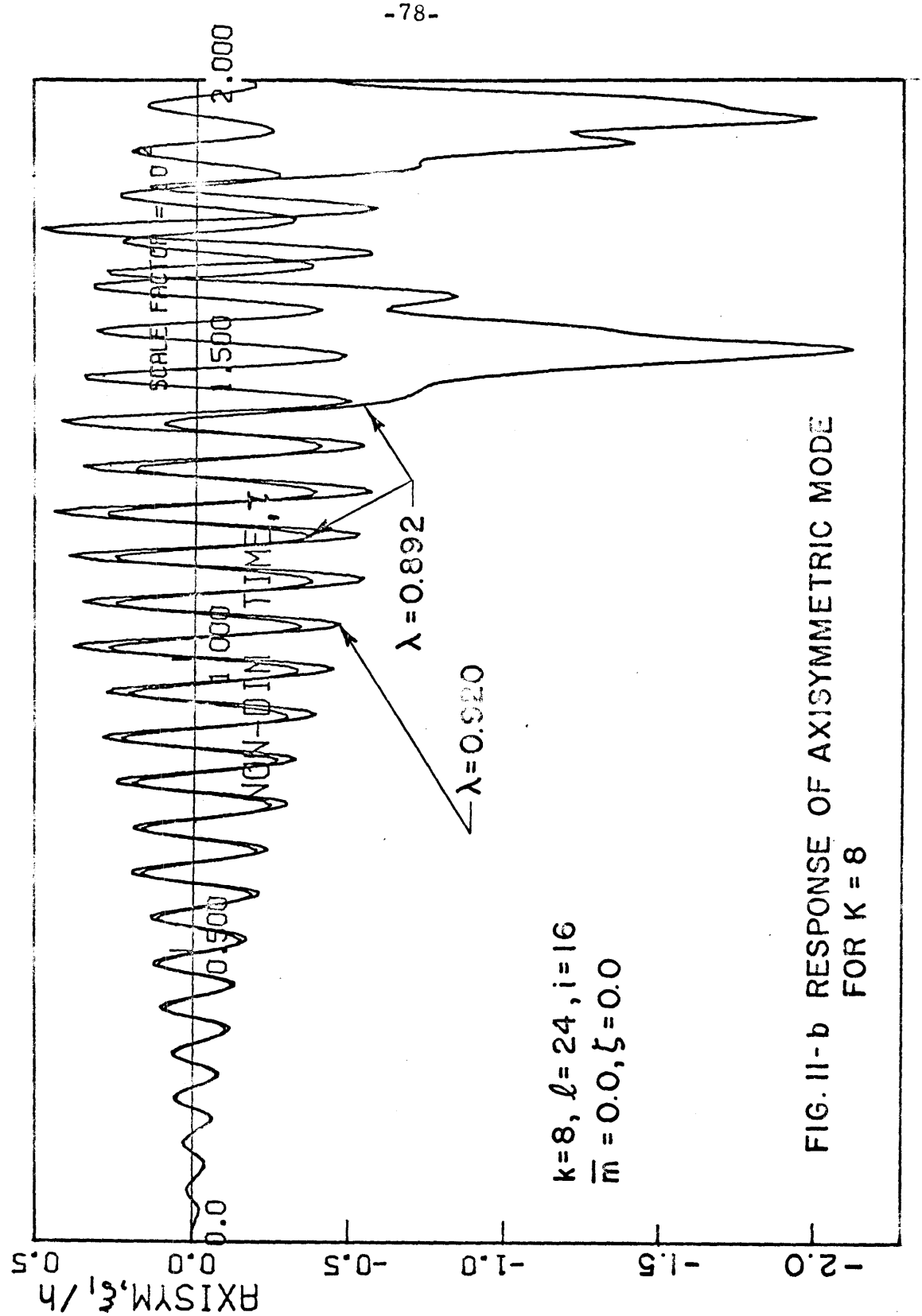

FIG. II-b RESPONSE OF AXISYMMETRIC MODE FOR K = 8

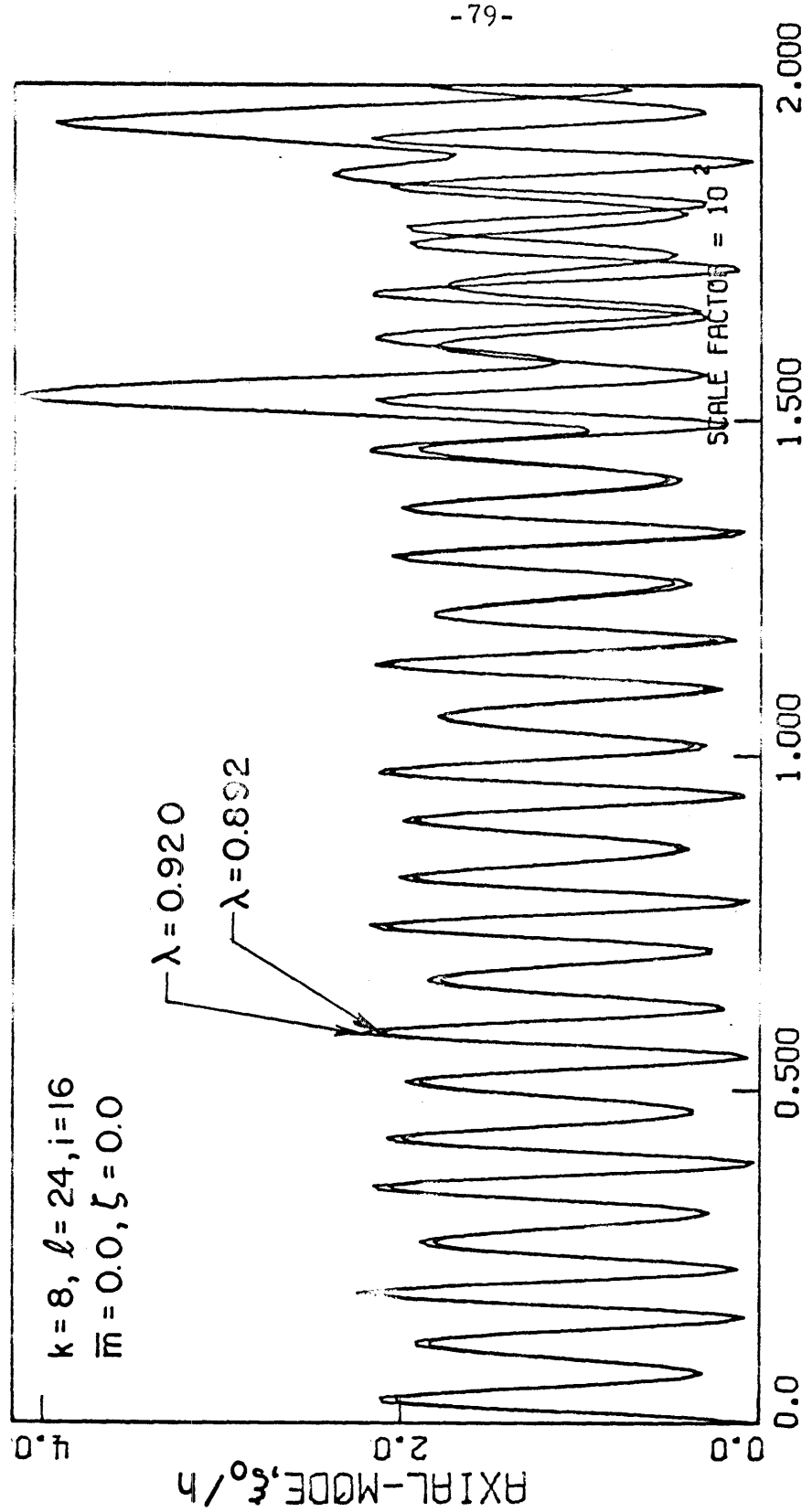

FIG. II-c RESPONSE OF AXIAL MODE FOR k = 8

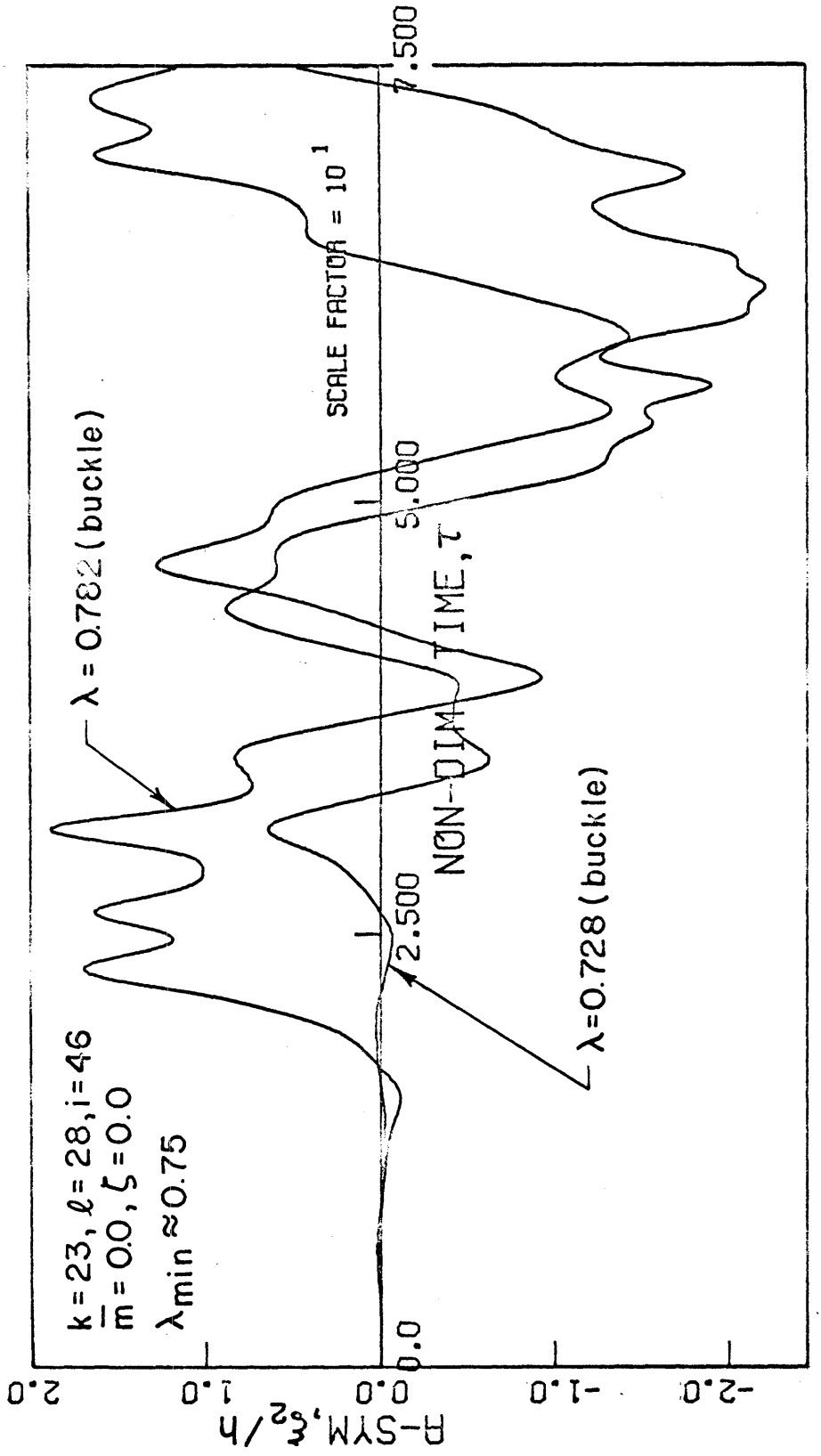

FIG. 12-a RESPONSE OF ASYMMETRIC MODE FOR k=23

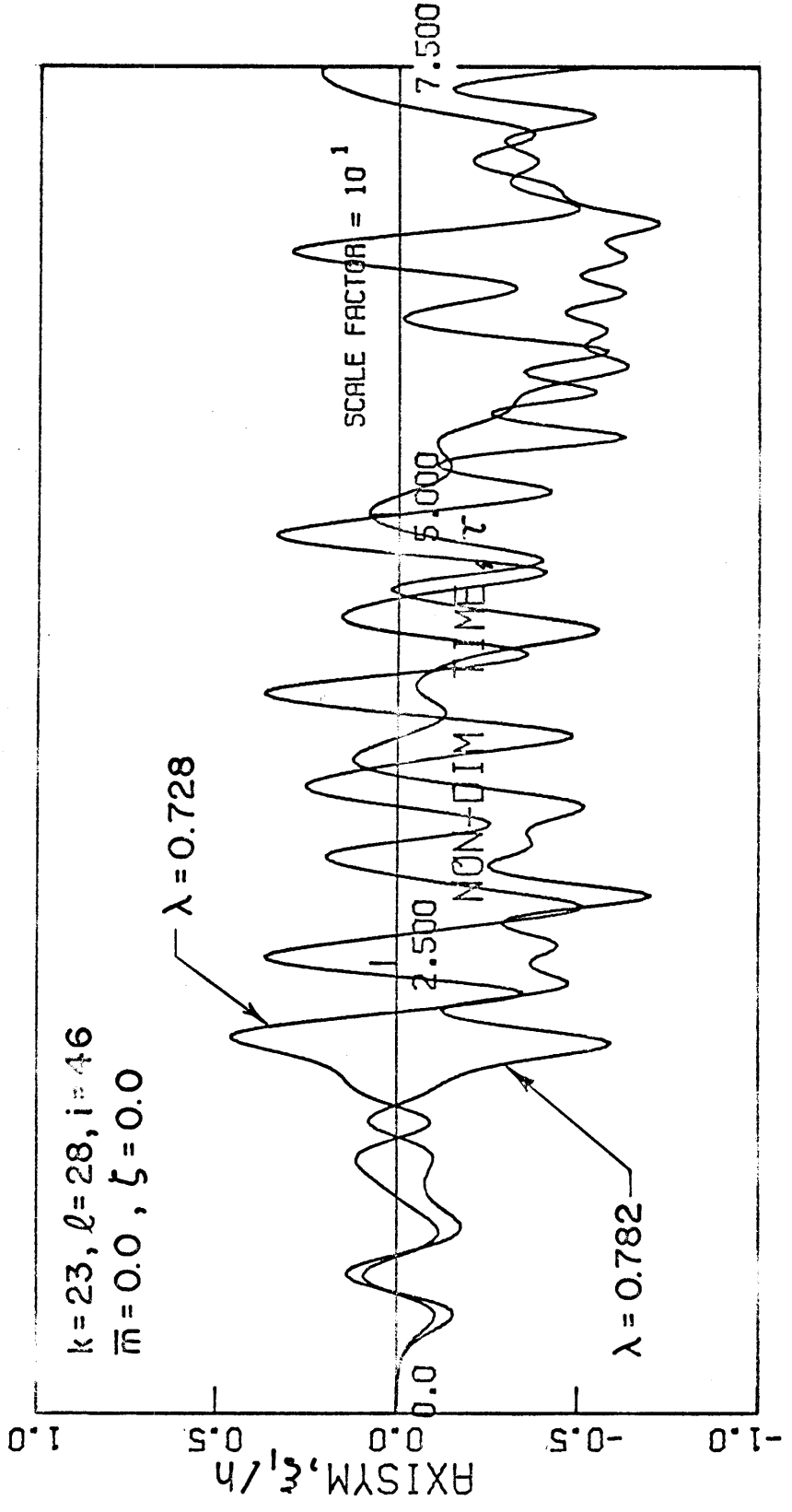

FIG. 12-b RESPONSE OF AXISYMMETRIC MODE FOR k=23

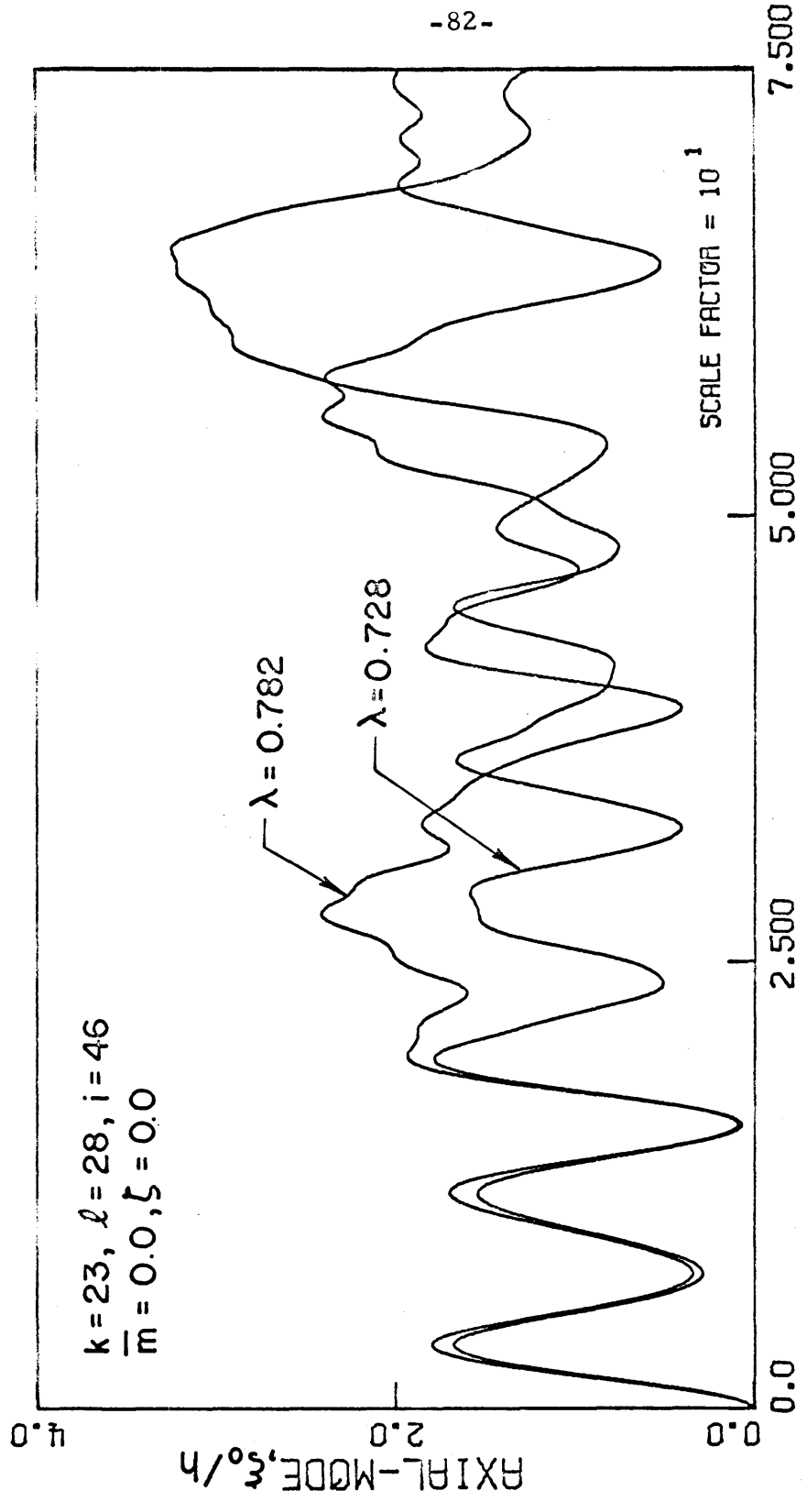

FIG. 12-c RESPONSE OF AXIAL MODE FOR k = 23

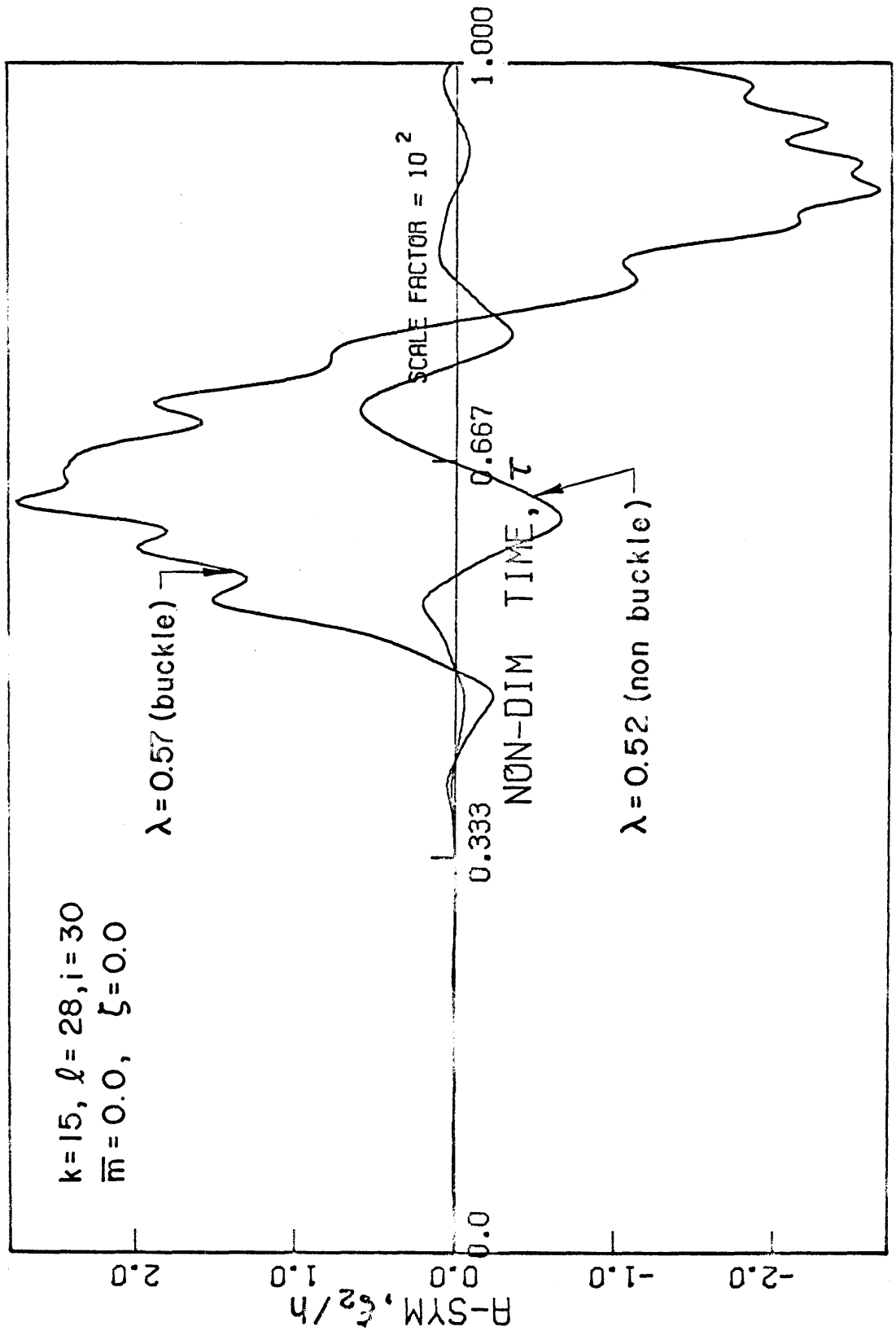

FIG. 13-a RESPONSE OF ASYMMETRIC MODE FOR k = 15

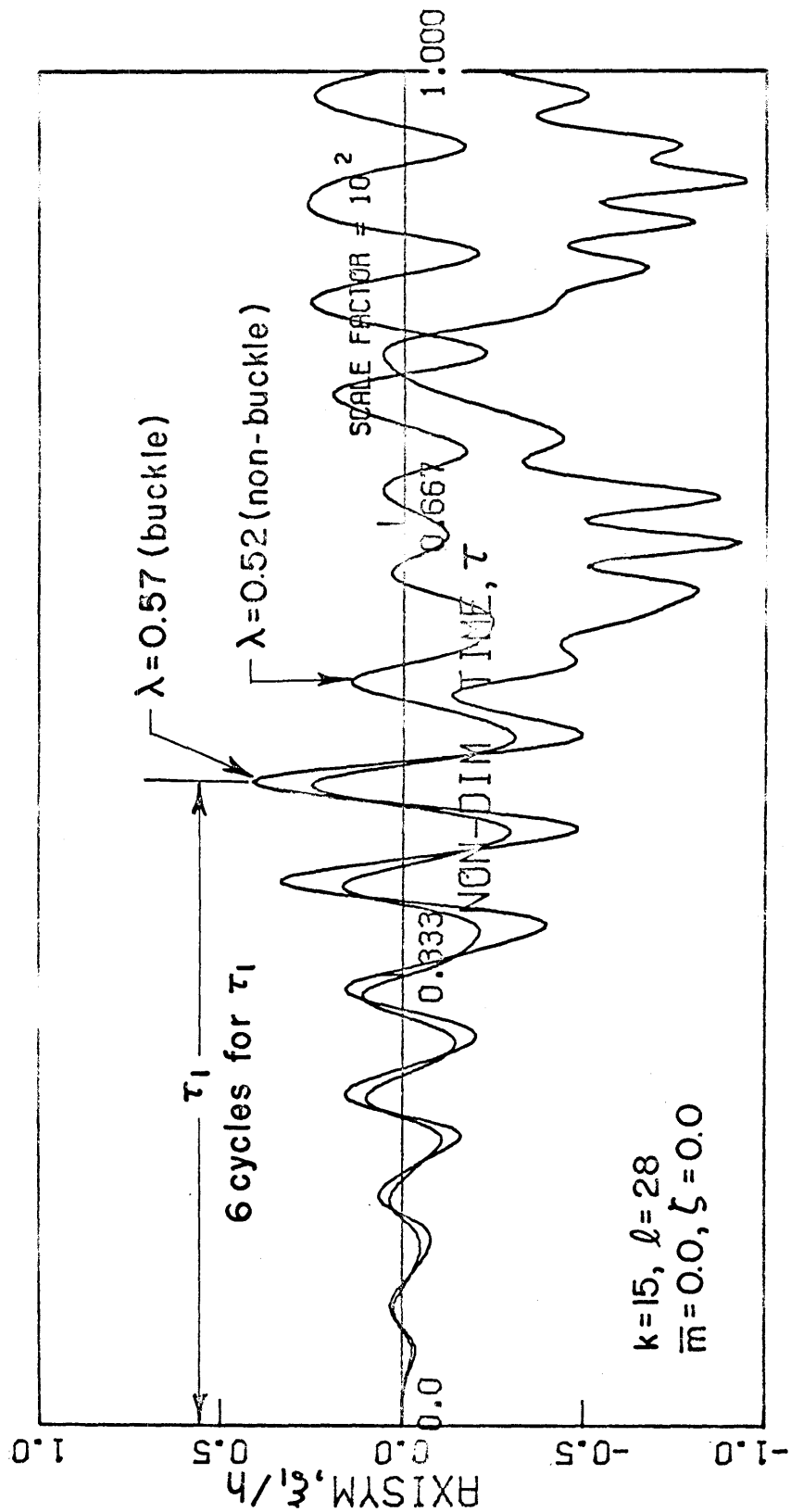

FIG. 13-b RESPONSE OF AXISYMMETRIC MODE FOR k=15

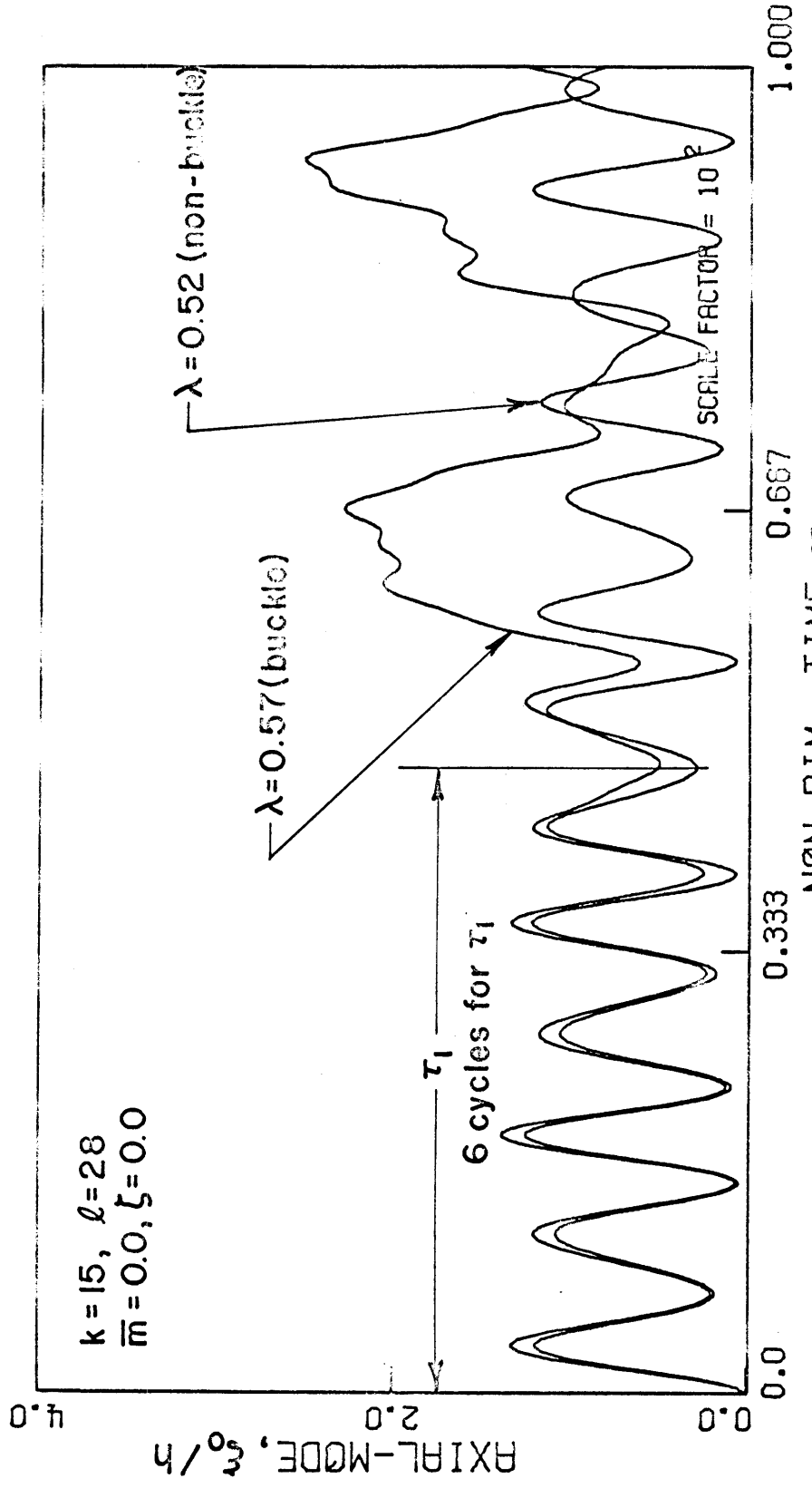

FIG. 13-c RESPONSE OF AXIAL MODE FOR k = 15

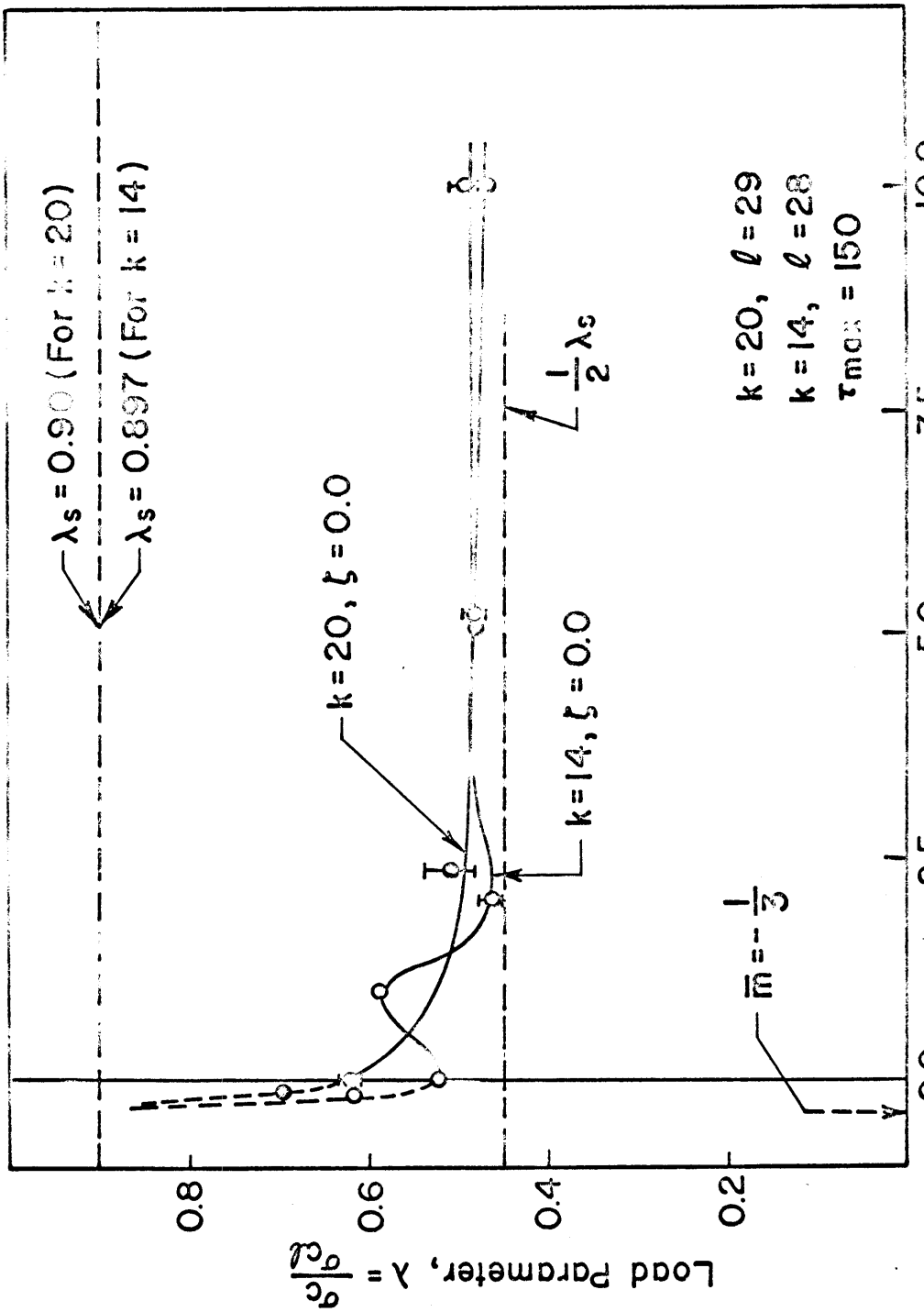

FIG. 14 EFFECT OF MASS ON THE DYNAMIC BUCKLING LOAD

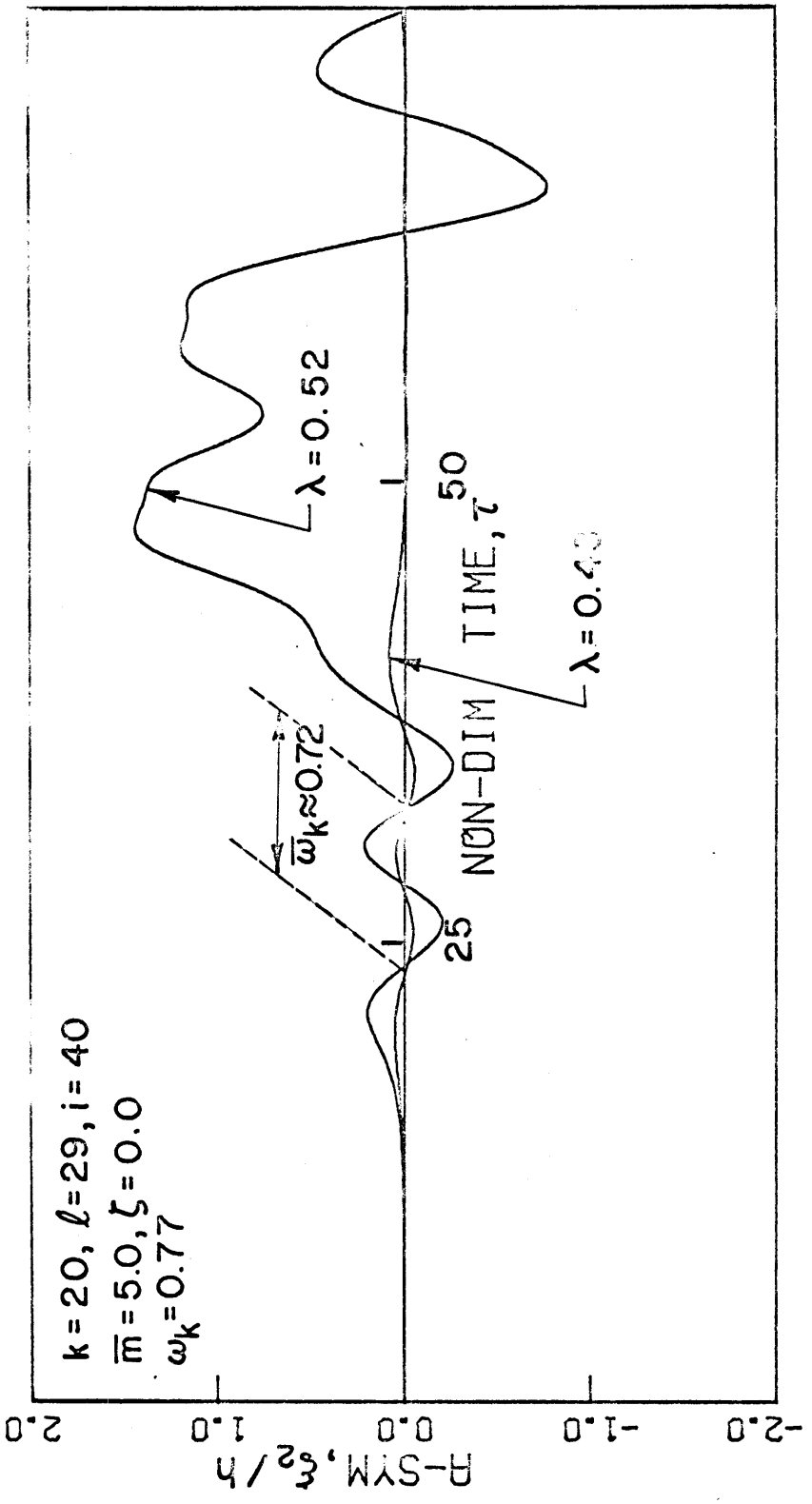

FIG. 15-a RESPONSE OF ASYMMETRIC MODE WITH MASS

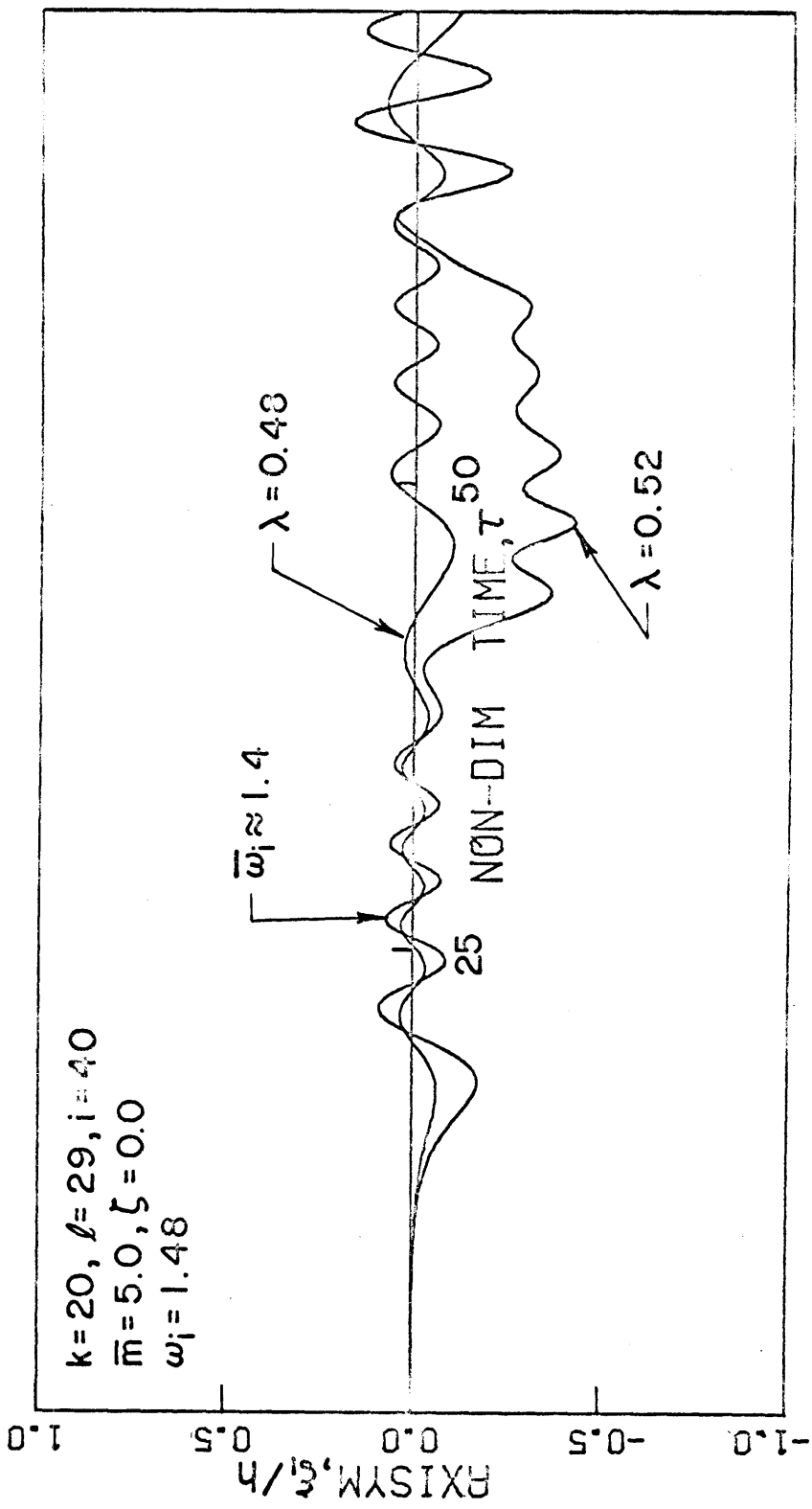

FIG. 15- 2 RESPONSE OF AXISYMMETRIC MODE WITH MASS

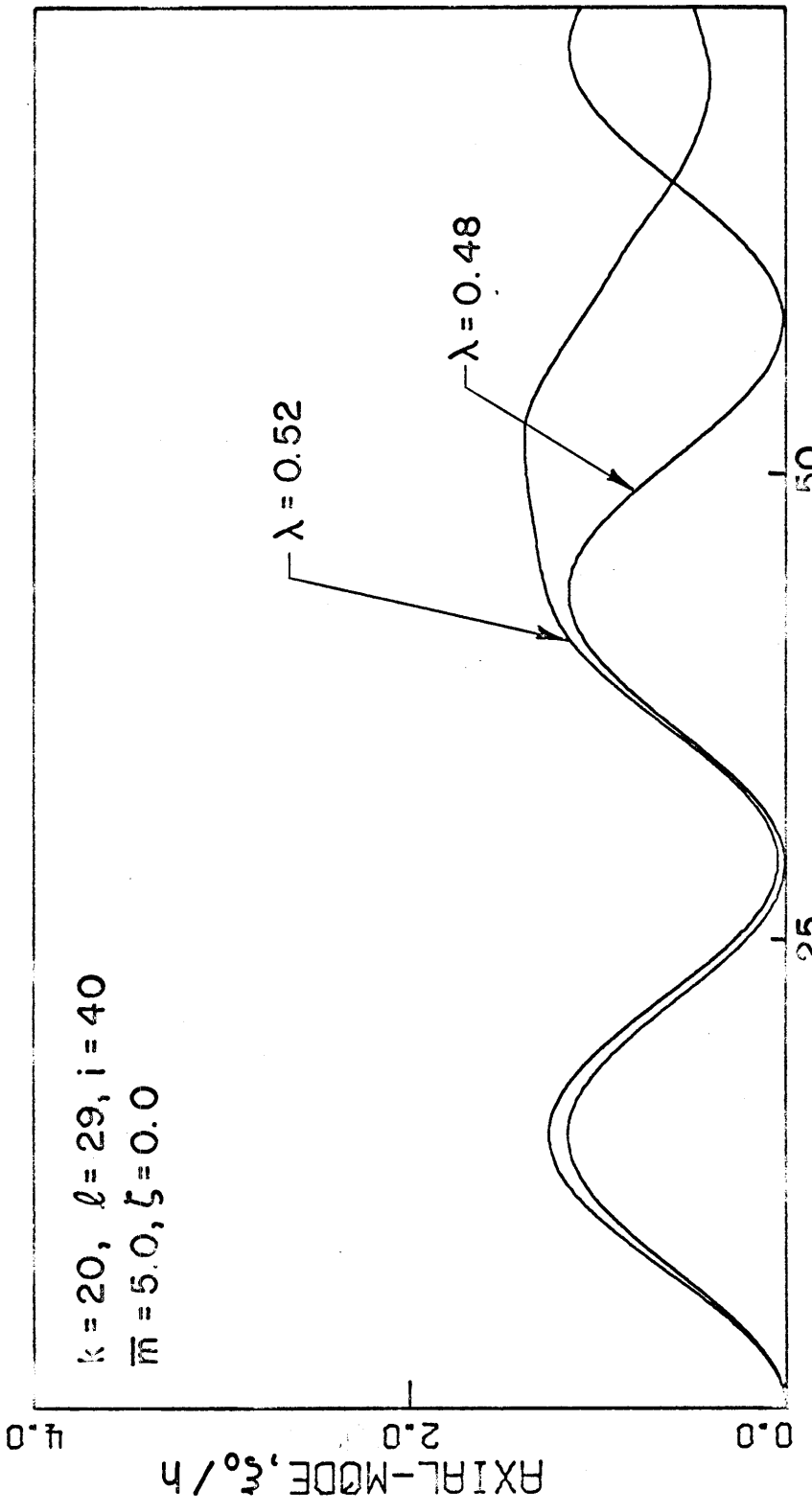

FIG. 15-c RESPONSE OF AXIAL MODE WITH MASS

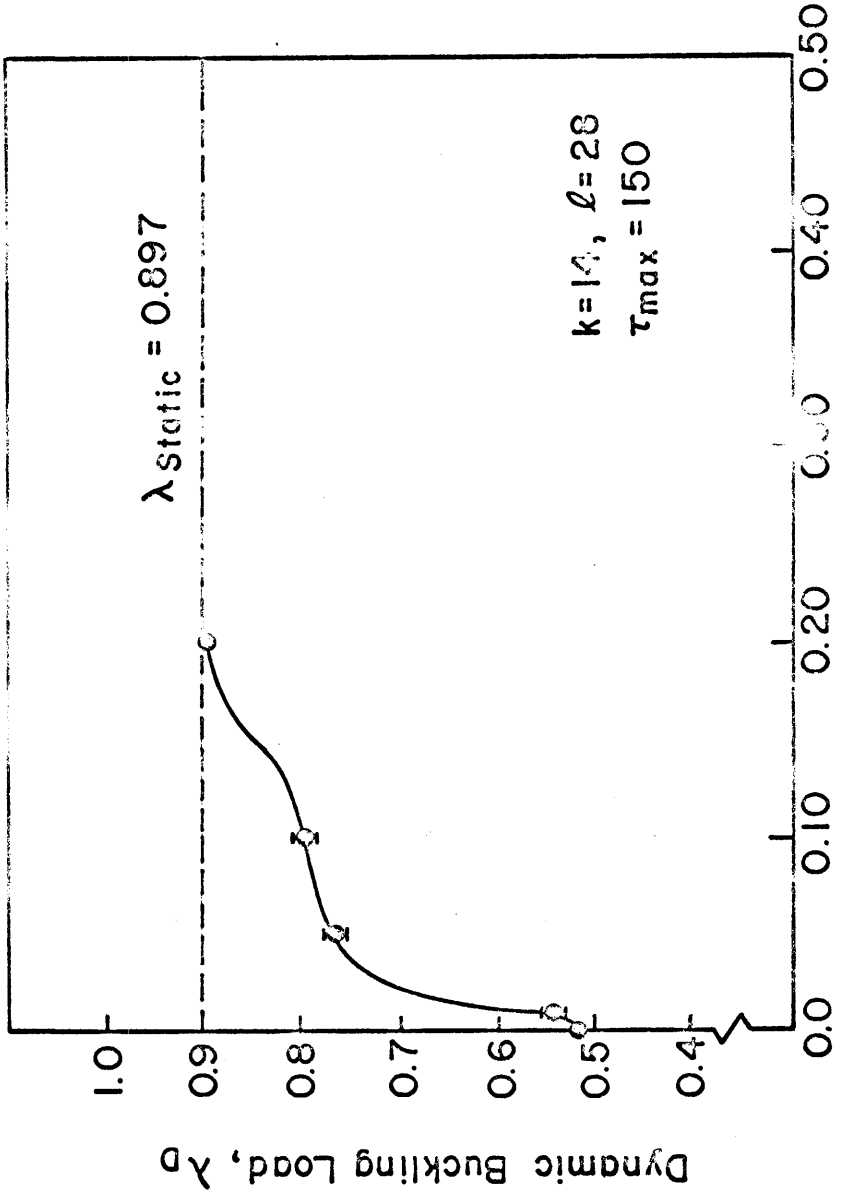

FIG. 16 EFFECT OF DAMPING ON DYNAMIC BUCKLING LOAD

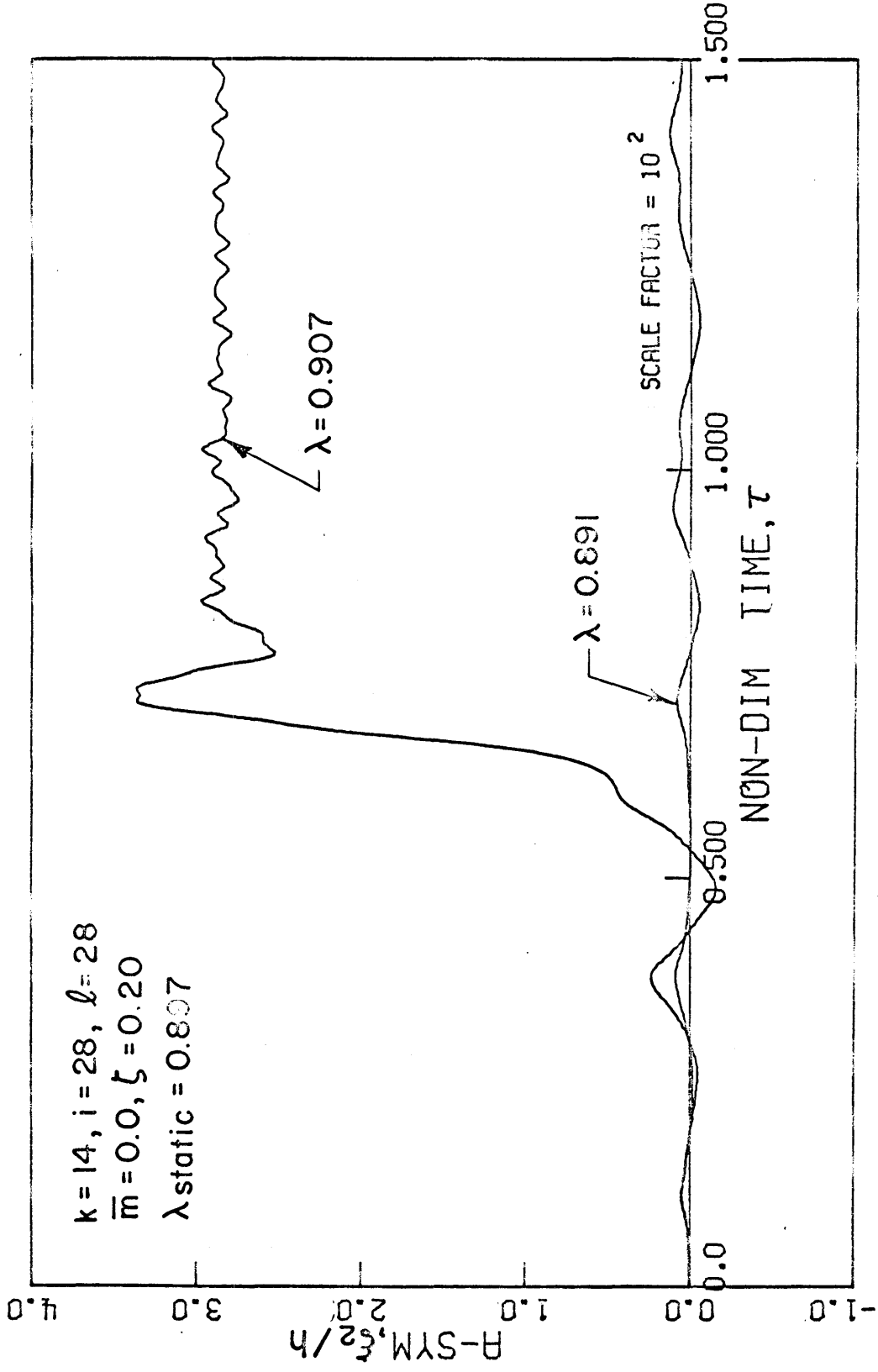

FIG. 17-a ASYMMETRIC RESPONSE WITH DAMPING, $\zeta = 0.20$

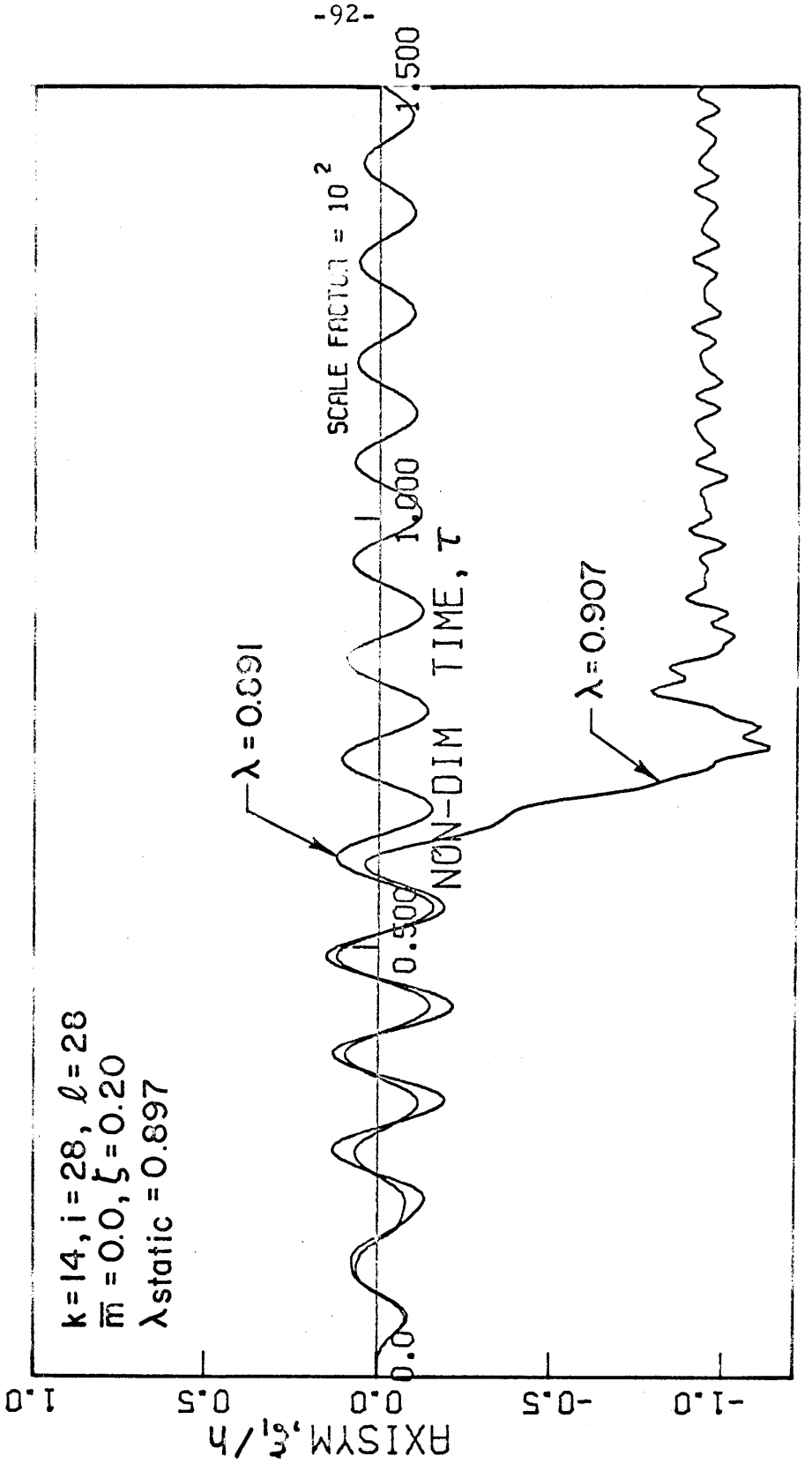

FIG. 17-b AXISYMMETRIC RESPONSE WITH DAMPING, ζ=0.20

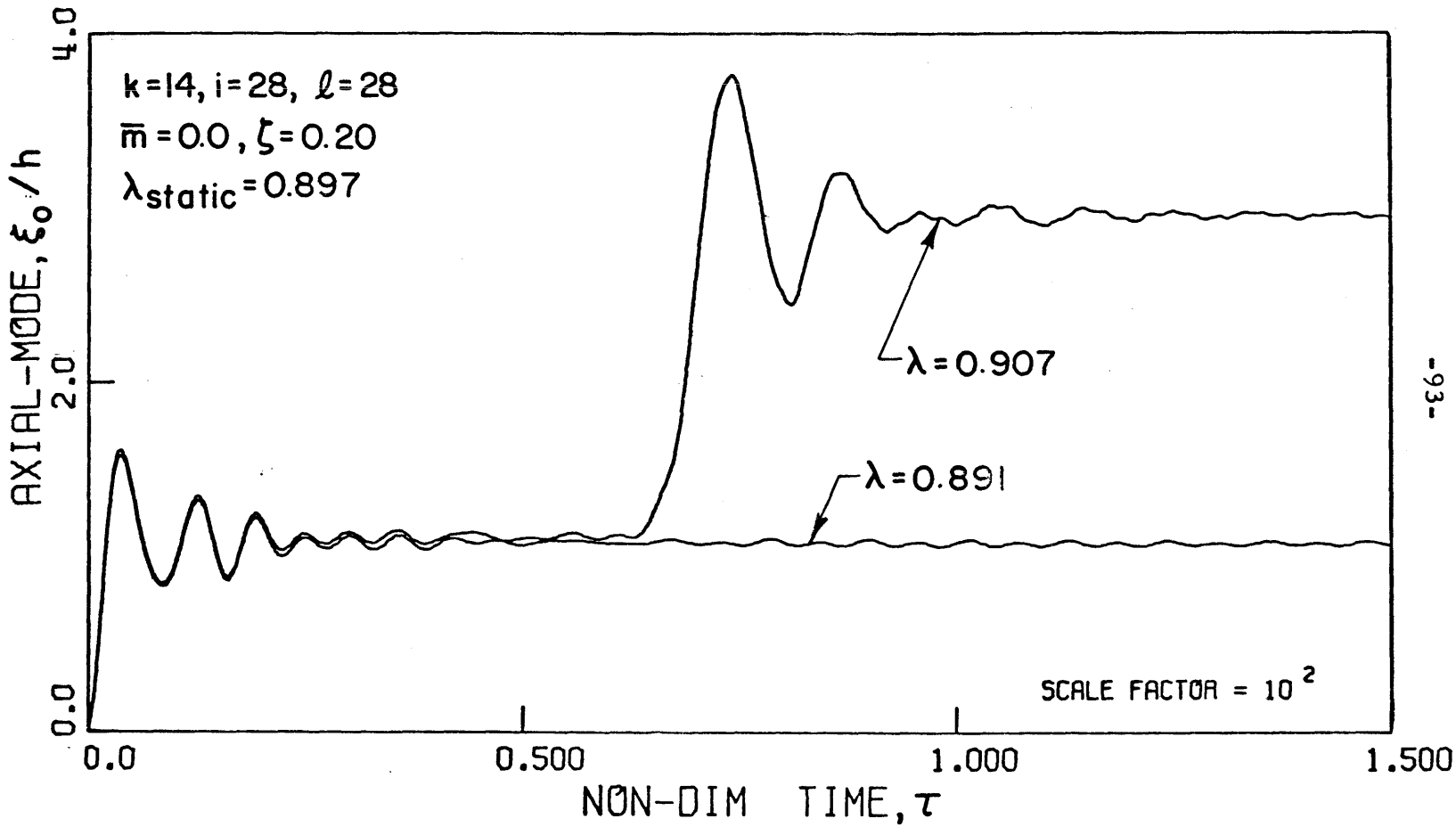

FIG. 17-c AXIAL RESPONSE WITH DAMPING, $\zeta = 0.20$

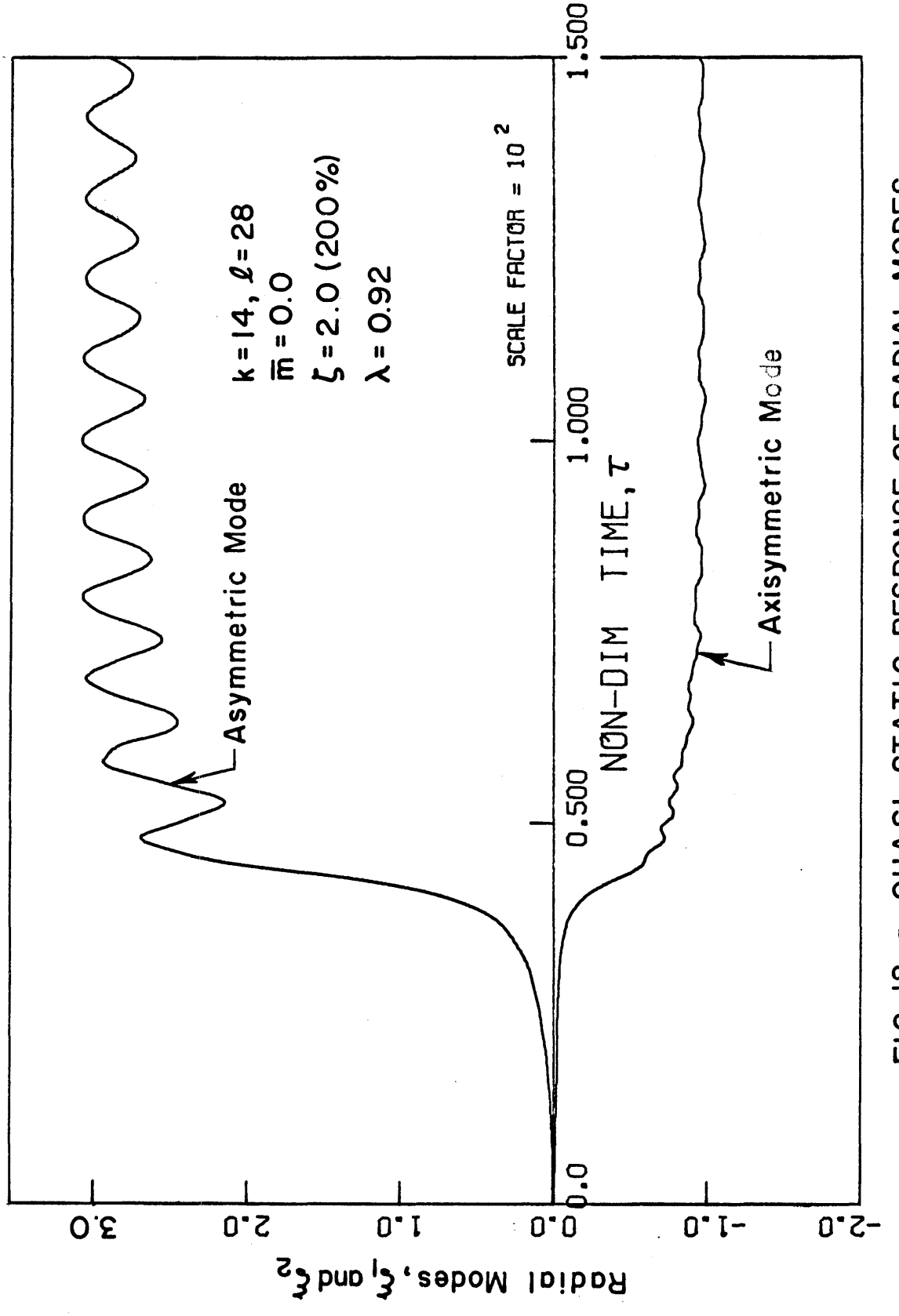

FIG. 18-a QUASI-STATIC RESPONSE OF RADIAL MODES

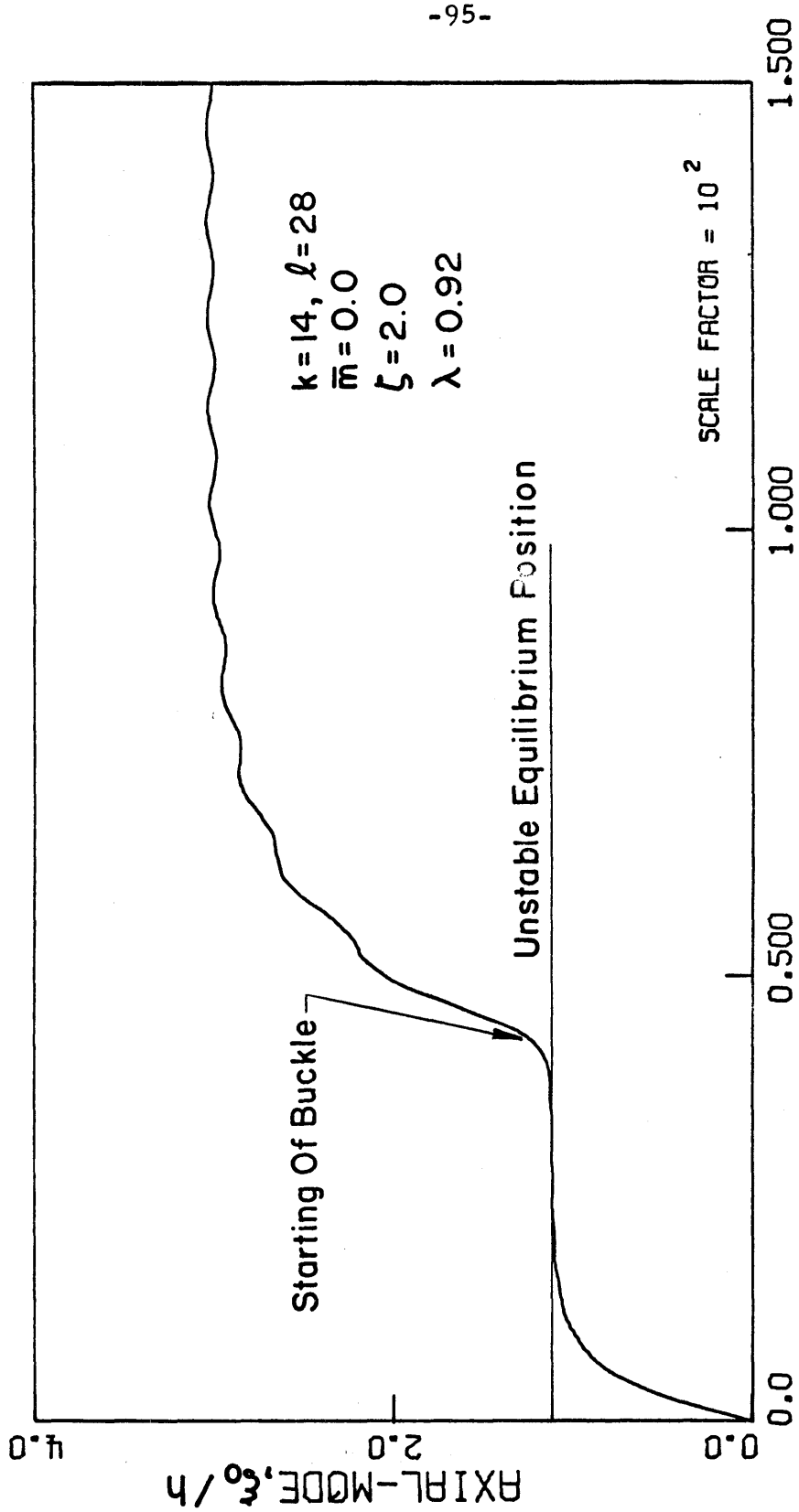

FIG.18-b QUASI-STATIC RESPONSE OF AXIAL MODE

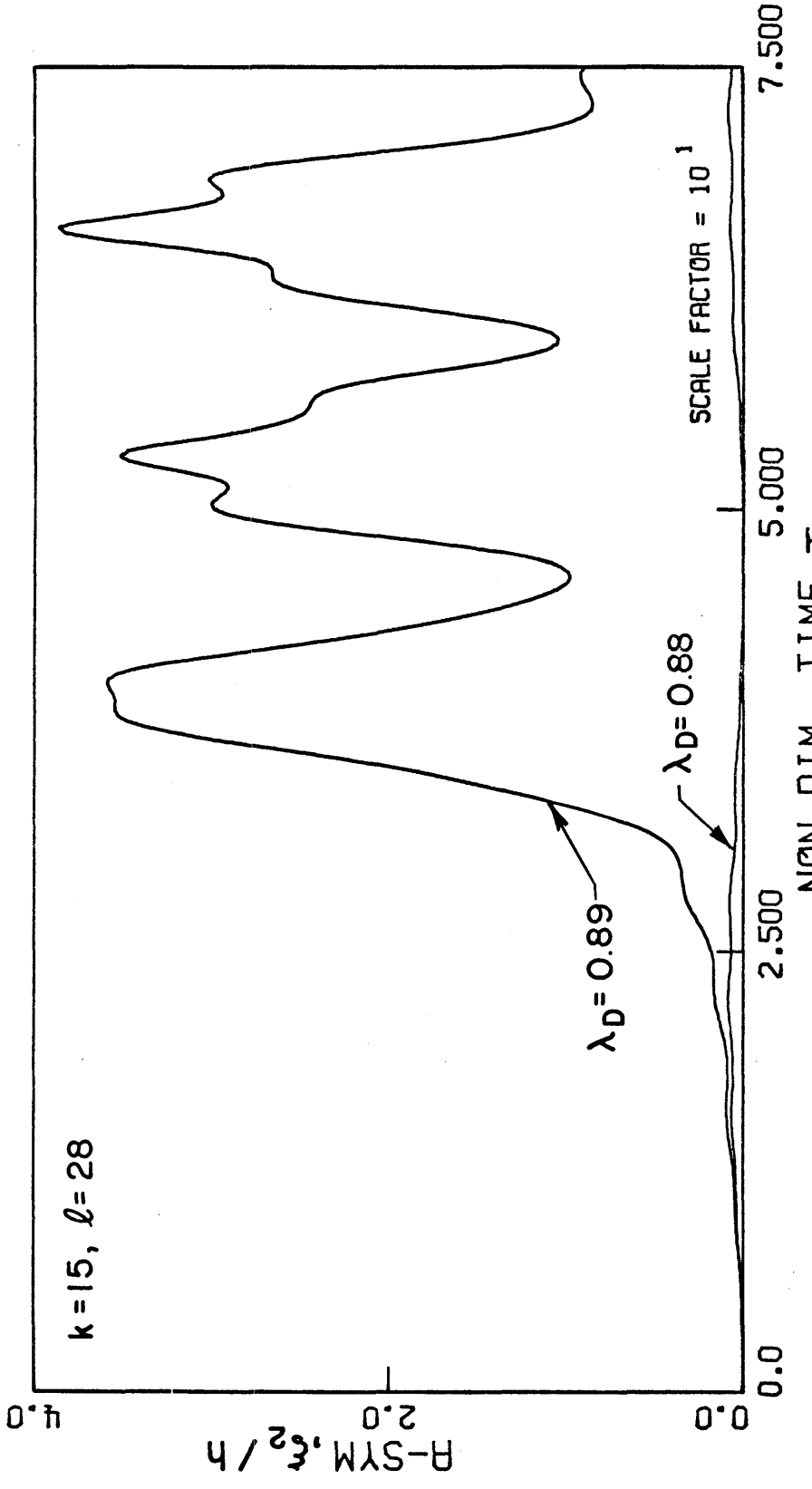

FIG. 19-a THE RESPONSE WITHOUT AXIAL INERTIA (ASYMMETRIC MODE)

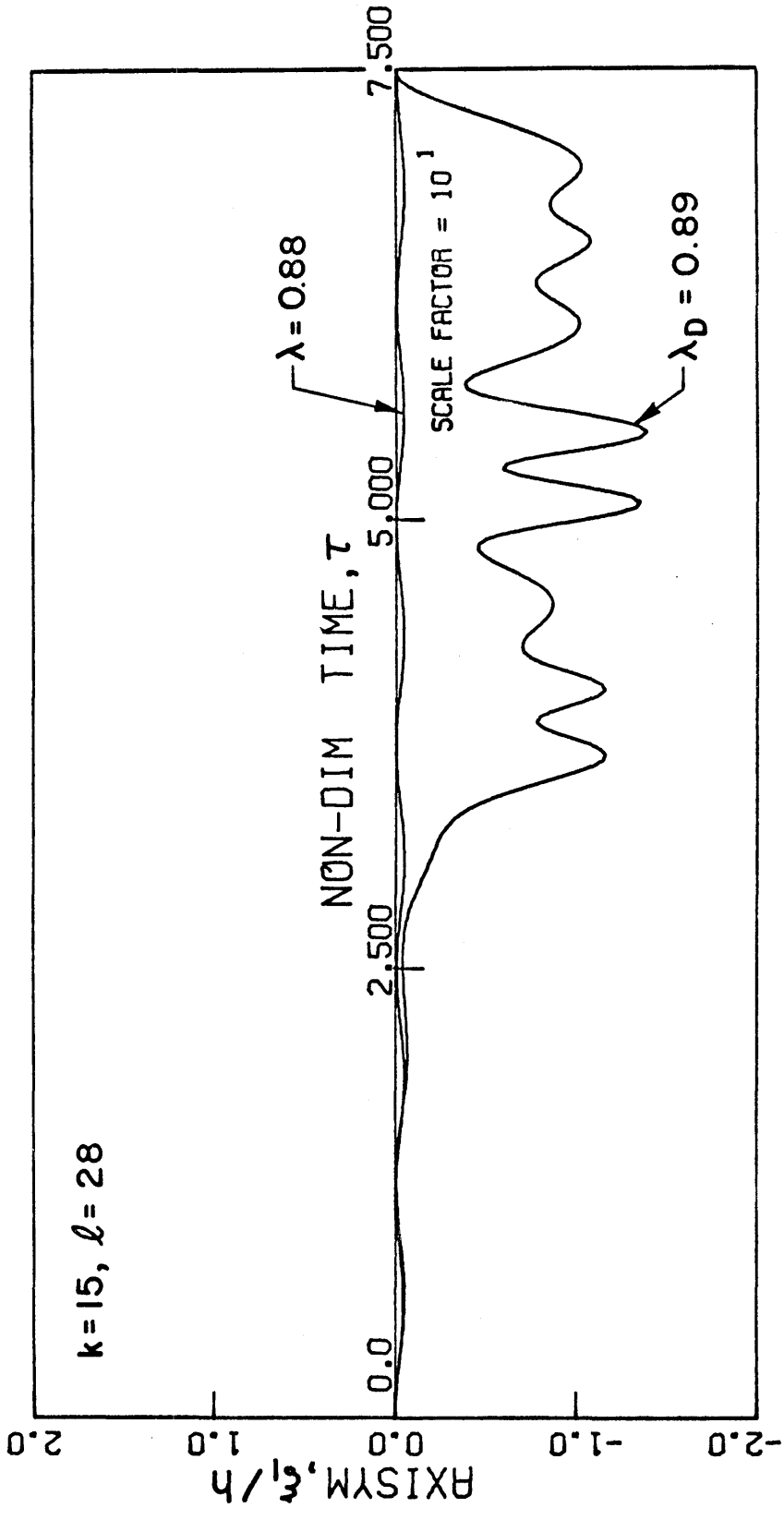

FIG. 19-b THE RESPONSE WITHOUT AXIAL INERTIA (AXISYMMETRIC MODE)

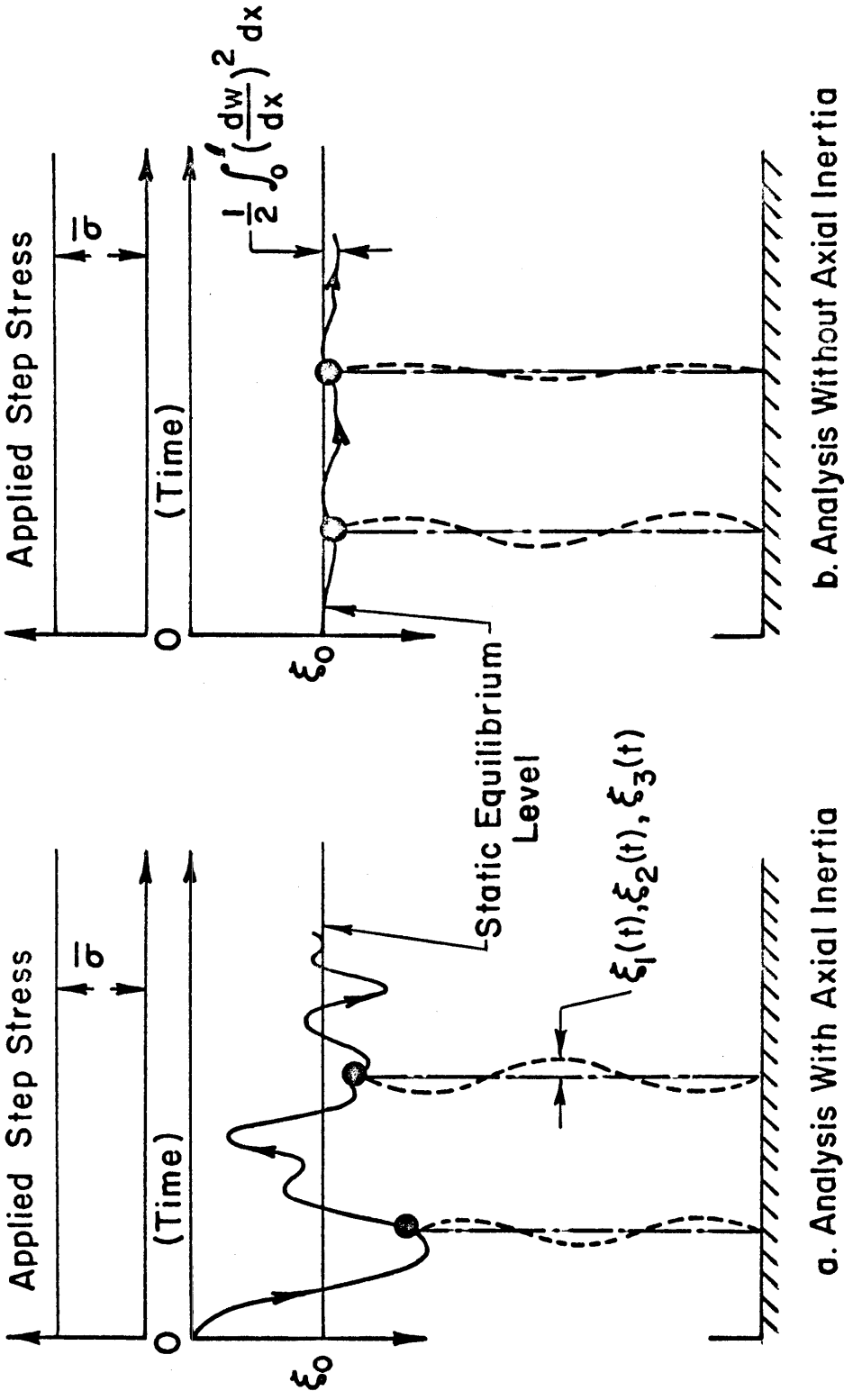

FIG. 20 SCHEMATIC SHELL MOTIONS

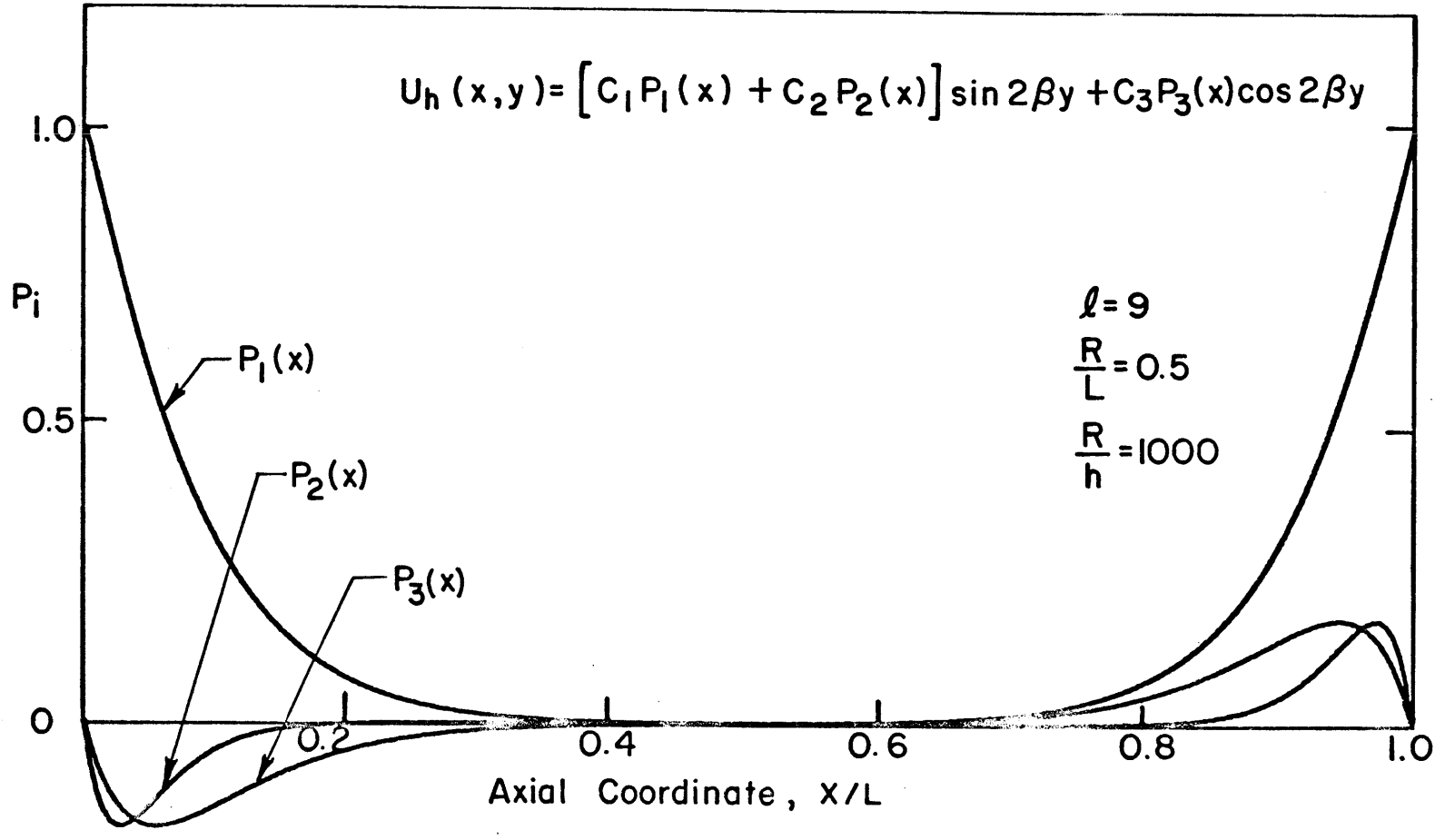

FIG. 21-a BOUNDARY LAYER-TYPE SOLUTION FOR AXIAL DISPLACEMENT

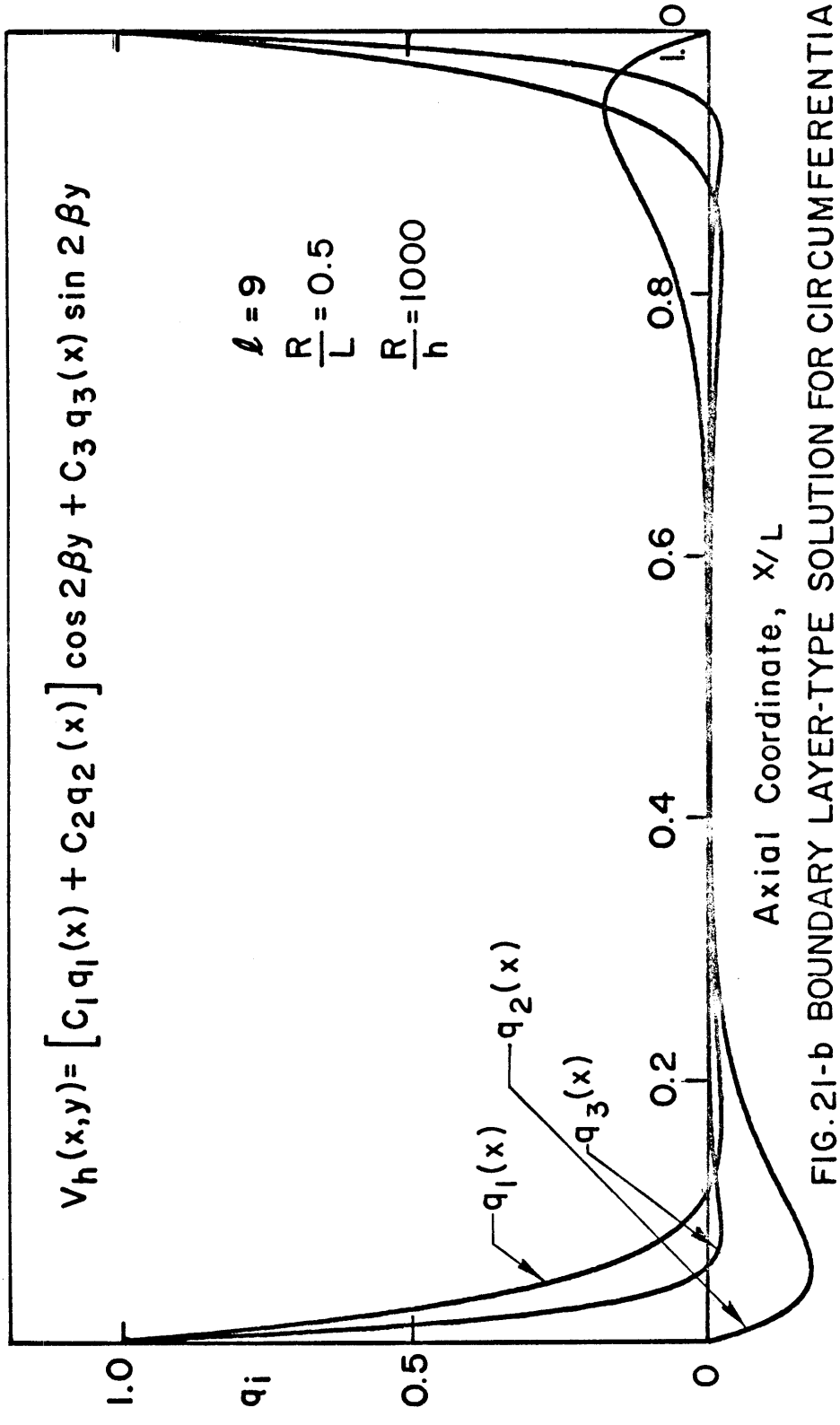

FIG. 21-b BOUNDARY LAYER-TYPE SOLUTION FOR CIRCUMFERENTIAL DISPLACEMENT